UNI. Y
OF MICHIGAN
MAR 1 0 1953
ENGINEERING
LIBRARY

JOURNAL OF THE AERONAUTICAL SCIENCES

VOLUME 20 MARCH, 1953 NUMBER 3

CONTENTS

Aerodynamic Coefficients of an Oscillating Airfoil with Control Surface in Two-Dimensional Subsonic Flow.....A. I. VAN DE VOOREN 153

On the Pure Rolling Motion of Winged and/or Finned Missiles in Varying Supersonic Flight.....JOHN D. NICOLAIDES AND RAY E. BOLZ 160

Theoretical Pressure Recovery Through a Normal Shock in a Duct with Initial Boundary Layer.....GEORGE MCLAFFERTY 169

Forced Convection Heat Transfer from Horizontal Cylinders in a Rarefied Gas.....F. M. SAUER AND R. M. DRAKE, JR. 175

Inelastic Instability and Incremental Theories of Plasticity.....E. T. ONAT AND D. C. DRUCKER 181

Thermal Distributions in Jeffery-Hamel Flows Between Nonparallel Plane Walls.....KNOX MILLSAPS AND KARL POHLHAUSEN 187

Quadruple Velocity Correlations and Pressure Fluctuations in Isotropic Turbulence.....MAHINDER S. UBEROI 197

A Field-Mapping Method for Analysis and Synthesis of Linear Closed-Loop Systems.....MIKE W. FOSSIER AND HAROLD A. ROSEN 205

Readers' Forum: "The Equations for Pressure and Momentum Using Linearized Theory for Compressible Flow," by Lee S. Wasserman; "Note on a Method of Root Area Analysis for Swept Wings," by John C. Bowman; "Lift of Highly Swept Wings," by Harold Mirels; "Effects of Angle of Attack on Local Skin-Friction Coefficients at $M_0 = 4$," by John Joseph Martin; "Comments on 'Remarks on Dynamic Loads in Landing,'" by Frederic M. Hoblit; "A Reply—Single Degree Flutter of an Aileron," by H. L. Runyan, H. J. Cunningham, and C. E. Watkins, with "Authors' Closure," by R. M. Rosenberg; "Approximate Calculation of Axisymmetric Flow Near the Vertex of a Body Traveling at High Supersonic Speeds," by A. J. Eggers, Jr., and Samuel Kraus; "Statement on References: On Air Forces on Oscillating Wings of Low Aspect Ratio," by I. E. Garrick; "Compressible Flow Past a Cascade of Thin Airfoils," by G. V. R. Rao; "The Pressure Distribution on Low Aspect Ratio Wings in Steady or Unsteady Incompressible Flow," by H. R. Lawrence; "Busemann Coefficients for a Supersonic Airfoil," by D. Naylor; "A Note on the Solution for the Rectangular Membrane," by S. F. Borg; "A Measurement of Turbulent Boundary-Layer Profiles and Heat-Transfer Coefficient at $M = 7$," by Peter P. Wegener, Eva M. Winkler, and M. Sibulkin.....210–222

Published by the
INSTITUTE OF THE AERONAUTICAL SCIENCES, INC.

JOURNAL OF THE AERONAUTICAL SCIENCES

Editor: HUGH L. DRYDEN, *Director, N.A.C.A.*

Associate Editor: ROBERT R. DEXTER *Managing Editor:* BERNEICE H. JARCK

Editorial Committee

Aerodynamics

Francis Clauser
Howard Emmons
Antonio Ferri
Alexander Flax
R. Paul Harrington
R. T. Jones
Carl Kaplan
H. W. Liepmann
C. C. Lin
H. F. Ludloff
Harold Luskin
John R. Markham
Carl B. Millikan
Shatswell Ober
W. Bailey Oswald
Allen E. Puckett
Elliott G. Reid
H. J. E. Reid
Russell Robinson
G. B. Schubauer
W. R. Sears
John Stack
Theodore von Kármán
Richard von Mises

Air Transport

Charles Froesch
J. A. Herlihy
R. D. Kelly
Otto E. Kirchner
Jerome Lederer
John C. Leslie
R. Dixon Speas

Flight Testing

W. K. Ebel
R. R. Gilruth
Melvin N. Gough
E. G. Stout

Structures and Materials

W. B. Bleakney
E. W. Conlon
L. H. Donnell
E. C. Hartmann
N. J. Hoff
Samuel Levy
E. E. Lundquist
Alfred S. Niles
W. Ramberg
E. Reissner
F. R. Shanley
H. W. Sibert
C. R. Strang
S. Timoshenko
H. S. Tsien
Chi-Teh Wang

Rotating Wing Aircraft

F. B. Gustafson
K. H. Hohenemser
Bartram Kelley
R. B. Maloy
Ralph McClarren
R. H. Miller
R. H. Prewitt
Igor I. Sikorsky

Vibration and Flutter

Lee Arnold
M. A. Biot
R. L. Bisplinghoff
William Bollay
Chieh-Chien Chang
I. E. Garrick
Martin Goland
J. P. Den Hartog

Aircraft Design

W. E. Beall
W. K. Ebel
Hall L. Hibbard
Richard Hutton
C. L. Johnson
A. A. Kartveli
C. J. McCarthy
Fred E. Weick
Robert J. Woods

Electronics in Aviation

K. C. Black
E. F. Herzog
David S. Little
D. K. Martin
George Rappaport
Paul Rosenberg
L. M. Sherer

Physiologic Problems

H. G. Armstrong
Louis H. Bauer
Robert J. Benford
Eugene Du Bois
W. Randolph Lovelace, II
Ross A. MacFarland

Fuels and Oils

D. P. Barnard
J. H. Doolittle
Graham Edgar
R. T. Goodwin
S. D. Heron
A. M. Rothrock

Flight Propulsion

George W. Brady
Frank W. Caldwell
L. S. Hobbs
E. E. Johnson
Joseph Keenan
R. P. Kroon
Hans Reissner
Abe Silverstein
C. Fayette Taylor
E. S. Taylor
P. Taylor
E. S. Thompson
H. S. Tsien

Instruments

Allan G. Binnie
J. R. Bradburn
Charles H. Colvin
C. S. Draper
S. G. Eskin
O. E. Esval
H. W. Holzapfel
W. L. Howland
George H. Purcell
C. F. Savage
O. Hugo Schuck
C. L. Seward, Jr.
L. D. Statham
R. C. Sylvander
D. K. Warner

Meteorology

C. F. Brooks
D. M. Little
E. J. Minser
F. W. Reichelderfer
H. C. Willett

SUBSCRIPTION RATES

JOURNAL OF THE AERONAUTICAL SCIENCES, Published Monthly.—United States and Possessions: 1 Year, $12.00; Single Copies, $1.50. Foreign Countries Including Canada (American Currency Rates): 1 Year, $13.00; Single Copies, $1.50.

AERONAUTICAL ENGINEERING REVIEW, Published Monthly.—United States and Possessions: 1 Year, $3.00; Single Copies, $0.50. Foreign Countries Including Canada (American Currency Rates): 1 Year, $3.50; Single Copies, $0.50.

Notices of change of address should be sent to the Institute at least 30 days prior to actual change of address.

Manuscripts for publication, proofs, and all correspondence should be addressed to the Editorial Office of the JOURNAL.

Correspondence regarding subscriptions may be addressed to Publication Office, 20th and Northampton Sts., Easton, Pa., or to the Editorial Office of the JOURNAL OF THE AERONAUTICAL SCIENCES, 2 East 64th Street, New York 21, New York.

Copyright, 1953, by the Institute of the Aeronautical Sciences, Inc.

Entered as Second Class Matter at the Post Office, Easton, Pa., May 1, 1937. Acceptance for mailing at a special rate of Postage provided for in the Act of August 24, 1912. Authorized April 29, 1937.

JOURNAL OF THE AERONAUTICAL SCIENCES

VOLUME 20 MARCH, 1953 NUMBER 3

Aerodynamic Coefficients of an Oscillating Airfoil with Control Surface in Two-Dimensional Subsonic Flow*

A. I. VAN DE VOOREN†

National Aeronautical Research Institute, Holland

SUMMARY

The method of reference 1, yielding a direct solution in terms of known functions for the aerodynamic forces acting on an oscillating wing in two-dimensional subsonic flow, is extended to the case of an airfoil with a control surface hinging about its leading edge. Hinge moment coefficients are calculated for translation and rotation of the whole airfoil, while, for rotation of the control surface lift, pitching moment and hinge moment coefficients are presented. Results are given for Mach Numbers $\beta = 0.35$, 0.5, 0.6, 0.7, and 0.8; for chord ratios $\tau = 0.1$, 0.2, and 0.3; and for a number of ω values smaller than 1.0.

LIST OF SYMBOLS

x, y = rectangular coordinates measured from the mid-chord point of the airfoil (x = chordwise coordinate)
$X = x/\sqrt{1-\beta^2}$
$Y = y$
l = semichord
τ = ratio of control surface chord to total chord
v = air speed
c = speed of sound
β = Mach Number, v/c
ν = frequency
ω = reduced frequency, $\nu l/v$
$\Omega = \omega/(1-\beta^2)$
φ = acceleration potential
ρ_0 = density of the undisturbed airflow
ξ, η = elliptic coordinates (see reference 1)
A = amplitude of translation (positive if downward)
B = amplitude of wing rotation about mid-chord (positive if trailing edge downward)
C = amplitude of control surface rotation (positive in the same sense as B)
K = total force on airfoil (positive if downward)
M = total moment about mid-chord point (positive if tail heavy)
N = control surface moment about hinge axis (positive if tail heavy)

Received September 9, 1952.

* This investigation was sponsored by the Netherlands Aircraft Development Board.

† Chief, Section for Flutter and Theoretical Aerodynamics.

INTRODUCTION

IT HAS BEEN DESCRIBED in reference 1 how exact formulas for the aerodynamic force and moment acting on an oscillating wing in two-dimensional subsonic compressible flow can be derived. These expressions are obtained from the analytical method, originally developed by Timman,[2] which solves the boundary-value problem of the time-free wave equation with pertaining boundary conditions and conditions of regularity. Complete analytical solutions in terms of Mathieu and modified Mathieu functions, applying to a plain wing and to a wing with an aerodynamically balanced control surface, have been elaborated by Timman in collaboration with the present author.[3] The numerical computations based on this theory have been performed by the Computation Department of the Mathematical Centre at Amsterdam under the direction of van Wijngaarden and with the assistance first of Scheen and later of Berghuis.

Since the coefficients for a plain wing have already been published, this paper contains only those coefficients that are introduced by the addition of a control surface. All tabulated values should be accurate up to one unit in the last decimal supplied.

To facilitate use in flutter calculations for tapered wings (strip theory), all coefficients are now being interpolated to Ω in the range $0 < \Omega < 1.0$ with an interval of $\Omega = 0.02$. Tabulated results can be applied for at the National Aeronautical Research Institute.

TABLE 1

$\tau = 0.1$

β	ω	n_a'	n_a''	n_b'	n_b''	k_c'	k_c''	m_c'	m_c''	n_c'	n_c''
0.35	0	0	0	−0.00234	0	−0.84509	0	+0.05556	0	−0.00601	0
	0.12536	0.00001	−0.00023	−0.00183	−0.00065	−0.65365	+0.15858	−0.04170	−0.09195	−0.00581	−0.00020
	0.25071	0.00017	−0.00040	−0.00152	−0.00172	−0.55870	0.15036	−0.09141	−0.09898	−0.00571	−0.00059
	0.37607	0.00048	−0.00055	−0.00126	−0.00282	−0.51007	0.12723	−0.11821	−0.09794	−0.00566	−0.00098
	0.50143	0.00095	−0.00071	−0.00100	−0.00393	−0.48302	0.10484	−0.13454	−0.09691	−0.00564	−0.00137
	0.62679	0.00158	−0.00089	−0.00072	−0.00506	−0.46736	0.08543	−0.14557	−0.09706	−0.00562	−0.00176
	0.75214	0.00236	−0.00108	−0.00040	−0.00619	−0.45840	0.06898	−0.15367	−0.09838	−0.00561	−0.00215
	1.00286	0.00441	−0.00155	+0.00034	−0.00854	−0.45186	+0.04365	−0.16552	−0.10378	−0.00561	−0.00291
0.5	0	0	0	−0.00254	0	−0.91410	0	+0.06009	0	−0.00650	0
	0.15	0.00004	−0.00028	−0.00185	−0.00092	−0.64356	+0.19948	−0.08045	−0.11401	−0.00623	−0.00030
	0.3	0.00031	−0.00049	−0.00150	−0.00234	−0.53583	0.18172	−0.14121	−0.11418	−0.00615	−0.00080
	0.45	0.00081	−0.00071	−0.00120	−0.00380	−0.48749	0.15824	−0.17301	−0.10915	−0.00613	−0.00131
	0.6	0.00157	−0.00095	−0.00090	−0.00529	−0.46279	0.14144	−0.19388	−0.10542	−0.00614	−0.00180
	0.75	0.00258	−0.00126	−0.00059	−0.00682	−0.44894	0.13153	−0.21003	−0.10287	−0.00617	−0.00229
	0.9	0.00385	−0.00166	−0.00027	−0.00840	−0.44007	0.12760	−0.22407	−0.10073	−0.00621	−0.00277
	1.125	0.00622	−0.00253	+0.00014	−0.01085	−0.42891	+0.13085	−0.24331	−0.09664	−0.00629	−0.00347
0.6	0	0	0	−0.00275	0	−0.98955	0	+0.06505	0	−0.00704	0
	0.10667	0.00001	−0.00022	−0.00209	−0.00057	−0.71759	+0.23409	−0.07740	−0.12731	−0.00678	−0.00017
	0.21333	0.00013	−0.00039	−0.00177	−0.00165	−0.58651	0.23443	−0.15122	−0.13065	−0.00668	−0.00056
	0.32	0.00039	−0.00055	−0.00155	−0.00277	−0.51921	0.21711	−0.19313	−0.12193	−0.00666	−0.00095
	0.42667	0.00080	−0.00073	−0.00135	−0.00391	−0.48003	0.20215	−0.22102	−0.11190	−0.00667	−0.00133
	0.53333	0.00132	−0.00093	−0.00117	−0.00507	−0.45455	0.19224	−0.24191	−0.10189	−0.00670	−0.00170
	0.64	0.00199	−0.00117	−0.00099	−0.00627	−0.43548	0.18713	−0.25898	−0.09164	−0.00674	−0.00207
	0.8	0.00325	−0.00164	−0.00078	−0.00811	−0.41268	0.18662	−0.27921	−0.07479	−0.00682	−0.00259
	0.96	0.00479	−0.00232	−0.00067	−0.00997	−0.38894	0.19109	−0.29429	−0.05502	−0.00692	−0.00310
	1.17333	0.00720	−0.00365	−0.00069	−0.01235	−0.35103	+0.19676	−0.30433	−0.02436	−0.00703	−0.00377
0.7	0	0	0	−0.00308	0	−1.10851	0	+0.07288	0	−0.00788	0
	0.10929	0.00001	−0.00024	−0.00223	−0.00066	−0.73275	+0.29143	−0.12818	−0.15236	−0.00755	−0.00020
	0.21857	0.00017	−0.00043	−0.00190	−0.00194	−0.57016	0.28654	−0.22380	−0.14091	−0.00747	−0.00065
	0.36429	0.00063	−0.00069	−0.00162	−0.00370	−0.47363	0.25810	−0.28697	−0.10383	−0.00751	−0.00124
	0.54643	0.00159	−0.00113	−0.00140	−0.00597	−0.41017	0.24014	−0.32656	−0.05207	−0.00763	−0.00191
	0.65571	0.00237	−0.00148	−0.00136	−0.00737	−0.38084	0.23633	−0.33649	−0.01889	−0.00773	−0.00227
	0.80143	0.00362	−0.00213	−0.00143	−0.00922	−0.34188	0.23271	−0.33381	+0.02523	−0.00784	−0.00274
	0.94714	0.00503	−0.00300	−0.00162	−0.01094	−0.30271	0.22438	−0.31322	0.06291	−0.00792	−0.00321
	1.16571	0.00729	−0.00472	−0.00197	−0.01312	−0.25259	+0.19686	−0.25977	+0.09216	−0.00800	−0.00403
0.8	0	0	0	−0.00366	0	−1.31939	0	+0.08674	0	−0.00938	0
	0.1125	0.00001	−0.00028	−0.00248	−0.00086	−0.71938	+0.39230	−0.24294	−0.18395	−0.00892	−0.00026
	0.225	0.00024	−0.00051	−0.00215	−0.00248	−0.52142	0.34642	−0.36008	−0.11046	−0.00892	−0.00082
	0.3375	0.00065	−0.00078	−0.00201	−0.00414	−0.43373	0.30719	−0.40055	−0.02508	−0.00906	−0.00130
	0.495	0.00153	−0.00128	−0.00204	−0.00649	−0.36257	0.28120	−0.38072	+0.08257	−0.00927	−0.00183
	0.585	0.00216	−0.00167	−0.00221	−0.00779	−0.32719	0.27333	−0.33949	0.12324	−0.00934	−0.00209
	0.72	0.00321	−0.00241	−0.00257	−0.00953	−0.27469	0.25876	−0.26406	0.13806	−0.00934	−0.00254
	0.9	0.00477	−0.00360	−0.00292	−0.01147	−0.21205	+0.22517	−0.20289	+0.09108	−0.00920	−0.00347

TABLE 2

$\tau = 0.2$

β	ω	n_a'	n_a''	n_b'	n_b''	k_c'	k_c''	m_c'	m_c''	n_c'	n_c''
0.35	0	0	0	−0.01357	0	−1.17388	0	+0.15199	0	−0.02509	0
	0.12536	0.00007	−0.00133	−0.01061	−0.00346	−0.91276	+0.19475	+0.01953	−0.13148	−0.02346	−0.00160
	0.25071	0.00092	−0.00231	−0.00889	−0.00933	−0.78542	0.16310	−0.04661	−0.14786	−0.02265	−0.00459
	0.37607	0.00264	−0.00322	−0.00756	−0.01541	−0.72135	0.11213	−0.08119	−0.15400	−0.02218	−0.00768
	0.50143	0.00522	−0.00416	−0.00626	−0.02156	−0.68667	0.06243	−0.10131	−0.16059	−0.02185	−0.01076
	0.62679	0.00866	−0.00517	−0.00487	−0.02776	−0.66750	+0.01667	−0.11405	−0.16912	−0.02158	−0.01383
	0.75214	0.01296	−0.00630	−0.00334	−0.03405	−0.65763	−0.02532	−0.12265	−0.17958	−0.02133	−0.01688
	1.00286	0.02425	−0.00912	+0.00010	−0.04699	−0.65493	−0.10000	−0.13326	−0.20530	−0.02083	−0.02296
0.5	0	0	0	−0.01468	0	−1.26975	0	+0.16441	0	−0.02714	0
	0.15	0.00017	−0.00162	−0.01073	−0.00488	−0.90220	+0.24526	−0.02645	−0.16601	−0.02498	−0.00230
	0.3	0.00163	−0.00283	−0.00886	−0.01271	−0.76074	0.19710	−0.10660	−0.17876	−0.02423	−0.00627
	0.45	0.00444	−0.00410	−0.00744	−0.02076	−0.70098	0.14253	−0.14747	−0.18610	−0.02396	−0.01025
	0.6	0.00858	−0.00558	−0.00609	−0.02899	−0.67478	0.09741	−0.17382	−0.19644	−0.02389	−0.01416
	0.75	0.01411	−0.00742	−0.00477	−0.03747	−0.66527	0.06202	−0.19445	−0.20965	−0.02394	−0.01801
	0.9	0.02105	−0.00983	−0.00358	−0.04622	−0.66514	0.03566	−0.21314	−0.22468	−0.02406	−0.02180
	1.125	0.03405	−0.01509	−0.00233	−0.05973	−0.67304	+0.01190	−0.24165	−0.24813	−0.02435	−0.02734
0.6	0	0	0	−0.01590	0	−1.37454	0	+0.17798	0	−0.02938	0
	0.10667	0.00000	−0.00129	−0.01213	−0.00291	−1.00469	+0.29918	−0.01590	−0.18375	−0.02728	−0.00128
	0.21333	0.00069	−0.00225	−0.01035	−0.00886	−0.83110	0.28202	−0.11461	−0.20019	−0.02648	−0.00430
	0.32	0.00212	−0.00321	−0.00924	−0.01503	−0.74521	0.24259	−0.17038	−0.20179	−0.02621	−0.00738
	0.42667	0.00428	−0.00424	−0.00837	−0.02132	−0.69846	0.20736	−0.20800	−0.20278	−0.02621	−0.01039
	0.53333	0.00719	−0.00545	−0.00763	−0.02774	−0.67148	0.17970	−0.23731	−0.20470	−0.02636	−0.01333
	0.64	0.01083	−0.00691	−0.00706	−0.03432	−0.65478	0.15968	−0.26293	−0.20714	−0.02661	−0.01619
	0.8	0.01768	−0.00984	−0.00661	−0.04446	−0.64035	0.14162	−0.29773	−0.20935	−0.02714	−0.02031
	0.96	0.02604	−0.01401	−0.00691	−0.05468	−0.62767	0.13581	−0.33075	−0.20729	−0.02776	−0.02420
	1.17333	0.03892	−0.02215	−0.00859	−0.06770	−0.60196	+0.14124	−0.36994	−0.19487	−0.02853	−0.02900

(Table 2 concluded on facing page)

TABLE 2 (*Concluded*)

$\tau = 0.2$

β	ω	n_a'	n_a''	n_b'	n_b''	k_c'	k_c''	m_c'	m_c''	n_c'	n_c''
0.7	0	0	0	−0.01781	0	−1.53979	0	+0.19937	0	−0.03291	0
	0.10929	0.00001	−0.00141	−0.01296	−0.00337	−1.02627	+0.38387	−0.07622	−0.22769	−0.03022	−0.00148
	0.21857	0.00087	−0.00250	−0.01117	−0.01040	−0.81591	0.35330	−0.20376	−0.22813	−0.02953	−0.00504
	0.36429	0.00335	−0.00406	−0.00998	−0.02004	−0.69501	0.29674	−0.29421	−0.20713	−0.02970	−0.00961
	0.54643	0.00856	−0.00668	−0.00953	−0.03253	−0.62506	0.25392	−0.36481	−0.17390	−0.03061	−0.01481
	0.65571	0.01276	−0.00889	−0.00992	−0.04019	−0.59628	0.24081	−0.39506	−0.14836	−0.03134	−0.01762
	0.80143	0.01938	−0.01292	−0.01140	−0.05018	−0.55894	0.23085	−0.42063	−0.10686	−0.03232	−0.02098
	0.94714	0.02673	−0.01838	−0.01381	−0.05935	−0.51803	0.22050	−0.42531	−0.06122	−0.03310	−0.02401
	1.16571	0.03813	−0.02906	−0.01794	−0.07069	−0.45669	+0.18922	−0.39204	−0.00554	−0.03364	−0.02844
0.8	0	0	0	−0.02119	0	−1.83272	0	+0.23730	0	−0.03917	0
	0.1125	0.00004	−0.00162	−0.01437	−0.00436	−1.02022	+0.51461	−0.21281	−0.28293	−0.03543	−0.00195
	0.225	0.00119	−0.00296	−0.01277	−0.01322	−0.75804	0.44108	−0.38230	−0.22049	−0.03533	−0.00629
	0.3375	0.00338	−0.00455	−0.01247	−0.02222	−0.64412	0.37695	−0.46206	−0.13816	−0.03629	−0.01002
	0.495	0.00800	−0.00769	−0.01386	−0.03493	−0.55952	0.32591	−0.48864	−0.01550	−0.03819	−0.01395
	0.585	0.01125	−0.01017	−0.01567	−0.04177	−0.52173	0.30925	−0.46383	+0.04502	−0.03907	−0.01560
	0.72	0.01651	−0.01484	−0.01921	−0.05067	−0.46675	0.28732	−0.38877	0.09445	−0.03964	−0.01778
	0.9	0.02390	−0.02231	−0.02341	−0.06007	−0.39880	0.25137	−0.28985	+0.06636	−0.03937	−0.02150

TABLE 3

$\tau = 0.3$

β	ω	n_a'	n_a''	n_b'	n_b''	k_c'	k_c''	m_c'	m_c''	n_c'	n_c''
0.35	0	0	0	−0.03837	0	−1.41072	0	+0.26935	0	−0.05905	0
	0.12536	0.00013	−0.00376	−0.03005	−0.00887	−1.10235	+0.20347	+0.11341	−0.15912	−0.05355	−0.00527
	0.25071	0.00236	−0.00653	−0.02541	−0.02459	−0.95413	0.14124	+0.03775	−0.18334	−0.05068	−0.01515
	0.37607	0.00695	−0.00911	−0.02202	−0.04092	−0.88017	+0.05735	−0.00004	−0.19634	−0.04887	−0.02539
	0.50143	0.01384	−0.01177	−0.01888	−0.05740	−0.84006	−0.02489	−0.02039	−0.21040	−0.04740	−0.03563
	0.62679	0.02304	−0.01466	−0.01564	−0.07405	−0.81785	−0.10268	−0.03155	−0.22717	−0.04601	−0.04586
	0.75214	0.03457	−0.01790	−0.01217	−0.09093	−0.80634	−0.17658	−0.03733	−0.24657	−0.04458	−0.05609
	1.00286	0.06483	−0.02601	−0.00455	−0.12568	−0.80340	−0.31547	−0.03961	−0.29213	−0.04145	−0.07672
0.5	0	0	0	−0.04151	0	−1.52592	0	+0.29135	0	−0.06387	0
	0.15	0.00039	−0.00456	−0.03042	−0.01256	−1.09364	+0.25659	+0.06747	−0.20377	−0.05655	−0.00752
	0.3	0.00423	−0.00802	−0.02553	−0.03354	−0.93220	0.17034	−0.02279	−0.22928	−0.05383	−0.02067
	0.45	0.01168	−0.01163	−0.02222	−0.05509	−0.86719	+0.07787	−0.06627	−0.25033	−0.05254	−0.03391
	0.6	0.02273	−0.01588	−0.01940	−0.07715	−0.84251	−0.00360	−0.09233	−0.27646	−0.05180	−0.04707
	0.75	0.03747	−0.02124	−0.01699	−0.09988	−0.83928	−0.07379	−0.11149	−0.30767	−0.05137	−0.06018
	0.9	0.05593	−0.02830	−0.01522	−0.12332	−0.84958	−0.13344	−0.12857	−0.34284	−0.05120	−0.07325
	1.125	0.09042	−0.04365	−0.01459	−0.15945	−0.88136	−0.20269	−0.15601	−0.40031	−0.05142	−0.09271
0.6	0	0	0	−0.04494	0	−1.65186	0	+0.31539	0	−0.06914	0
	0.10667	−0.00006	−0.00364	−0.03432	−0.00722	−1.21649	+0.32838	+0.08740	−0.22502	−0.06206	−0.00410
	0.21333	+0.00171	−0.00637	−0.02954	−0.02307	−1.01721	0.28630	−0.02584	−0.25472	−0.05922	−0.01406
	0.32	0.00549	−0.00907	−0.02685	−0.03959	−0.92204	0.22007	−0.08836	−0.26894	−0.05812	−0.02426
	0.42667	0.01121	−0.01204	−0.02503	−0.05639	−0.87349	0.15956	−0.12696	−0.28395	−0.05783	−0.03437
	0.53333	0.01889	−0.01555	−0.02381	−0.07355	−0.84931	0.10845	−0.16249	−0.30150	−0.05803	−0.04432
	0.64	0.02853	−0.01986	−0.02326	−0.09110	−0.83897	0.06709	−0.19162	−0.32104	−0.05860	−0.05409
	0.8	0.04658	−0.02846	−0.02395	−0.11810	−0.83911	+0.02074	−0.23409	−0.35065	−0.06009	−0.06842
	0.96	0.06847	−0.04074	−0.02716	−0.14516	−0.84575	−0.00628	−0.27930	−0.37705	−0.06217	−0.08213
	1.17333	+0.10173	−0.06462	−0.03564	−0.17920	−0.85158	−0.01722	−0.34237	−0.39907	−0.06549	−0.09907
0.7	0	0	0	−0.05034	0	−1.85045	0	+0.35332	0	−0.07746	0
	0.10929	−0.00005	−0.00399	−0.03665	−0.00828	−1.24729	+0.42663	+0.02943	−0.28288	−0.06831	−0.00468
	0.21857	+0.00214	−0.00705	−0.03194	−0.02697	−1.00777	0.37007	−0.11794	−0.30200	−0.06583	−0.01639
	0.36429	0.00863	−0.01154	−0.02958	−0.05264	−0.87695	0.28028	−0.22457	−0.30679	−0.06600	−0.03169
	0.54643	0.02226	−0.01923	−0.03036	−0.08576	−0.81218	0.20454	−0.31771	−0.30843	−0.06879	−0.04954
	0.65571	0.03314	−0.02578	−0.03310	−0.10588	−0.79120	0.17705	−0.36627	−0.30253	−0.07136	−0.05937
	0.80143	0.05004	−0.03772	−0.03982	−0.13181	−0.76605	0.15520	−0.42239	−0.28111	−0.07528	−0.07118
	0.94714	0.06837	−0.05383	−0.04955	−0.15499	−0.73444	0.14076	−0.46148	−0.24396	−0.07904	−0.08145
	1.16571	+0.09558	−0.08492	−0.06588	−0.18221	−0.67419	+0.10929	−0.47221	−0.17612	−0.08289	−0.09508
0.8	0	0	0	−0.05992	0	−2.20248	0	+0.42053	0	−0.09219	0
	0.1125	0.00000	−0.00454	−0.04063	−0.01057	−1.25037	+0.58131	−0.10929	−0.36417	−0.07941	−0.00604
	0.225	0.00290	−0.00836	−0.03679	−0.03403	−0.95069	0.48003	−0.31453	−0.32939	−0.07865	−0.02038
	0.3375	0.00850	−0.01296	−0.03724	−0.05770	−0.82328	0.39118	−0.42820	−0.27136	−0.08155	−0.03312
	0.495	0.02014	−0.02221	−0.04389	−0.09050	−0.73610	0.31207	−0.51120	−0.16492	−0.08831	−0.04720
	0.585	0.02809	−0.02953	−0.05090	−0.10760	−0.70204	0.28443	−0.51795	−0.09807	−0.09227	−0.05299
	0.72	0.04041	−0.04323	−0.06381	−0.12870	−0.65273	0.25122	−0.47347	−0.01874	−0.09629	−0.05965
	0.9	0.05658	−0.06476	−0.07950	−0.14894	−0.59148	+0.20789	−0.36517	−0.00342	−0.09758	−0.06863

The graphs and tables in this paper will be accompanied by a short review of the complications introduced by the control surface.

THE SINGULARITY AT THE LEADING EDGE OF THE CONTROL SURFACE

As has been shown in reference 1, the problem is to determine a function u related to the acceleration potential φ by the formula

$$u(X, Y) = \varphi(X\sqrt{1-\beta^2}, Y)\exp(-i\nu\beta X/c\sqrt{1-\beta^2})$$

which satisfies the time-free wave equation with corresponding boundary conditions and conditions of regularity. Besides the usual singularity at the leading edge of the airfoil, there exists in the case of a control surface a second singularity, which is logarithmical for

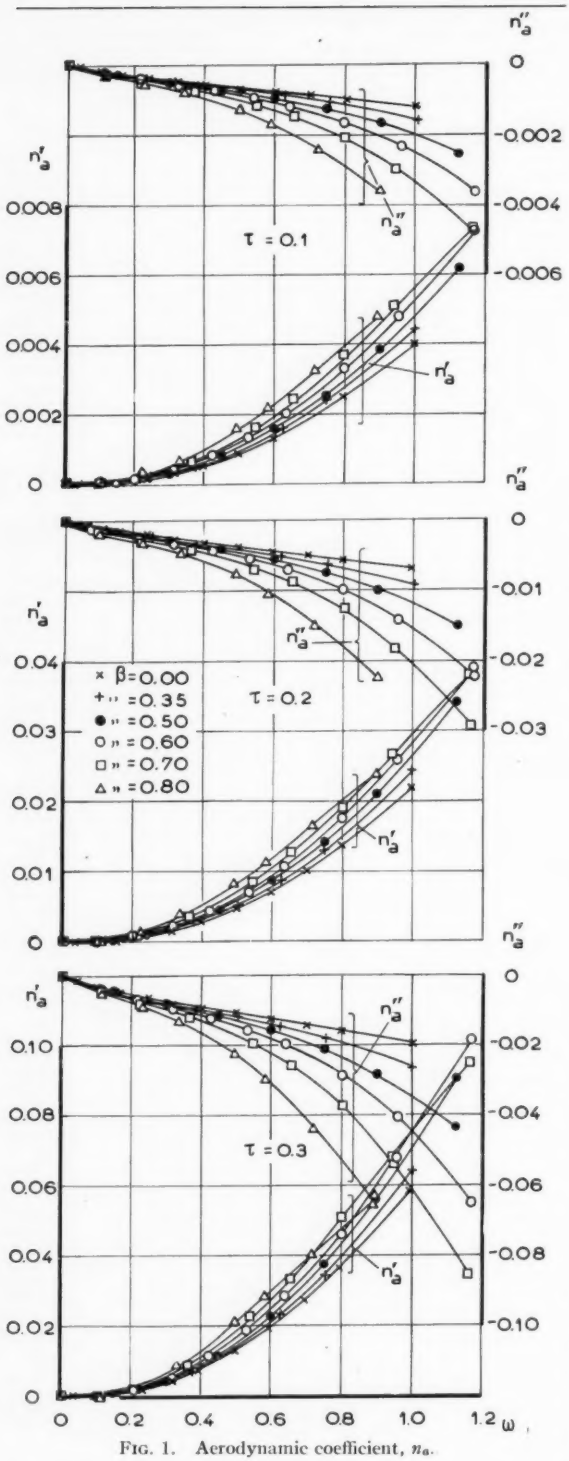

FIG. 1. Aerodynamic coefficient, n_a.

linearized flow, at the leading edge of the control surface.

The corresponding singular part in u can be obtained from the function

$$f(\xi, \eta) = \log\left[\frac{\cosh \xi - \cos(\eta + \eta_1)}{\cosh \xi - \cos(\eta - \eta_1)}\right]$$

representing the acceleration potential of the steady flow about an airfoil with zero angle of incidence and a control surface with an infinitely small angle of deflection. In the same way as for the singularity at the leading edge, correction terms must be added to obtain a solution of the wave equation. The result is

$$u(\xi, \eta) = v^2 \left\{\log\left[\frac{\cosh \xi - \cos(\eta + \eta_1)}{\cosh \xi - \cos(\eta - \eta_1)}\right] - 4\sum_{n=1}^{\infty}\left[se_n(\eta_1)\frac{Ne_n^{(2)}(\xi)}{Ne_n^{(2)\prime}(0)} + \sum_{m=1}^{\infty} B_m^{(n)}\frac{e^{-m\xi}\sin m\eta_1}{m}\right] se_n^{(\eta)}\right\}$$

The factor by which this singular potential enters into the expression for the resulting potential is obtained by identifying the vertical velocity of the flow in an arbitrary point of the control surface as calculated from the resulting potential with its prescribed value. Obviously, the factor is proportional to the discontinuity in the prescribed normal velocity at the leading edge of the control surface. From the complete function $u(\xi, \eta)$ the acceleration potential and the pressure distribution follow, and the aerodynamic forces and moments can then be obtained by appropriate integrations.

NUMERICAL CALCULATIONS

The complex dimensionless derivatives k_c, m_c, n_a, n_b, and n_c defined by

$$K = \pi\rho_0 l^2 v^2 e^{i\nu t}(Ak_a + Bk_b + Ck_c)$$
$$M = \pi\rho_0 l^2 v^2 e^{i\nu t}(Am_a + Bm_b + Cm_c)$$
$$N = \pi\rho_0 l^2 v^2 e^{i\nu t}(An_a + Bn_b + Cn_c)$$

were calculated for the same β and ω values for which in reference 1 the coefficients k_a, k_b, m_a, and m_b have been given, with the exception of ω values larger than 1, which were omitted in the calculations referring to a wing with control surface. Three values were given to the chord ratio; viz., 0.1, 0.2, and 0.3.

As new basic functions the incomplete Bessel functions,

$$R_n(\beta^2\Omega, \eta_1) = \int_0^{\eta_1} e^{i\beta^2\Omega\cos\eta}\cos n\eta\, d\eta$$

appeared in the calculations for the control surface system. The method of computation was by expanding $e^{i\beta^2\Omega\cos\eta}$ into its Fourier series and performing the integration. This leads to a series of Bessel functions $J_m(\beta^2\Omega)$, $m = 1.2\ldots$, with coefficients depending on η_1. In this way the incomplete Bessel functions were computed[4] in eight decimal places for $n = 0(1)20$, $\cos\eta = 0.3(0.1)0.8$, and for a varying number (47 for $n = 0$ to 1 for $n = 20$) of $\beta^2\Omega$ values between 0 and 4.8.

The resulting values for the aerodynamic derivatives are given in Tables 1–3. Partially, they can be compared with results given by Dietze[5] [$\omega = 0$, (0.02), 0.1,

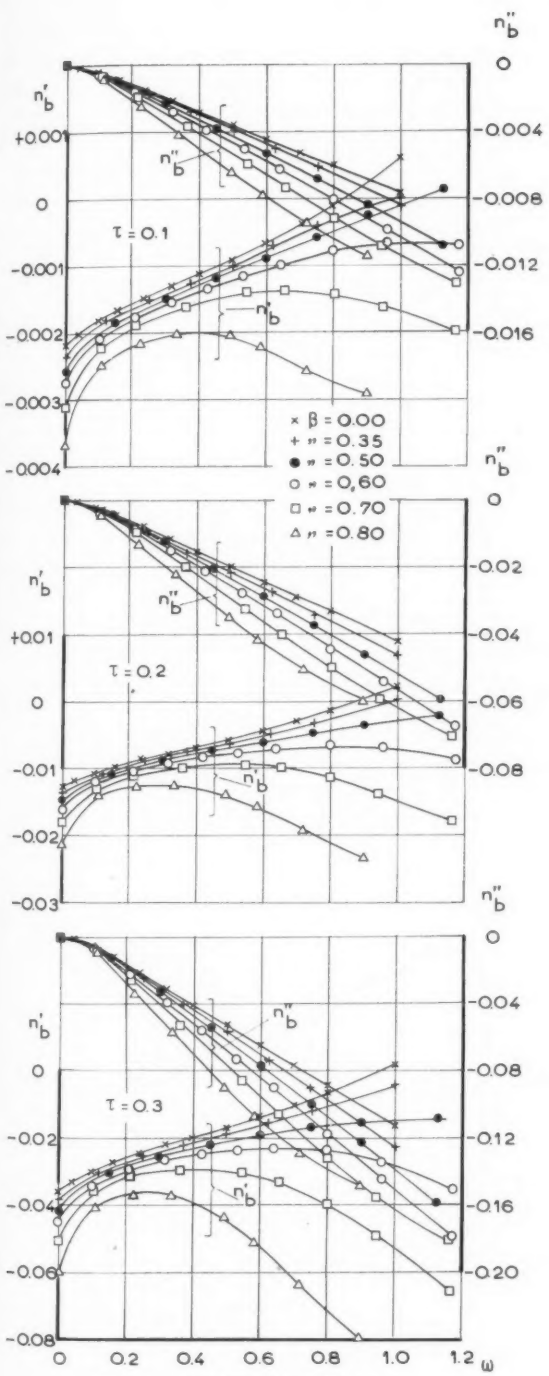

FIG. 2. Aerodynamic coefficient, n_b.

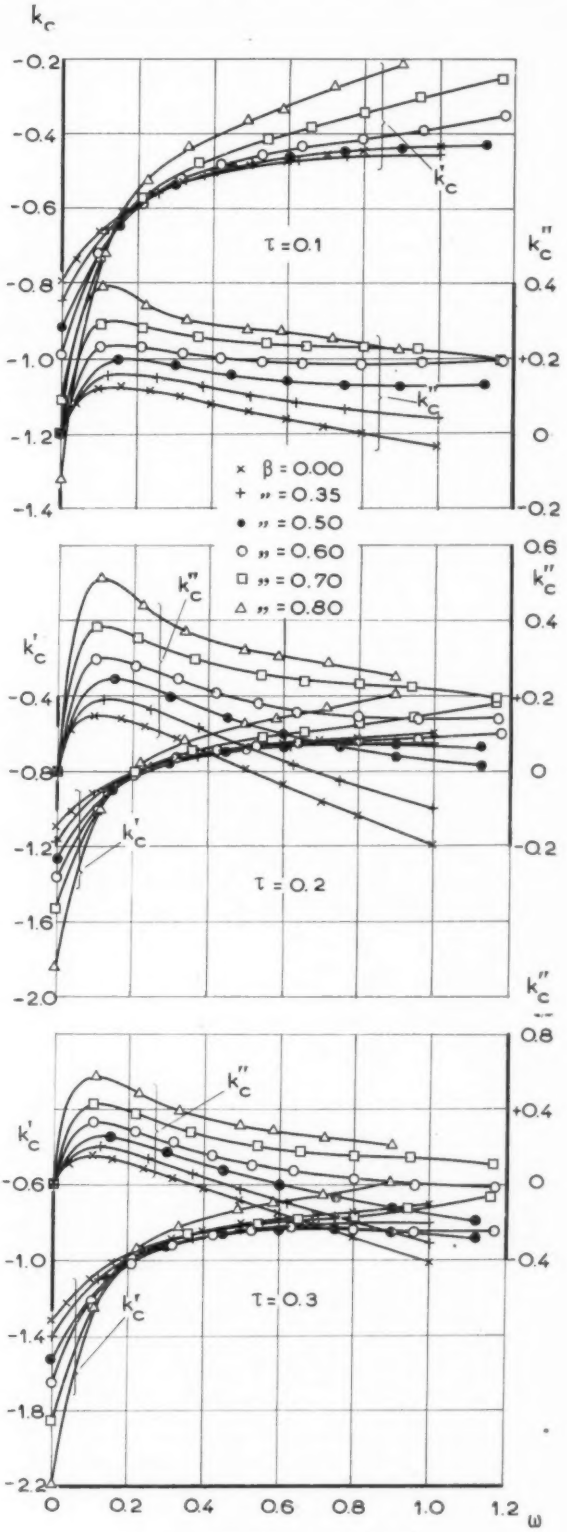

FIG. 3. Aerodynamic coefficient, k_c.

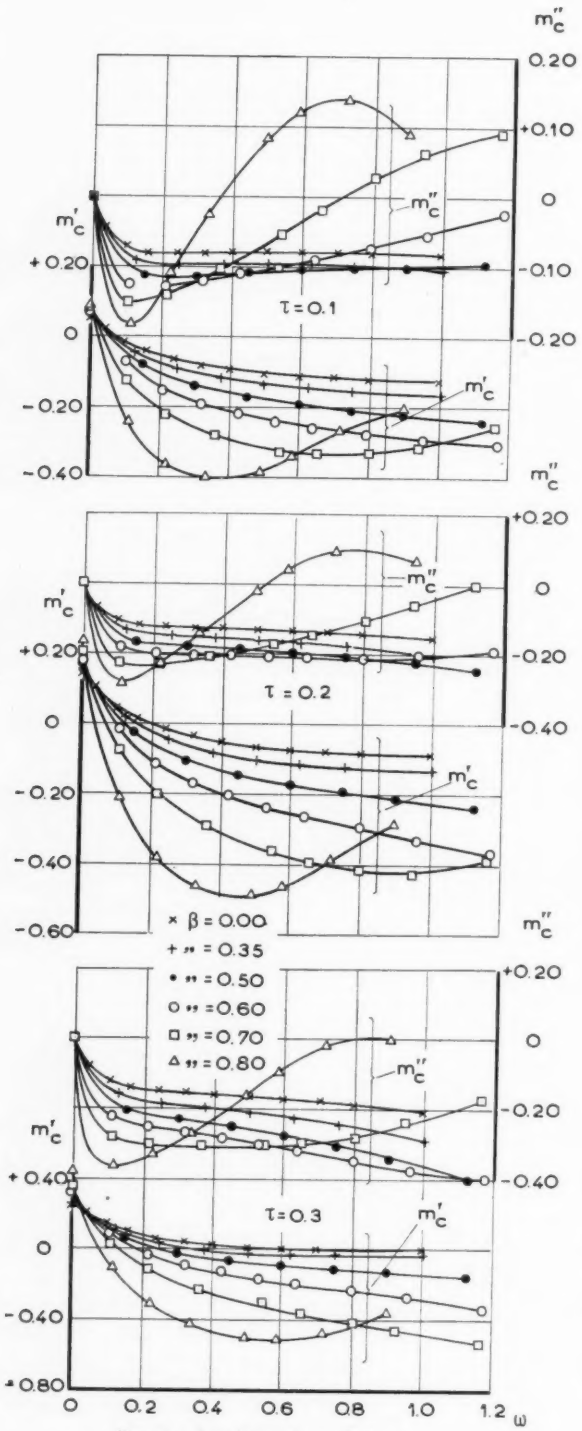

FIG. 4. Aerodynamic coefficient, m_c.

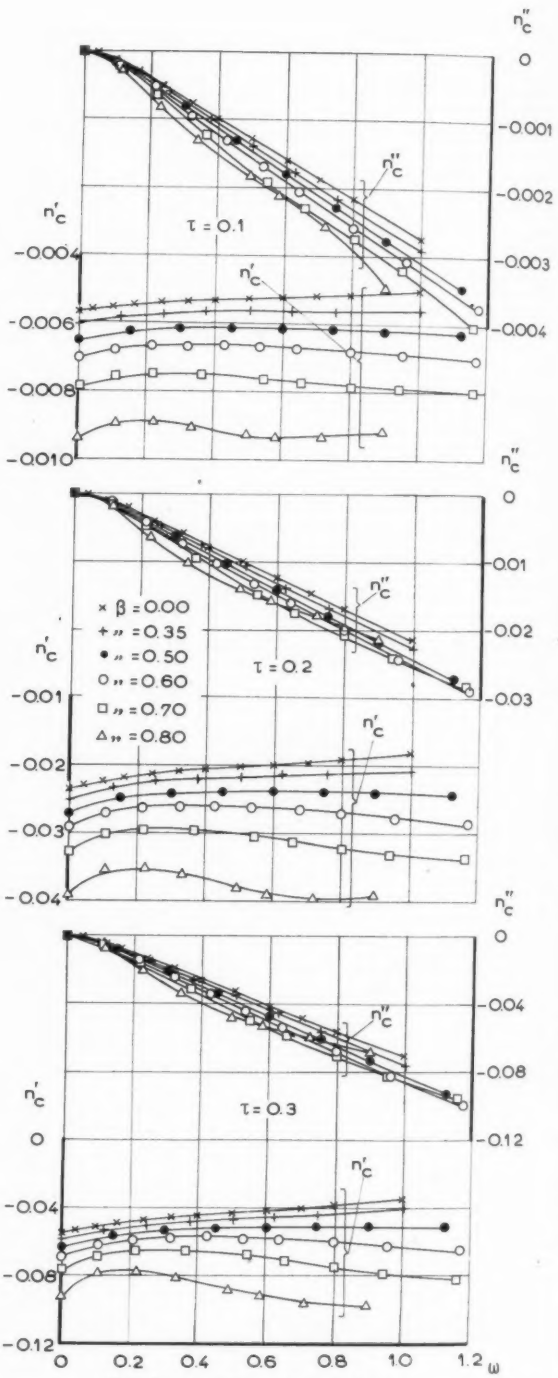

FIG. 5. Aerodynamic coefficient, n_c.

(0.1), 0.7, $\beta = 0.7$, $\tau = 0.15$] and recalculated and extended by Turner and Rabinowitz,[6] using Dietze's method [$\omega = 0$, (0.02), 0.1, (0.1), 0.7, $\beta = 0.7$, $\tau = 0.15$, (0.09), 0.42]. Though an accurate comparison is hampered by the different chord ratios, general agreement is good, the largest discrepancies being 4 per cent in the modulus and 5 deg. in the argument, which occurs in k_c for large values of ω and τ. It may, however, be repeated that the coefficients given in this paper are the more accurate. (See Figs. 1–5.)

REFERENCES

[1] Timman, R., van de Vooren, A. I., and Greidanus, J. H., *Aerodynamic Coefficients of an Oscillating Airfoil in Two-Dimensional Subsonic Flow*, Journal of the Aeronautical Sciences, Vol. 18, No. 12, pp. 797–802, 834, December, 1951.

[2] Timman, R., *Beschouwingen over de luchtkrachten op trillende vliegtuigvleugels*, Thesis Delft, 1946.

[3] Timman, R., and van de Vooren, A. I., *Theory of the Oscillating Wing with Aerodynamically Balanced Control Surface in a Two-Dimensional Subsonic Compressible Flow*, Report F. 54 National Aeronautical Research Institute, Amsterdam, 1949.

[4] Computation Department Mathematical Centre, *The Oscillating Wing in a Subsonic Flow*, Reports R.53, 1949, 1950.

[5] Dietze, F., *Die Luftkräfte des harmonisch schwingenden Flügels im kompressiblen Medium bei Unterschall-geschwindigkeit*, Z.W.B., FB 1733 and 1733/2, 1943, 1944.

[6] Turner, M. J., and Rabinowitz, S., *Aerodynamic Coefficients for an Oscillating Airfoil with Hinged Flap with Tables for a Mach Number of 0.7*, N.A.C.A. T.N. No. 2213, 1950.

Library Facilities of the
Institute of the Aeronautical Sciences

To serve Institute members and others in the aeronautical industry, the Institute of the Aeronautical Sciences offers the facilities of:

The W. A. M. Burden Library
2 East 64th Street
New York 21, N.Y.

The facilities of this library are available for reference study at the Institute.

The Paul Kollsman Lending Library
2 East 64th Street
New York 21, N.Y.

This library loans books without charge to members and others in the United States over eighteen years of age. Full information will be sent on request.

The Pacific Aeronautical Library
7660 Beverly Boulevard
Los Angeles 36, Calif.

This is a service and reference library for West Coast members and organizations. Full information as to its facilities will be sent on request.

On the Pure Rolling Motion of Winged and/or Finned Missiles in Varying Supersonic Flight*

JOHN D. NICOLAIDES† AND RAY E. BOLZ‡

Ballistic Research Laboratories and Case Institute of Technology, Respectively

ABSTRACT

Based on the assumption that the aerodynamic force acting at any point on a lifting surface is linearly dependent upon the local angle of attack at that point and that the aerodynamic coefficients vary in a particular manner with Mach Number, the pure rolling motion of a winged and/or finned missile with large or small variation in flight Mach Number is given.

This refined theory of pure rolling motion and a suggested reduction technique are investigated in the Aerodynamics Range for small changes in Mach Number where it is found that the "fit" of the theory to the observed motion is consistent with the small errors of measurement. The results obtained from the refined theory of motion are compared with those obtained from the standard theory based on constant aerodynamic coefficients, and it is found that for these particular tests the differences are extremely small and may be reconciled by a simple empirical relation.

The aerodynamic coefficients, C_{l_p} and C_{l_δ}, and the effectiveness parameter, $pb/2V$, associated with the pure rolling motion of an arrow-type missile configuration having rectangular, single wedge, 8 per cent thickness fins are determined over a Mach Number range of $1.3 < M < 3.0$. These experimental values are compared with those obtained from previous experiments on the same configuration with 16 per cent thickness fins and with theoretical values as determined by the linearized theory for rectangular fins of 0 per cent thickness. Qualitatively, the results show that the values for the 8 per cent thickness fins lie in between.

The aerodynamic coefficients are also obtained at two Mach Numbers on two additional configurations, wing only and wing plus fins, to indicate the suitability of the Range for a study of wing-fin roll interference. The results indicate that for the two models studied the damping effectiveness of the fins was almost eliminated, being 14 per cent at a Mach Number of 1.95 and 0 per cent at a Mach Number of 1.73.

SYMBOLS

A_P	=	area of fin or wing panel
A, B	=	arbitrary constants depending on boundary conditions
b	=	wing span
C_{1_0}	=	damping constant
C_{2_0}	=	control constant
C_D	=	drag coefficient, drag/qS
C_{l_δ}	=	roll moment derivative due to canted surface, $(\partial C_l/\partial\delta)_{\delta\to 0}$
C_{l_p}	=	roll moment derivative due to rolling velocity, $\lvert\partial C_l/\partial(pb/2V)\rvert_{(pb/2V)\to 0}$
C_l	=	roll moment coefficient, L/qAb
d	=	diameter of body
δL_δ	=	rolling moment due to angle of cant, $(C_{l_\delta}\delta qbA_P n_\delta)$
pL_p	=	rolling moment due to rolling velocity, damping moment, $C_{l_p}(pb/2V)qbA_P n$
I	=	axial moment of inertia, slugs per sq.ft
M	=	Mach Number
m	=	mass, slugs
n_δ	=	number of canted fins
n	=	total number of fins and/or wings
p	=	Rolling velocity, ϕ, rad. per sec.
q	=	$\rho V^2/2$
P.E.	=	probable error
$pb/2V$	=	fin tip helix angle
$p_s b/2V$	=	steady-state fin tip helix angle
S	=	$\pi d^2/4$
s_1	=	steady-state rolling velocity
V	=	linear velocity of missile along trajectory, ft. per sec.
z	=	linear distance along the missile flight trajectory
α, β, λ	=	constants
γ	=	$-\lambda/[1 + (\beta/\alpha M_0)]$
δ	=	angle of cant
ρ	=	free-stream air density, slugs per cu.ft.
ϕ	=	angle of roll
$\psi(\gamma, z)$	=	$\ln(1 + \gamma z)/\gamma z$

Superscripts

Prime mark is the derivative with respect to z, distance along the trajectory.

INTRODUCTION

IN REFFRENCES 1 AND 2, a technique was suggested for determining the aerodynamic coefficients associated with the pure rolling motion of free-flight missiles. This technique was applied to free-flight data obtained in the Aerodynamics Range with the result that the aerodynamic coefficients were determined with good statistical accuracy and were reproducible.

However, the theory of rolling motion employed was derived under the assumption that the aerodynamic coefficients were constant during any one test flight. For the Aerodynamics Range where the observational distance is approximately equal to the significant transient rolling distance for the models employed, the total change in Mach Number was 7 per cent maximum, for which the associated variation of the aerodynamic coefficients from the average value was about 3 per cent.

Therefore, in view of the change of the coefficients associated with the variation in Mach Number both in the Aerodynamics Range and also in full-scale free flight, it is one of the purposes of this paper to present a refined theory of pure rolling motion of free-flight missiles which allows for variation of the aerodynamic coefficients with the varying flight Mach Number. The value of this theory is to: (1) provide a more

Received March 27, 1952.

* The authors wish to acknowledge the contributions of Dr. A. C. Charters to the general program and the assistance of Miss Karolyn Skegas in the reduction of the data.

† Aerodynamicist, Free-Flight Aerodynamics Branch, Exterior Ballistics Laboratory.

‡ Associate Professor of Aeronautical Engineering.

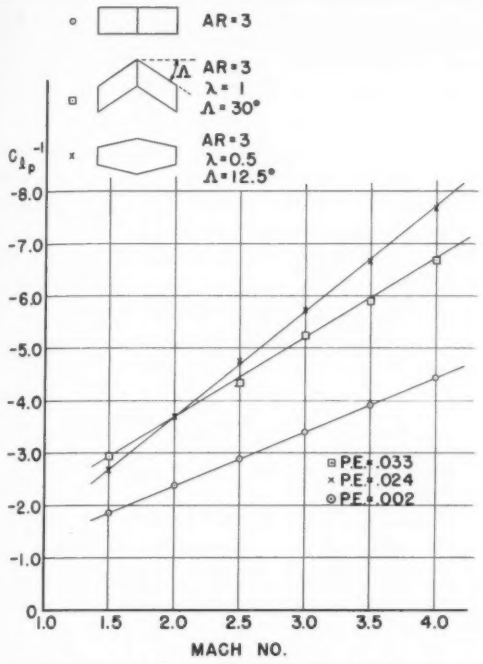

FIG. 1. Variation of $C_{l_p}^{-1}$ with Mach Number for three arbitrarily selected plan forms.

general reduction technique applicable to other test facilities where the change in the coefficients is large, and (2) investigate the association between Mach Number and the values of coefficients as obtained in the Range by the previous theory.

Also in reference 1, the aerodynamic coefficients in roll are presented over a range of test Mach Numbers from 1.7 to 2.6 for missiles with 16 per cent thick fins. As discussed in the reference, the deviation of the experimental results from those calculated from the linearized theory was thought to be primarily a result of the large wing thickness. It is, as a consequence, a second purpose of this paper to present data for identical test configurations except with 8 per cent thick fins, over a range of Mach Numbers from 1.3 to 3.0, in order to evaluate the effect of fin thickness on the aerodynamic coefficients.

Finally, it is the third purpose of this paper to explore in a preliminary fashion the applicability of the test technique to an experimental determination of wing-tail interference phenomena.

Solution of the Roll Equation

The differential equation of motion[1] of a missile in pure roll is given by

$$\phi'' + C_1(z)\phi' = C_2(z) \tag{1}$$

where

$$C_1(z) = \frac{\rho b^3 n A_P}{4I} C_{l_p}(z) - \frac{\rho S}{2m} C_D(z) \tag{1a}$$

$$C_2(z) = \frac{\rho b n_\delta A_P \delta}{2} C_{l_\delta}(z) \tag{1b}$$

ϕ $\equiv$ roll angle

and where the primes refer to derivatives with respect to z, the distance along the trajectory. In reference 1, C_1 and C_2 were taken as constant; here, however, they are functions of the Mach Number, M, because of the variation of the aerodynamic coefficients with M, itself a function only of z.

From Eq. (1), one may observe that, for a constant rolling velocity, $\phi'' = 0$, the ratio C_2/C_1 is a constant and is the steady-state rolling velocity of the missile. As such, it is directly proportional to the steady-state fin tip helix angle, $pb/2V$ [reference 1, Eq. (34*b*)]. For many configurations the value of $pb/2V$ has a small variation with Mach Number (e.g., see Fig. 14 of reference 1) and thus $C_2(z)/C_1(z)$ might be treated as a constant; however, for generality we shall let

$$C_2(z)/C_1(z) = s_1 + s'z \tag{2}$$

where s_1 is the steady-state rolling velocity corresponding to the Mach Number at the beginning of the trajectory.

The solution of Eq. (1) may thus be written in integral form as

$$\phi = B_0 + s_1 z + \frac{s'}{2} z^2 + A_0 \int e^{-\int C_1(z)\,dz} - s' \int e^{-\int C_1(z)\,dz} \int e^{\int C_1(z)\,dz} dz\,dz \tag{3}$$

The variation of $C_1(z)$ from Eq. (1a), neglecting the drag term* is

$$C_1(z) = K_1 C_{l_p}(z) \tag{4}$$

where

$$K_1 = -\rho b^2 n A_P/4I \tag{5}$$

Now $C_{l_p}(z)$ may be expressed with good accuracy both theoretically and experimentally by a linear relation

$$C_{l_p}^{-1} = \alpha M + \beta \tag{6}$$

(α, $\beta \equiv$ constants) for the configuration of reference 1† and many others investigated (e.g., see Figs. 1 and 2).‡

This variation of C_{l_p}, together with a linear variation of $M(z)$, approximating the true variation over relatively small Mach Number ranges, or a variation of $C_D \sim 1/M$ for large Mach Number ranges, yields

$$M = M_0(1 - \lambda z) \tag{7}$$

* The contribution of the drag term to C_1 may be estimated by considering the values in Table 4, reference 1, where it is seen that $[(K_R/m)/C_1]100 = 1.73$ per cent maximum (for Model 6).

† The variation being 2–3 per cent for $1.5 < M < 3.0$ for the configuration of reference 1.

‡ Data from references 6, 7, and 8 were used in preparing Figs. 1 and 2.

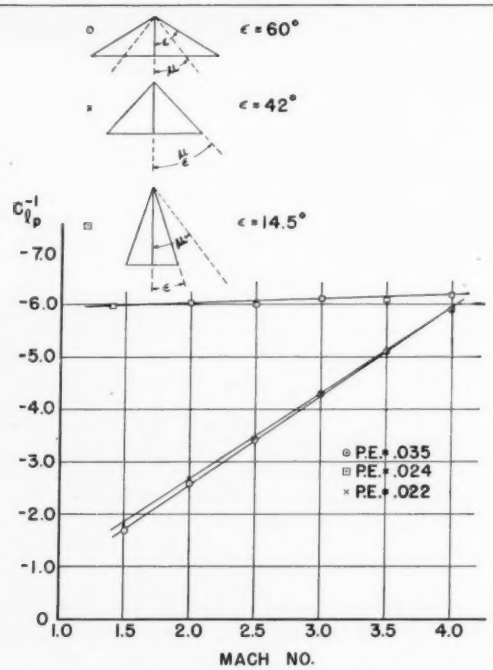

FIG. 2. Variation of $C_{l_p}^{-1}$ with Mach Number for three delta plan forms.

where M_0 = Mach Number at the beginning of the trajectory and λ = constant, when substituted into Eq. (5) yields*

$$C_l(z) = C_{l_0}/(1 + \gamma z) \tag{8}$$

where

$$\left.\begin{aligned} C_{l_0} &= K_1/(\beta + \alpha M_0) \\ \gamma &= -\lambda/[1 + (\beta/\alpha M_0)] \end{aligned}\right\} \tag{9}$$

Now, employing this variation of $C_l(z)$, the refined roll equation becomes

$$\phi = B + \left[s_1 - \frac{s'}{C_{l_0} + \gamma} + \frac{s'}{2}\left(1 - \frac{\gamma}{C_{l_0} + \gamma}\right)z\right]z + Ae^{-\{[(C_{l_0} - \gamma)/\gamma]\ln(1+\gamma z)\}} \tag{10}$$

When $s' = \gamma = 0$, the equation reduces to

$$\phi = B + s_1 z + Ae^{-C_{l_0} z} \tag{11}$$

the relation of the previous paper.[1]

The aerodynamic coefficients are obtained from the constants of the roll equation [Eq. (10)] by

$$C_{l_\delta} = (2I/\rho b A_P n_\delta \delta) s_1 C_{l_0} \tag{12}$$

$$C_{l_\delta} = \frac{4I}{\rho b^2 A_P n}\left(C_{l_0} + \frac{\rho S C_D}{2m}\right) \tag{13}$$

$$\frac{pb}{2V}/\delta = \frac{s_1 b}{2(57.3)\delta}\left[\frac{1}{1 + (\rho S C_D/2mC_{l_0})}\right] \tag{14}$$

* The authors are indebted to R. A. Turetsky, Ballistician, Naval Ordnance Laboratory, for his assistance in the development of the theory and, in particular, for his contributions to the reduction technique.

METHOD OF DATA REDUCTION[9]

The method of data reduction is fundamentally the same as in references 1 and 2. The roll equation [Eq. (10)] is expanded in a Taylor's series about the initial values of the constants, and the higher order terms are neglected. The resultant equation is linear in the differentials of the constants, and thus the method of Least Squares may be applied directly to determine the values of these differential corrections. The corrected initial values of the constants, obtained by adding these differential corrections to the original values of the constants, may in turn be used as initial values, and the process may be repeated until the sum of the squares of the residuals of the fit reaches a minimum.

EXPERIMENTAL TESTS

The purpose of the experimental program may be stated in four parts:

(1) To determine the accuracy and consistency of the refined form of the theoretical roll equation in representing the experimental free-flight data obtained in the Aerodynamics Range (for description see references 1–4).

(2) To compare the results obtained by applying the refined theory and the standard theory to data obtained in the Aerodynamics Range for small variation in flight Mach Number.

(3) To determine the effect of fin thickness on the aerodynamic coefficients over a large range of Mach Numbers and to compare these values with those obtained from linearized theory.

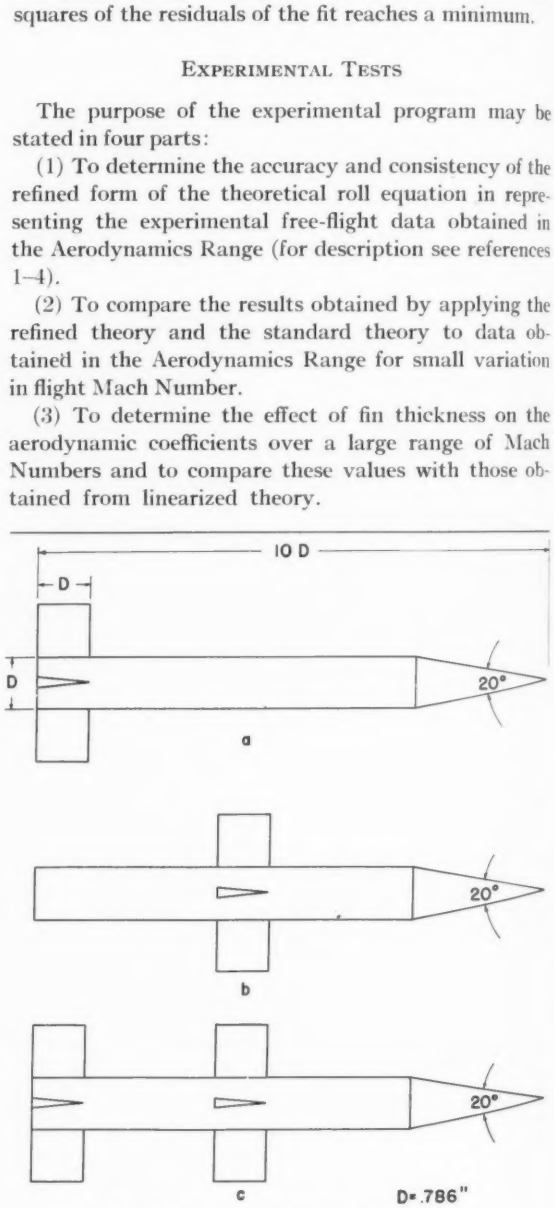

FIG. 3. Configurations of test missiles.

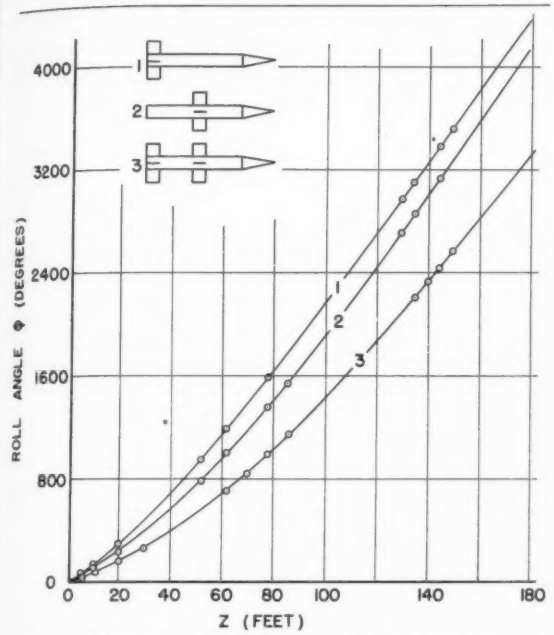

FIG. 4. Measured values of the missiles' roll angles at the Range station locations plotted with the "fitted" theoretical curve of rolling motion.

(4) To investigate the applicability of the Range for experimental studies of wing-fin interference phenomena for rolling missiles.

The basic design of the missile used in the program is identical to that used in the tests of reference 1—namely, a cone-cylinder fuselage ($l/d = 10$) with fixed rectangular-plan-form single-wedge fins and/or wings in cruciform arrangement. The three variations in the basic design are: (1) fin-only models 8 per cent thick at the trailing edge (Fig. 3a); (2) wing-only models 16 per cent thick at trailing edge (Fig. 3b); and (3) wing-fin configuration (Fig. 3c) with 16 per cent thick wings and fins.

RESULTS AND DISCUSSION

Presentation of Results

To illustrate the data obtained from the Range, Fig. 4 presents the angular orientation in roll of three representative tests as measured from the shadowgraphs (Photos 1, 2, and 3) taken at each spark station along the trajectory.

In this same figure are plotted the equations of the curves that best fit the data as obtained by the methods discussed in the previous section. The agreement of the data to within a degree of the fitted curve cannot be shown in the figure because of the insensitivity of the scale. (The difference between the curves should not be interpreted as a result of the variation in the configuration designs only, since the moments of inertia are not identical.)

The "excellent fit" of both roll equations to the experimental points for the various models is given by their probable errors (P.E.), which varied from 0.14° to 0.64° and had an average of 0.41°. Since the probable errors are small and of the same order of magnitude as the estimated error in roll angle measurements, it may be concluded that both roll equations represent

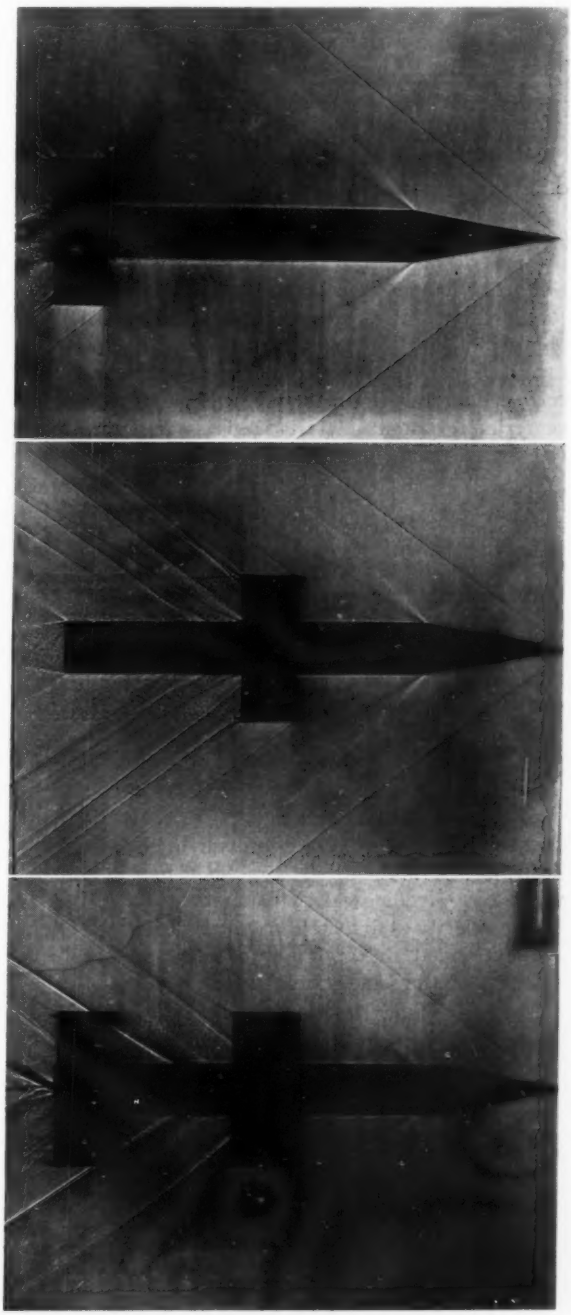

PHOTOS 1, 2, AND 3. Typical shadowgraphs of three types of missiles in free flight showing roll measurement pins and supersonic flow phenomena.

the actual motion of the models tested to within the experimental error. The small P.E.'s also indicate that rolling motion is unaffected by the yawing motion for the mean square yaws encountered in the tests.

Discussion of Results

(*a*) *Comparison of the Two Reduction Techniques.*—For five projectiles, the observed motion was "fitted" and the aerodynamic coefficients were determined both by means of the Standard Reduction Technique of reference 1—assuming the coefficients constant over the Mach Number variation for any given flight—and by means of the Refined Reduction Technique discussed in this paper, which allows for variation of the coefficients. From the values obtained from the two techniques, it was seen (1) that the total change in Mach Number for each of the models is small, (2) that both theories "fit" the experimental data equally well and considerably within the previously estimated measurement accuracy of 0.7°, (3) that the constants and the aerodynamic coefficients are also equally well determined by both theories as indicated by their probable errors, and (4) that a small (from 0.5–2 per cent) but consistent trend toward increasing the values of the coefficients results from the refined technique when the center of the timing data is used as a reference point (see Figs. 5 and 6).

In reference to this last observation it should be noted that the values of the aerodynamic coefficients calculated from the constants of the Refined Technique are those at z_1, the center of the timing data which, for this discussion, may be considered as the center of the observational data; whereas the values of the aerodynamic coefficients obtained from the Standard Technique were arbitrarily associated with z_1 as in reference 1. Since the Refined Technique yields the variation of the aerodynamic coefficients with distance along the trajectory, it is now possible to determine the distance down range at which the values of the coefficients from the Standard Technique occurred. It was found that this distance could be approximated by the following empirical relation: z at $\phi' = (1/2)\ (\phi_L' + \phi_F')$ where ϕ_L' = rolling velocity at last station and ϕ_F' = rolling velocity at first station, which effectively weights the stations at the beginning of the range where the transient motion is most pronounced.

Comparing now the differences between the aerodynamic coefficients obtained from the two reduction techniques and the use of this empirical relation, it is

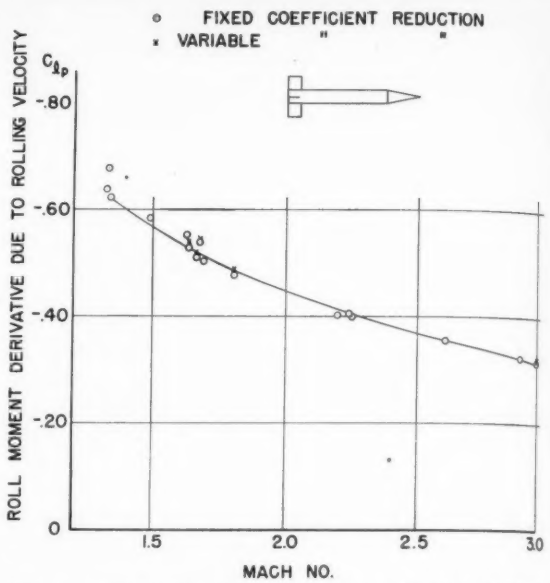

FIG. 5. Experimental values of C_{l_p} as a function of Mach Number plotted with the "Weighted Fit" curve.

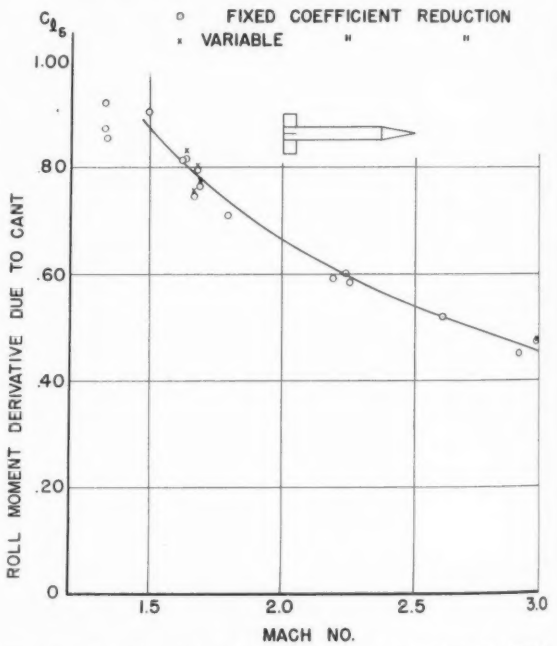

FIG. 6. Experimental values of $C_{l\delta}$ as a function of Mach Number plotted with the "Weighted Fit" curve.

TABLE 1

(A) Round Number	(B) Standard Reduction Values of C_{l_p}	(B) Standard Reduction Values of $C_{l\delta}$	(C) Refined Reduction Values at z^* C_{l_p}	(C) Refined Reduction Values at z^* $C_{l\delta}$	(D) Per Cent Difference in Values (C − B) of C_{l_p}	(D) Per Cent Difference in Values (C − B) of $C_{l\delta}$	(E) Refined Reduction Values at z When $\phi' = (1/2) \times (\phi_F' + \phi_L')$ C_{l_p}	(E) Refined Reduction Values at z When $\phi' = (1/2) \times (\phi_F' + \phi_L')$ $C_{l\delta}$	(F) Per Cent Difference in Values (E − B) of C_{l_μ}	(F) Per Cent Difference in Values (E − B) of $C_{l\delta}$
6	0.530	0.819	0.541	0.834	1.94%	1.88%	0.539	0.817	−0.13%	−0.21%
7	0.511	0.749	0.519	0.760	1.49%	1.49%	0.510	0.748	−0.16%	−0.18%
8	0.541	0.798	0.547	0.806	1.14%	1.10%	0.542	0.798	0.10%	0.04%
9	0.506	0.765	0.515	0.779	1.88%	1.84%	0.507	0.767	0.23%	0.17%

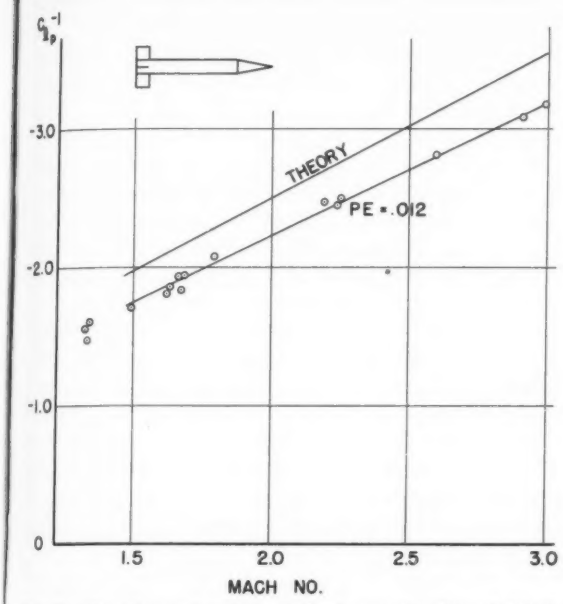

FIG. 7. Experimental values of $C_{l_p}^{-1}$ as a function of Mach Number plotted with the "Weighted Fit" curve.

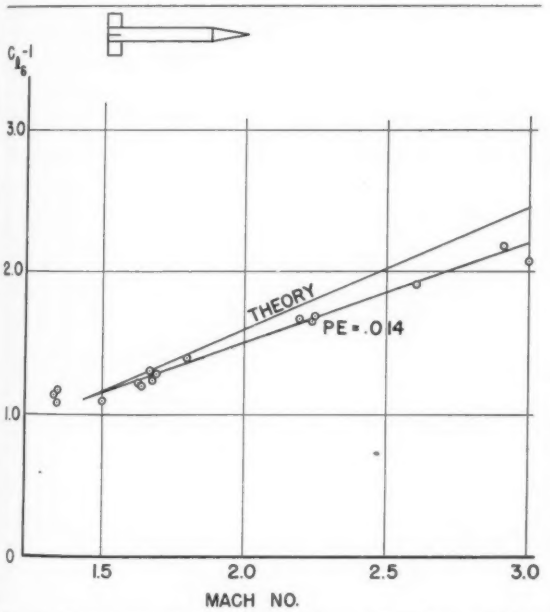

FIG. 8. Experimental values of $C_{l\delta}^{-1}$ as a function of Mach Number plotted with the "Weighted Fit" curve.

seen from Table 1 that the agreement is considerably improved. Although the empirical relation appears to provide a good method for associating the aerodynamic coefficients obtained from the Standard Technique with Mach Number, it should be noted that the original differences were small (0.5–2 per cent) and of little consequence in most engineering work.

Therefore, the comparison of the two reduction techniques as applied to this particular Aerodynamic Range data reveals that the Standard Technique is certainly adequate. However, for models and full-scale missiles where the change in the aerodynamic coefficients for a particular test run are large, the Refined Theory should yield significantly better results.

(*b*) *Linearity of* $(C_{l\delta}^{-1})$ *and* $(C_{l_p})^{-1}$ *with Mach Number; Consistency of the Data.*—It was found [see Eq. (6)] both experimentally and theoretically that, for all of the many configurations investigated, $(C_{l\delta})^{-1}$ and $(C_{l_p})^{-1}$, when plotted against Mach Number, yielded a linear variation. Since the Refined Roll Reduction Technique was based on this variation, the values of the reciprocal of the coefficients obtained from the various firings are plotted in Figs. 7 and 8. These experimental values* were "fitted" by straight lines in a manner that weighted the influence of each test value by the probable error associated with it.

In Figs. 5 and 6, the coefficients C_{l_p} and $C_{l\delta}$ are plotted in conventional manner against Mach Number. Also included in the figures are the weighted lines obtained from the reciprocal plots. It is noted that the maximum deviation of any of the experimental values from the weighted line is about 5 per cent (for $M > 1.4$) in both figures.

(*c*) *Effectiveness Parameter per Cant Angle* $(pb/2V/\delta)$. —In order to obtain the consistency of the effectiveness parameter with Mach Number, a weighted straight line was "fitted" to the data ($M > 1.4$) and is plotted in Fig. 9, together with the data. The maximum deviation of the data from the "fitted" line is 6 per cent (Model 16). It should be noted that the values of both $C_{l\delta}$ and $pb/2V/\delta$ for Models 15 and 16 differ from the

* The coefficients obtained for $M < 1.4$ have been excluded because of the suspected presence of transonic effects.

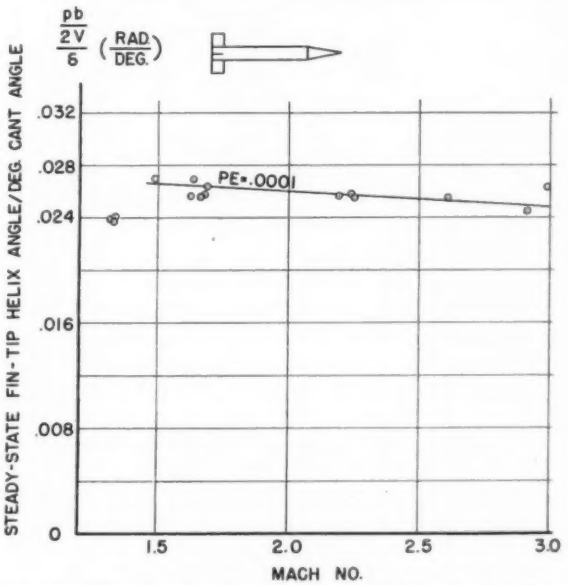

FIG. 9. The effectiveness parameter per cant angle plotted as a function of Mach Number.

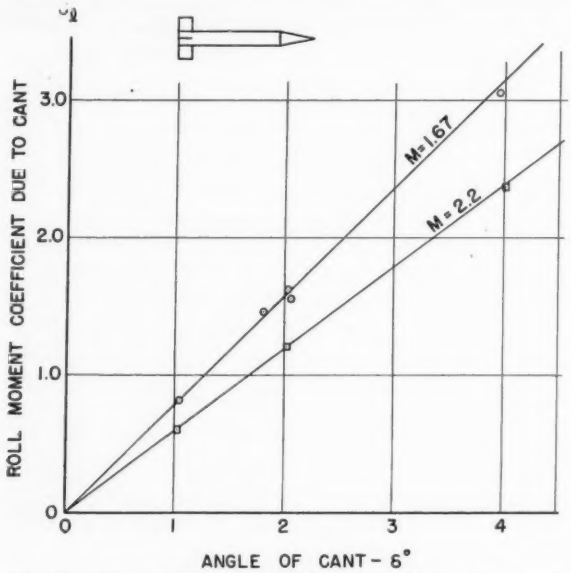

FIG. 10. The roll moment coefficient produced by a canted fin surface plotted as a function of the cant angle.

respective curves by approximately 4.8 and 7.8 per cent, respectively. Since the determination of both of these coefficients depends on an accurate knowledge of the angle of cant and since both models were subject to relatively severe launching conditions in order to obtain the largest Mach Numbers of the program, it is conjectured that there may have been distortion of the aluminum fins.

One of the assumptions of the reduction technique was that $s' = 0$ and thus

$$C_2/C_1 = s = \text{constant}$$

since [from Eq. (14)]

$$s/\delta \sim (pb/2V)/\delta$$

This assumption may be investigated by inspection of Fig. 9, where it is seen that the maximum departure of any value from a constant taken as the average is approximately 3 per cent over $1.4 < M < 3.0$, excluding the results of Model 16.

(*d*) *Linearity of Roll Moment and $pb/2V$ with Cant Angle.*—The analysis presented in this paper is based upon the assumption of a linear relationship between the lift coefficient at any point of the lifting surfaces and the angle of cant of the surface. This in turn implies a linearity of both the roll moment, C_l, and the steady-state effectiveness parameter, $pb/2V$, with angle of cant. Figs. 10 and 11 show the experimental values of roll moment and the effectiveness parameter angle as functions of cant angle for two Mach Numbers. The resultant straight lines passing through the origin substantiate the original assumption and are an indication of the accuracy and reliability of the test results.

It should be noted that the values of effectiveness parameter extend over an extremely large range; the value obtained for 4° cant is equivalent to the spin that would be obtained by firing a shell of a diameter equal to the fin span from a 1–30 twist gun, which is the standard rifling for many guns.

(*e*) *Effect of Fin Thickness on the Coefficients.*—In Figs. 12 and 13 are presented the roll damping moment and the roll moment coefficients as a function of Mach Number for the seven missiles with 16 per cent thick fins[4] and the 16 missiles with 8 per cent thick fins. In all other respects the geometry of the missiles was identical within machining tolerances. Also plotted in these figures are the linearized theoretical curves as calculated in reference 1. Since the linearized theory becomes more applicable with thinner surfaces, the data substantiated the expectations of lower coefficients for the thinner surfaces. Note that the deviation of the coefficients from the linearized values for the thin-fin missiles is less than 12 per cent over the complete range of Mach Numbers.

A comparison of the theoretical lift of an infinite-aspect-ratio single-wedge wing obtained from the linearized theory with that obtained from the exact theory using the two-dimensional expansion and shock equations results in a value approximately 9 per cent lower for the linearized lift at a Mach Number of 2.5 for the 8 per cent thick fins and 15 per cent lower for the 16 per cent thick fins. The trend then in the two-

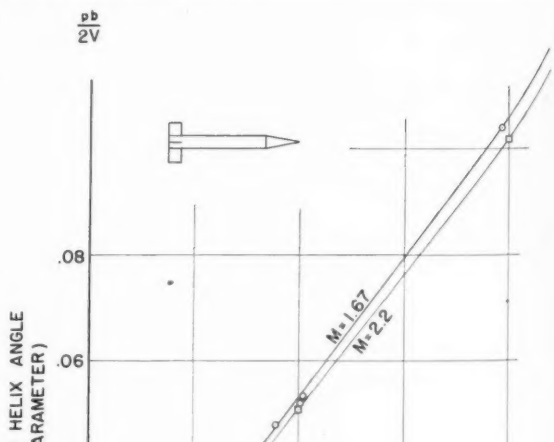

FIG. 11. The effectiveness parameter plotted as a function of the angle of cant on each of four fins.

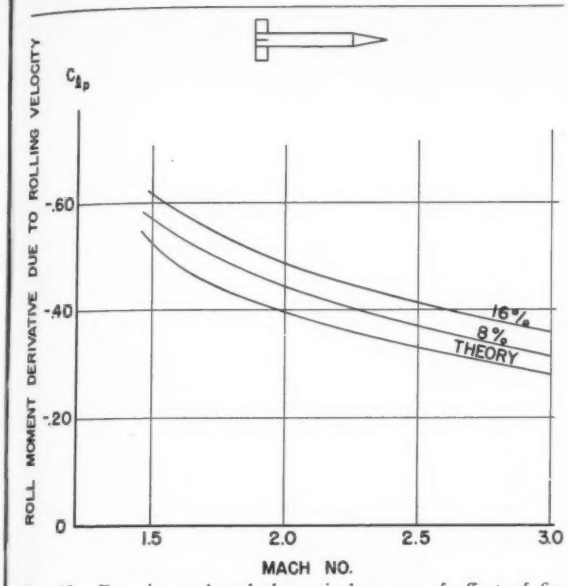

FIG. 12. Experimental and theoretical curves of effect of fin thickness on C_{l_p}.

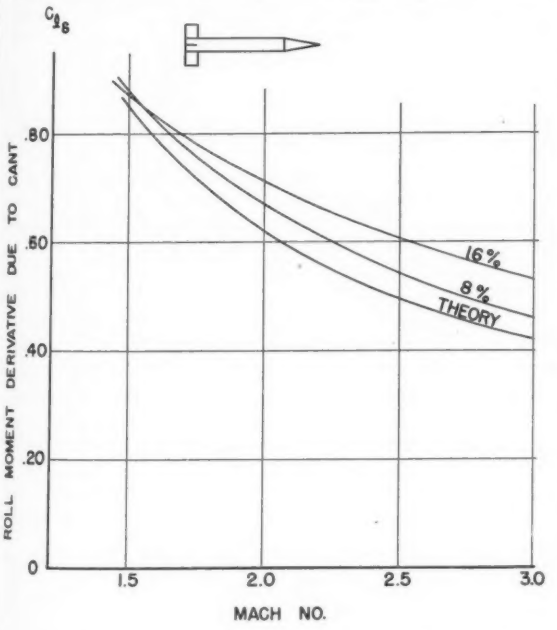

FIG. 13. Experimental and theoretical curves of effect of fin thickness on $C_{l\delta}$.

dimensional case is qualitatively similar to that in the three-dimensional case as would be expected.

(*f*) *Wing-Fin Interference.*—The experimental values for the aerodynamic coefficients, $C_{l\delta}$, C_{l_p}, and $(p_s b \div 2V)/\delta$ obtained from the 16 per cent thickness surfaces for (1) the seven models with fins only over $1.6 < M < 3.0$, (2) the two models with wings only at $M = 1.7$ and 1.95, and (3) the two models with wings and fins (aligned) at $M = 1.7$ and 1.95, are plotted in Figs. 14, 15, and 16. For the models with both wings and fins, only the four fins were canted ($\delta = 2°$); as a result, the fins were in a region of downwash behind the wing resulting only from the angle of attack induced by the rolling velocity of the missile. Since the maximum roll rate was about 25° per ft. and since the distance between the wing trailing edge and fin leading edge was about 3 in., the tail rotates a maximum of about 6° for a 3-in. flight path, which is quite insufficient to allow it to escape the downwash region of the wing. However, it is not located symmetrically with respect to this region.

The data from the wing-fin models, Fig. 14, indicate an extremely large downwash effect on the damping coefficient for the tail surfaces. At a Mach Number of 1.95, the surfaces are only 14 per cent as effective as when acting alone, and at a $M = 1.73$ they contribute no damping at all.

The large interference effect of the wings on the tail surfaces damping moment seems due to the fact that the greatest part of the moment is contributed by the surface area near the fin tip, and it is this region that is most seriously influenced by the downwash field of the wing. The geometry of the single-wedge airfoil results in a comparatively large wake, which also tends to decrease the aerodynamic effectiveness of the fin surfaces in this wake.

The roll moment produced by the canted fin surfaces appears to be unaffected by the presence of the wing. This result seems reasonable, since the downwash field*

* The turbulent rotational motion of the fluid also caused by the wing could conceivably influence the roll moment; however, this effect appears small from the data.

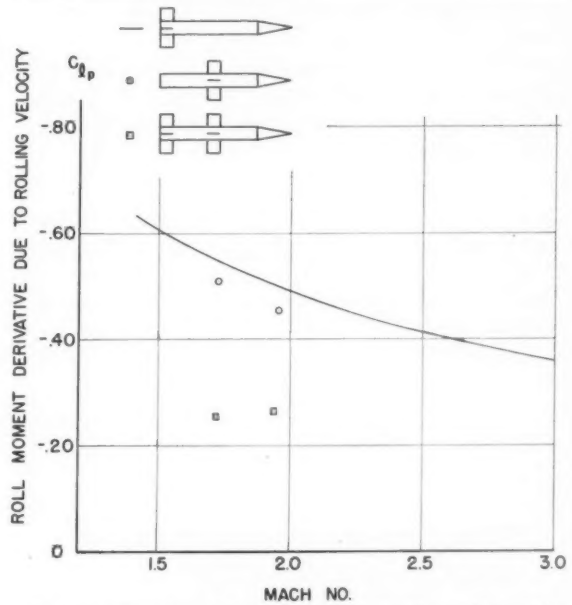

FIG. 14. Experimental values of C_{l_p} for various wind and/or fin configurations demonstrating effect of wing location and interference.

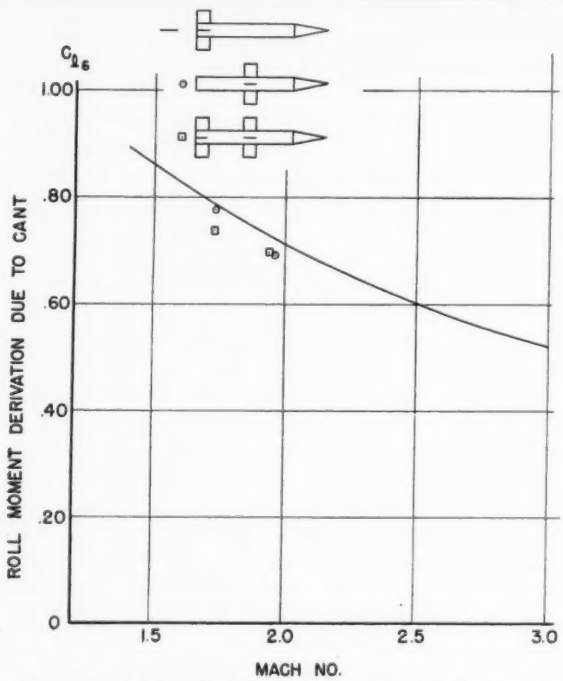

FIG. 15. Experimental values of $C_{l\delta}$ for various wing and/or fin configurations demonstrating effects of wing location and interference.

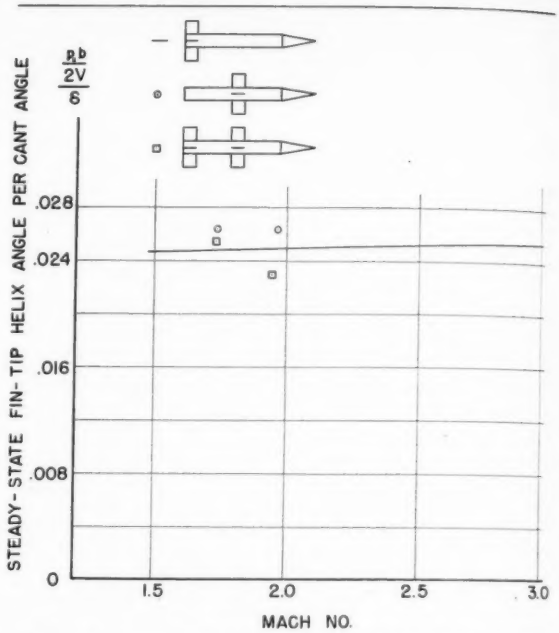

FIG. 16. Experimental values of $(p_s b/2V)/\delta$ for various wing and/or fin configurations demonstrating effects of wing location and interference.

of the wing arises solely as a result of the rolling velocity and as such can influence only the fin damping moment.

One might interpret the small differences in the coefficients for the wing-only models and for the fin-only models as a result of the variation in body-wing interference for the different geometrical arrangements. Additional tests, however, would be necessary for exploitation of this possibility.

The data are only sufficient to indicate that the range technique is successfully adaptable to a study of wing-tail interference phenomena under different flight and design conditions.

REFERENCES

[1, 2] Bolz, R. E., and Nicolaides, J. D., *A Method of Determining Some Aerodynamic Coefficients from Supersonic Free-Flight Tests of a Rolling Missile*, Journal of the Aeronautical Sciences, Vol. 17, No. 10, p. 609, October, 1950, and B. R. L. No. 711, April, 1949.

[3] Charters, A. C., *Some Ballistic Contributions to Aerodynamics*, Journal of the Aeronautical Sciences, Vol. 14, No. 3, p. 155, March, 1947.

[4] Charters, A. C., and Thomas, R. N., *The Aerodynamic Performance of Small Spheres from Subsonic to High Supersonic Velocities*, Journal of the Aeronautical Sciences, Vol. 12, No. 4, p. 468, October, 1945.

[5] Scarborough, J. B., *Numerical Mathematical Analysis*; The Johns Hopkins Press, 1930.

[6] Ribner, Herbert S., *Damping in Roll of Cruciform and Some Related Delta Wings at Supersonic Speeds*, N.A.C.A. T.N. No. 2285, February, 1951.

[7] Harman, Sidney, and Jeffreys, Isabella, *Theoretical Lift and Damping in Roll of Thin Wings with Arbitrary Sweep and Taper at Supersonic Speeds, Supersonic Leading and Trailing Edges*, N.A.C.A. T.N. No. 2114, May, 1950.

[8] Jones, Arthur L., and Alksne, Alberta, *The Damping Due to Roll of Triangular Trapezoidal and Related Plan Forms in Supersonic Flow*, N.A.C.A. T.N. No. 1548, March, 1948.

[9] Nicolaides, J. D., and Bolz, R. E., *On the Pure Rolling Motion of Winged and/or Finned Missiles in Varying Supersonic Flight*, B.R.L. Report 799, March, 1952.

Theoretical Pressure Recovery Through a Normal Shock in a Duct with Initial Boundary Layer

GEORGE McLAFFERTY*
United Aircraft Corporation

Abstract

The theoretical pressure recovery through a normal shock in a duct having an initial boundary layer has been calculated on the basis of continuity and conservation of momentum. The results can be used to determine the maximum theoretical pressure recovery in supersonic compressors, supersonic wind-tunnel diffusers, supersonic ram-jet diffusers, and in any other case in which a wall boundary layer is present upstream of a normal shock. This calculation procedure has also been applied to diffusing passages having boundary-layer bleed systems to determine the maximum theoretical pressure recovery in both the main stream and the boundary-layer passage.

It is shown that the theoretical total pressure recovery through a normal shock in a duct is reduced by an amount proportional to the displacement thickness of the boundary layer approaching the shock for a wide range of approach boundary-layer profiles and approach Mach Numbers.

Introduction

THE EXPERIMENTAL PERFORMANCE of supersonic diffuser passages is usually evaluated on the basis of the relation of this performance to the isentropic performance with ideal approach conditions. In the application of diffusers to supersonic compressors and other cases where the inlet conditions are not ideal because of the presence of initial boundary layers, the ultimate theoretical performance must be modified by this consideration to provide a realistic basis for performance evaluation.

Discussion

Pressure recovery through a normal shock with a uniform profile approaching the shock is calculated by classical theory on the basis of the following three assumptions: (1) continuity of flow, (2) conservation of momentum, and (3) conservation of energy.

These same assumptions were used to calculate the pressure recovery through a normal shock in a duct with an initial boundary layer approaching the shock. The method of analysis is discussed in the Appendix. Airflow and momentum of the initial boundary layer were calculated from tabulated values of boundary-layer displacement thickness and momentum thickness. The results of the analysis are presented in Figs. 1 and 2 for a $1/7$-power turbulent boundary-layer profile approaching the shock and a uniform profile downstream of the shock. The theoretical pressure recovery is plotted as a function of the ratio of displacement thickness of the boundary layer to the semiheight of the passage.

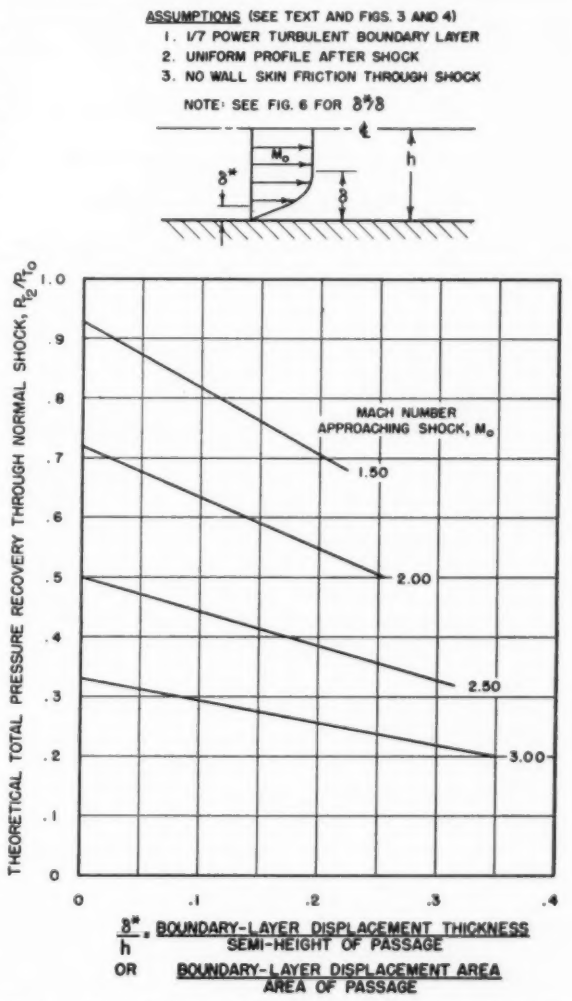

FIG. 1. Theoretical normal shock pressure recovery vs. displacement thickness of initial boundary layer.

Received March 17, 1952. Revised and received October 20, 1952.

* Aeronautical Research Engineer, Research Department.

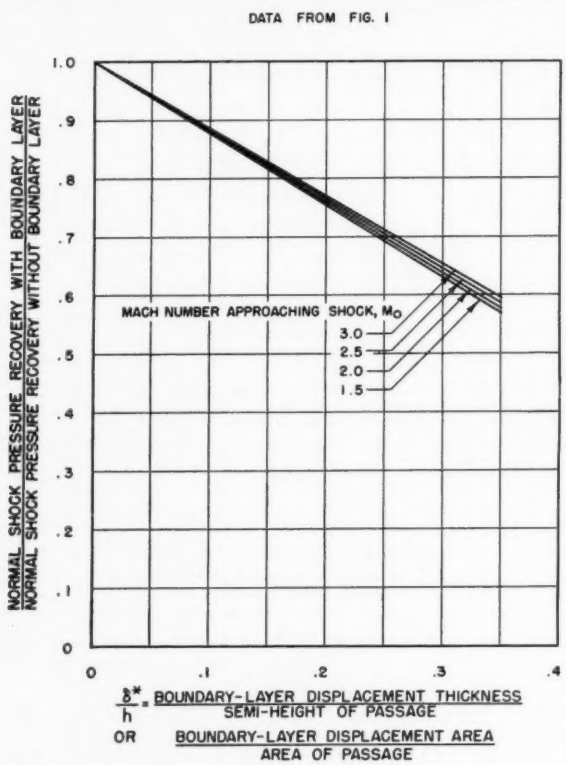

FIG. 2. Summary of effect of initial boundary layer on theoretical normal shock pressure recovery.

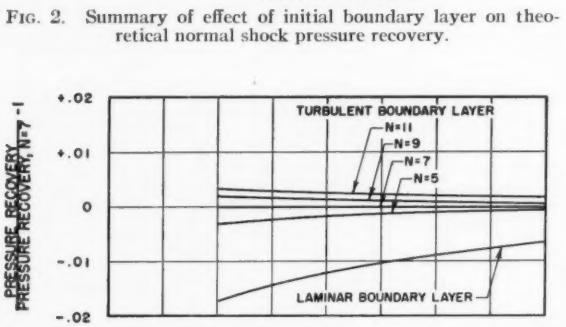

FIG. 3. Theoretical pressure recoveries for various approach boundary-layer profiles, calculated for $\delta^*/h = 0.10$.

Theoretical pressure recoveries for different assumed boundary-layer velocity distributions upstream of the shock are plotted in Fig. 3. It is shown that the theoretical pressure recovery is relatively insensitive to changes in distribution from the $^1/_7$-power profile, even for the case of a laminar profile, where the difference in pressure recovery is only 2 per cent. The theoretical pressure recovery for velocity profiles downstream of the shock other than the assumed uniform profile is not changed if one type of momentum average total pressure is used to calculate the pressure recovery. Other total pressure averages provide pressure recoveries slightly greater or slightly less than the momentum average total pressure recovery. On the basis of these considerations, it is not felt that the results of the analysis would be radically changed if the velocity profiles upstream and downstream of the shock-boundary-layer interaction differed somewhat from the assumed profiles.

It has been shown experimentally that a normal shock in the presence of a boundary layer occurs over a substantial length of passage. According to references 1 and 2, the length required to produce the complete static pressure rise through a normal shock is on the order of 6 to 15 hydraulic diameters. It was also noted in references 1 and 2 that a constant-area passage in the region of the normal shock allows a considerably greater pressure recovery than would be obtained if the normal shock occurs in a divergent passage. This result is expected because a normal shock in a divergent passage occurs at an average area greater than the throat area and, hence, at an average effective Mach Number greater than the Mach Number at the throat.

The effect of wall skin friction on the pressure recovery through a normal shock may also be calculated using the methods discussed in the Appendix. The results of this analysis are given in Fig. 4 for a Mach Number of 2.0 approaching the shock. The wall skin friction is expressed as a fraction of the total stream thrust approaching the shock. An example of the use of Fig. 4 is calculated in the Appendix for a round pipe 10 diameters in length. If the skin-friction force is calculated from the dynamic pressure of the flow ap-

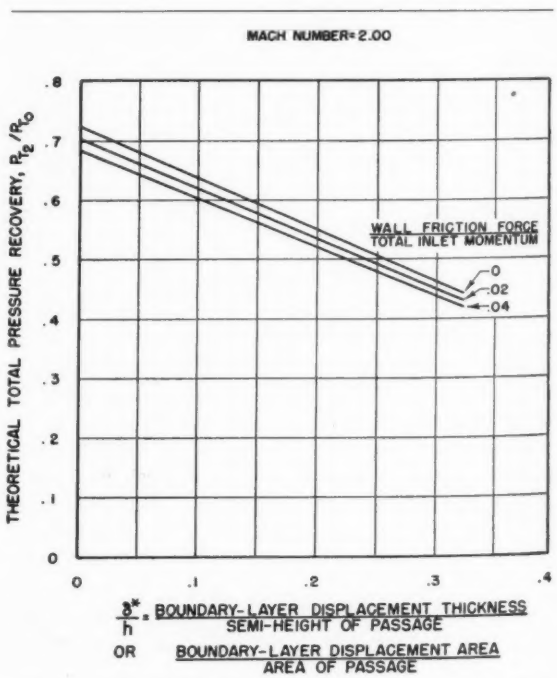

FIG. 4. Example of effect of wall friction forces on the pressure recovery through a normal shock occurring over a length of passage.

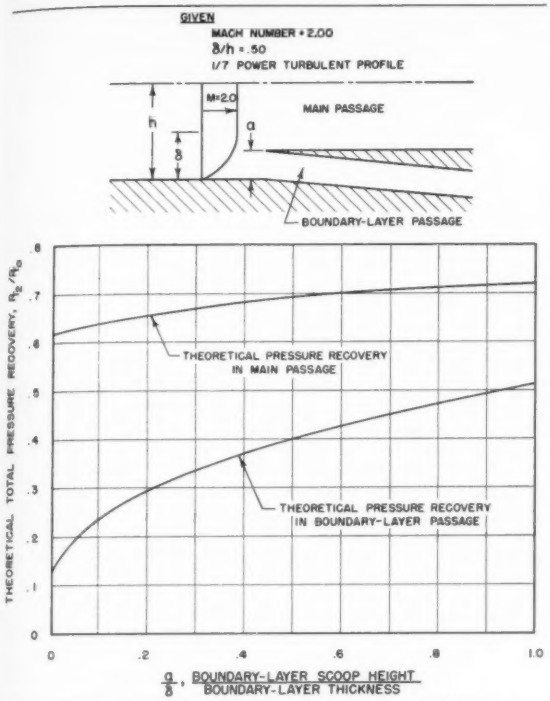

FIG. 5. Example of calculated pressure recoveries in inlet system with boundary-layer bleed.

proaching the shock, the ratio of wall friction to total inlet momentum in this example is 0.034, which reduces the maximum total pressure recovery about 4 per cent. The skin-friction coefficient used in this example is high for two reasons. First, the average dynamic pressure is substantially less than the dynamic pressure of the stream approaching the shock. Second, the skin-friction coefficient would be reduced because the boundary layer is separated in the region of the shock. From this reasoning it is believed that the total pressure recovery would be reduced on the order of only 1 or 2 per cent by wall skin friction in this example.

It is often undesirable to have a constant-area throat of sufficient length to obtain the complete static pressure rise through a normal shock. The length of the required throat can be reduced by removing the boundary layer approaching the shock. Removing the boundary layer also has the effect of increasing the pressure recovery through the shock in the main passage. The maximum pressure recovery in the boundary-layer passage and the maximum pressure recovery in the main stream can be calculated as a function of the amount of boundary layer bled off by the same type of analysis used to obtain the results in Figs. 1 and 2. The results of a sample calculation are given in Fig. 5. In this example, bleeding off the complete boundary layer provided a maximum theoretical pressure recovery of 72 per cent in the main passage as compared to 62 per cent with no boundary-layer bleed. The theoretical pressure recovery in the boundary-layer passage for complete removal of main-passage boundary layer was 52 per cent.

It can be shown theoretically that isolation of the high-velocity main stream and the low-velocity boundary-layer stream will result in less overall increase in entropy. This results from elimination of losses due to mixing the main-stream high total pressure air and the boundary-layer low total pressure air.

Calculated values of the ratio of boundary-layer displacement thickness to boundary-layer total thickness are shown in Fig. 6 as a function of Mach Number for several different boundary-layer profiles. The turbulent boundary-layer profile values were obtained from reference 3, and the laminar boundary-layer profile values were obtained by integration of the boundary-layer equations.

The results shown in Figs. 1 through 6 have a large range of application to all cases where the pressure rise through a normal shock is affected by an initial boundary layer, such as in supersonic compressors, in supersonic wind-tunnel diffusers, and in most types of supersonic ram-jet diffusers.

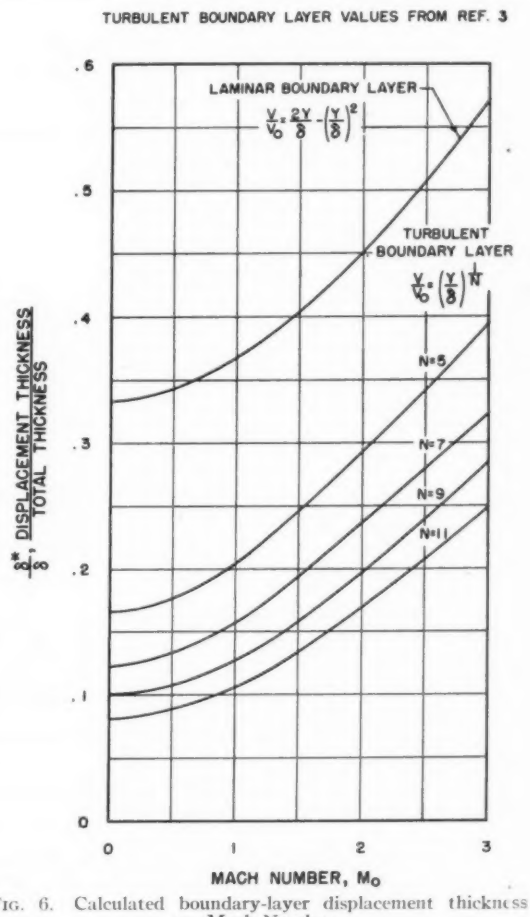

FIG. 6. Calculated boundary-layer displacement thickness vs. Mach Number.

References

[1] Neumann, E. P., and Lustwerk, F., *Supersonic Diffusers for Wind Tunnels*, M.I.T. Meteor Report No. 13, November, 1947.

[2] Neumann, E. P., and Lustwerk, F., *High-Efficiency Supersonic Diffusers*, M.I.T. Meteor Report No. 56, June, 1950.

[3] Tucker, Maurice, *Approximate Calculation of Turbulent Boundary-Layer Development in Compressible Flow*, N.A.C.A. T.N. No. 2337, April, 1951.

Appendix

List of Symbols

a = height of boundary-layer scoop (see Fig. 5)
A = cross-sectional area
A_f = surface area for determination of skin-friction drag
A/A_* = isentropic area ratio, a function of Mach Number only
C = airflow constant $= \sqrt{\frac{\gamma}{RT_T}\left(\frac{2}{\gamma+1}\right)^{(\gamma+1)/(\gamma-1)}}$
C_{f_0} = skin-friction coefficient (see example in Appendix)
D = hydraulic passage diameter (see example in Appendix)
F = stream thrust [see Eq. (1)]
h = semiheight of passage
K_F = stream thrust parameter [see Eq. (2)]
K_W = airflow parameter [see Eq. (10)]
l = length of passage required to obtain complete static pressure rise through normal shock (see example in Appendix)
M = Mach Number
N = velocity profile parameter in turbulent boundary-layer equation, $V/V_0 = (y/\delta)^{1/N}$
P_S = static pressure
P_T = total pressure
R = gas constant for air
T_T = total temperature
V = velocity
W = airflow
y = distance from wall of passage
γ = ratio of specific heats
δ = boundary-layer total thickness
δ^* = boundary-layer displacement thickness, $\frac{1}{\rho_0 V_0}\int_0^\delta (\rho_0 V_0 - \rho V)\,dy$
Δ = wall-friction force expressed as a fraction of upstream stream thrust [see Eq. (5)]
ρ = density
θ = boundary-layer momentum thickness, $\frac{1}{\rho_0 V_0^2}\int_0^\delta \rho V(V_0 - V)\,dy$

Subscripts

0 = midstream conditions upstream of shock-wave boundary-layer interaction
1 = average conditions upstream of shock-wave boundary-layer interaction
2 = average conditions downstream of shock-wave boundary-layer interaction

In a nonuniform stream with constant static pressure in a symmetrical passage with semiheight h and unit area, the stream thrust is defined as

$$F = P_S \frac{1}{h}\int_0^h (1 + \gamma M^2)\,dy \tag{1}$$

Let

$$K_F = \frac{1}{h}\int_0^h (1 + \gamma M^2)\,dy \tag{2}$$

Eq. (1) becomes

$$F = P_S K_F \tag{3}$$

The stream thrust before and after a shock must be equal if there is no wall skin friction.

$$F_1 = F_2 \tag{4}$$

If the wall skin friction is a fraction, Δ, of the upstream stream thrust, Eq. (4) becomes

$$F_1(1 - \Delta) = F_2 \tag{5}$$

Substituting quantities from Eq. (3),

$$P_{S_1} K_{F_1}(1 - \Delta) = P_{S_2} K_{F_2} \tag{6}$$

or

$$P_{S_2}/P_{S_1} = (K_{F1}/K_{F2})(1 - \Delta) \tag{7}$$

In the same manner, the airflow in the passage of unit area is

$$W = C\frac{1}{h}\int_0^h \frac{P_T}{(A/A_*)}\,dy \tag{8}$$

or

$$\frac{W}{C} = P_S \frac{1}{h}\int_0^h \frac{1}{(P_S/P_T)(A/A_*)}\,dy \tag{9}$$

where C is a function of T_T, R, and γ.

Let

$$K_W = \frac{1}{h}\int_0^h \frac{1}{(P_S/P_T)\,(A/A_*)}\,dy \tag{10}$$

so that Eq. (9) becomes

$$W/C = P_S K_W \tag{11}$$

The airflow before and after the shock must be equal,

$$W_2 = W_1 \tag{12}$$

Since T_T, R, and γ do not change through the shock,

$$C_2 = C_1 \tag{13}$$

Eq. (12) can then be written

$$W_2/C_2 = W_1/C_1 \tag{14}$$

From Eq. (11), this becomes

$$P_{S_2} K_{W_2} = P_{S_1} K_{W_1} \tag{15}$$

or

$$P_{S_2}/P_{S_1} = K_{W_1}/K_{W_2} \tag{16}$$

Combining Eqs. (7) and (16),

$$(K_{F_1}/K_{F_2})\,(1 - \Delta) = K_{W_1}/K_{W_2} \tag{17}$$

or

$$K_{W_2}/K_{F_2} = [1/(1 - \Delta)]\,(K_{W_1}/K_{F_1}) \tag{18}$$

It is convenient to express K_{W_1} and K_{F_1} in terms of K_{W_0} and K_{F_0}, which are evaluated assuming that the mid-stream conditions in the nonuniform flow approaching the shock exist across the complete stream. Eq. (18) can be written

$$\frac{K_{W_2}}{K_{F_2}} = \frac{1}{1 - \Delta}\frac{K_{W_0}}{K_{F_0}}\frac{K_{W_1}/K_{W_0}}{K_{F_1}/K_{F_0}} \tag{19}$$

The quantities K_{W_1}/K_{W_0} and K_{F_1}/K_{F_0} are determined by the flow conditions approaching the shock. They are expressed in terms of more conventional boundary-layer parameters by the following derivation. By definition,

$$\frac{K_{F_1}}{K_{F_0}} = \frac{1}{h}\left[\int_0^h (1 + \gamma M^2)\,dy\right]\Big/(1 + \gamma M_0^2) \tag{20}$$

$$\frac{K_{F_1}}{K_{F_0}} = \frac{\int_0^\delta (1 + \gamma M^2)\,dy + \int_\delta^h (1 + \gamma M^2)\,dy}{h(1 + \gamma M_0^2)} \tag{21}$$

$$\frac{K_{F_1}}{K_{F_0}} = \frac{\delta + \int_0^\delta \gamma M^2\,dy + (h - \delta)(1 + \gamma M_0^2)}{h(1 + \gamma M_0^2)} \tag{22}$$

The quantity $\int_0^\delta \gamma M^2\,dy$ can be obtained by proper manipulation of the expressions for boundary-layer displacement thickness, δ^*, and boundary-layer momentum thickness, θ.

$$\delta^* + \theta = \frac{1}{\rho_0 V_0}\int_0^\delta (\rho_0 V_0 - \rho V)\,dy + \frac{1}{\rho_0 V_0^2}\int_0^\delta \rho V(V_0 - V)\,dy \tag{23}$$

$$\delta^* + \theta = \int_0^\delta \left(1 - \frac{\rho V}{\rho_0 V_0}\right)dy + \int_0^\delta \left(\frac{\rho V}{\rho_0 V_0} - \frac{\rho V^2}{\rho_0 V_0^2}\right)dy \tag{24}$$

$$\delta^* + \theta = \int_0^\delta \left(1 - \frac{\rho V}{\rho_0 V_0} + \frac{\rho V}{\rho_0 V_0} - \frac{\rho V^2}{\rho_0 V_0^2}\right)dy \tag{25}$$

$$\delta^* + \theta = \int_0^\delta \left(1 - \frac{\rho V^2}{\rho_0 V_0^2}\right)dy \tag{26}$$

$$\delta^* + \theta = \delta - \int_0 \frac{\rho V^2}{\rho_0 V_0^2} \tag{27}$$

It can be shown that

$$\rho V^2 = P_S \gamma M^2 \tag{28}$$

Substituting in Eq. (27),

$$\delta^* + \theta = \delta - \int_0^\delta \frac{P_S \gamma M^2}{P_{S_0}\gamma M_0^2} \tag{29}$$

Since the static pressure is assumed constant across the passage

$$\delta^* + \theta = \delta - \frac{1}{\gamma M_0^2}\int_0^\delta \gamma M^2 \tag{30}$$

or

$$\int_0^\delta \gamma M^2 = \gamma M_0^2\,[\delta - \delta^* - \theta] \tag{31}$$

Substituting Eq. (31) in Eq. (22),

$$\frac{K_{F_1}}{K_{F_0}} = \frac{\delta + \gamma M_0^2(\delta - \delta^* - \theta) + (h - \delta)(1 + \gamma M_0^2)}{h(1 + \gamma M_0^2)} \tag{32}$$

$$\frac{K_{F_1}}{K_{F_0}} = \frac{h(1 + \gamma M_0^2) - \delta - \delta\gamma M_0^2 + \delta + \gamma M_0^2(\delta - \delta^* - \theta)}{h(1 + \gamma M_0^2)} \tag{33}$$

$$\frac{K_{F_1}}{K_{F_0}} = 1 - \frac{\gamma M_0^2(\delta^* + \theta)}{h(1 + \gamma M_0^2)} \tag{34}$$

$$\frac{K_{F_1}}{K_{F_0}} = 1 - \frac{\delta}{h}\frac{\gamma M_0^2}{(1 + \gamma M_0^2)}\left(\frac{\delta^*}{\delta} + \frac{\theta}{\delta}\right) \tag{35}$$

From the definition of boundary-layer displacement thickness, δ^*,

$$K_{W_1}/K_{W_0} = 1 - (\delta^*/h) \tag{36}$$

or

$$K_{W_1}/K_{W_0} = 1 - (\delta/h)(\delta^*/\delta) \tag{37}$$

Substitute Eqs. (35) and (37) in Eq. (19),

$$\frac{K_{W_2}}{K_{F_2}} = \left(\frac{1}{1 - \Delta}\right)\frac{K_{W_0}}{K_{F_0}}\frac{\left(1 - \frac{\delta}{h}\frac{\delta^*}{\delta}\right)}{\left[1 - \frac{\delta}{h}\frac{\gamma M_0^2}{(1 + \gamma M_0^2)}\left(\frac{\delta^*}{\delta} + \frac{\theta}{\delta}\right)\right]} \tag{38}$$

If a uniform profile is assumed downstream of the shock, K_{W_2}/K_{F_2} calculated from Eq. (38) determines the Mach Number downstream of the shock, M_2, which in turn determines K_{W_2} and P_{S_2}/P_{T_2}. From Eq. (16),

$$\frac{P_{S_2}}{P_{S_1}} = \frac{K_{W_1}}{K_{W_2}} = \frac{K_{W_0}\,[1 - (\delta^*/h)]}{K_{W_2}} \tag{39}$$

The following tautology exists:

$$\frac{P_{T_2}}{P_{T_0}} = \frac{P_{S_2}}{P_{S_1}}\frac{P_{S_1}}{P_{S_0}}\frac{P_{S_0}/P_{T_0}}{P_{S_2}/P_{T_2}} \tag{40}$$

P_{S_1}/P_{S_0} is equal to unity from the original assumption of uniform static pressure in the upstream flow. Substituting Eq. (39) in Eq. (40),

$$\frac{P_{T_2}}{P_{T_0}} = \frac{P_{S_0}/P_{T_0}}{P_{S_2}/P_{T_2}} \frac{K_{W_0}}{K_{W_2}} \left(1 - \frac{\delta^*}{h}\right) \tag{41}$$

The theoretical total pressure recoveries through a normal shock presented in the present report were calculated using Eqs. (38) and (41). The wall friction term, Δ, was assumed equal to zero except for the calculation of the results shown in Fig. 4. As an example of the use of Fig. 4, calculate Δ for flow in a round pipe at Mach Number 2.00.

$$\Delta = \frac{\text{wall friction force}}{\text{total inlet stream thrust}} \tag{42}$$

$$\Delta = \frac{C_{f_0} A_f (\gamma/2) P_{S_0} M_0^2}{P_{S_0} A (1 + \gamma M_0^2)} \tag{43}$$

$$\Delta = \frac{C_{f_0} \pi D l (\gamma/2) M_0^2}{(\pi/4) D^2 (1 + \gamma M_0^2)} \tag{44}$$

$$\Delta = 1.70(l/D) C_{f_0} \tag{45}$$

The wall skin-friction coefficient in the region of the shock is difficult to determine but would probably be low because of the separated flow due to the adverse pressure gradient through the shock. Also, the friction force should be based on an average dynamic pressure through the shock instead of the dynamic pressure upstream of the shock. However, as an example, assume $l/D = 10$ and $C_{f_0} = 0.002$. The skin-friction coefficient of 0.002 was obtained from a standard chart of turbulent flat-plate skin-friction coefficients for a Mach Number of 2.0 and a Reynolds Number of 20×10^6. From Eq. (45),

$$\Delta = 1.70(10)\ (0.002) = 0.034 \tag{46}$$

From Fig. 4, this amount of wall skin friction will reduce the total pressure recovery approximately 4 per cent. The 4 per cent figure is probably an upper limit according to the reasoning stated previously, and the actual reduction in total pressure recovery is probably more nearly on the order of 1–2 per cent in this example.

Changes of Address

Since the Post Office Department does not as a rule forward magazines to forwarding addresses, it is important that the Institute be notified of changes in address 30 days in advance of publishing date to ensure receipt of every issue of the JOURNAL and REVIEW.

Notices should be printed legibly and sent directly to:

Institute of the Aeronautical Sciences, Inc.

2 East 64th Street, New York 21, New York

Forced Convection Heat Transfer from Horizontal Cylinders in a Rarefied Gas

F. M. SAUER* AND R. M. DRAKE, JR.†
University of California at Berkeley

ABSTRACT

An approximate analytical treatment of the energy equation is given which yields a specification for the average heat-transfer coefficients from horizontal circular cylinders to gases flowing at high Mach Numbers and low Reynolds Numbers. The results are given for continuum and slip-flow regions in comparison with available experimental data.

NOMENCLATURE

a	=	thermal diffusivity, sq.ft. per sec.
D	=	diameter of cylinder, ft.
h	=	heat transfer coefficient, local, B.t.u./hr. ft.^{2} °F.
J_ν	=	Bessel's functions of first kind
K_ν	=	Bessel's functions of second kind
k	=	thermal conductivity of the gas, B.t.u.-ft./hr. ft.^{2} °F.
L	=	reciprocal length proportional to molecular mean free path
M	=	Mach Number (dimensionless)
n	=	an arbitrary constant
Nu	=	Nusselt Number, (hD/k), (dimensionless)
r, θ, z	=	spatial coordinates, ft. or rad.
r_1	=	radius of cylinder, $D/2$, ft.
Re	=	Reynolds Number, V_0D/ν (dimensionless)
t	=	temperature at any point, °F.
t_0	=	temperature of the free stream, °F.
t_w	=	temperature of the cylinder surface, °F.
u, v, w	=	velocity components in the r, θ, z directions, ft. per sec.
V	=	any constant velocity in the θ direction, ft. per sec.
V_0	=	free-stream velocity, ft. per sec.
α	=	thermal accommodation coefficient (dimensionless)
γ	=	ratio of specific heats of constant pressure and constant volume (dimensionless)
μ	=	absolute viscosity, lbs. sec./ft.^{2}
λ	=	molecular mean free path, ft.
ρ	=	density, lbs. sec.^{2}/ft.^{4}
ϑ	=	temperature ratio, $(t - t_w)/(t_0 - t_w)$ (dimensionless)
σ	=	Prandtl Number (dimensionless)
τ	=	time, sec.

INTRODUCTION

THE SUBJECT OF HEAT TRANSFER from bodies in a high-speed rarefied gas stream has become important in several fields of investigation. If a gas is sufficiently rarefied, it is clear that a continuum treatment fails because the mean distance between molecular encounters becomes comparable with significant body dimensions, and the effect of the molecular structure on the flow and heat transfer must be considered. The nature of the rarefaction effects with regard to the aerodynamic effects has been examined by Tsien[1] and with regard to heat transfer by Drake and Kane.[2] Although the requirements attendant to the design of high-speed high-altitude missiles have provided the stimulus for most investigations, the results are of interest for other systems. Rarefaction effects may occur at fairly ordinary pressures if the body dimensions are small, as for instance in a hot-wire anemometer or thermoelement[3] to be used in high-speed flows.

The use of hot wires as turbulence measuring devices requires extremely thin wires in order to reduce the thermal lag. These wires operate at Reynolds Numbers of the order of 10–1,000. The wire diameter and the molecular mean free path are comparable, and at supersonic speeds, the flow around the wire is in some cases slip flow.

It is the purpose of this paper to introduce approximate solutions for the specification of the average heat-transfer coefficients for horizontal cylinders appropriate to laminar flow in the continuum and slip-flow regions in order to estimate the effect of the temperature jump associated with slip flow on the heat transfer.

A comparison between continuum and slip-flow heat transfer is possible if considerations are made on the basis of a continuum formulation of the energy equation wherein the rarefaction effects, as specified by the temperature jump condition, are relegated to the boundary values of the problem.[2] In particular, if the mean tangential velocity at the cylinder surface is taken as an arbitrary constant the energy equation may be reduced to a heat conduction equation which can be solved to yield a specification of the average heat transfer coefficient for continuum flow conditions. The results so obtained may be made to correspond to existing experimental data for average heat-transfer coefficients from horizontal cylinders[6, 11] in continuum flow by specifying the magnitude of the mean tangential velocity. Using the value of the mean tangential velocity thus determined, another solution of the heat conduction equation for temperature jump boundary conditions yields an average heat-transfer coefficient for the slip-flow case which may be compared with the continuum results for effect of the temperature jump on the heat transfer.

Received June 17, 1952. Revised and resubmitted November 17, 1952.

* Formerly Assistant Professor Mechanical Engineering; now Physicist, Fire Research Division, California Forest and Range Experiment Station.

† Assistant Professor, Mechanical Engineering.

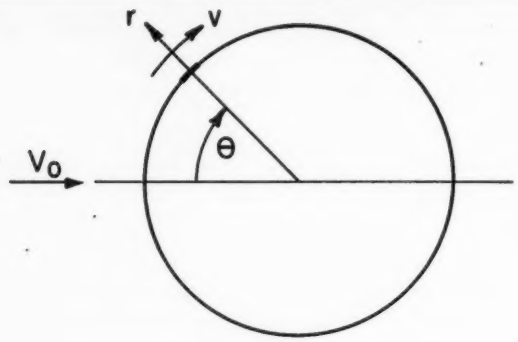

FIG. 1. Coordinate system.

ANALYSIS

Consider an infinite cylinder placed normal to a uniform gas stream. Neglecting the terms relating to compressibility and dissipation of mechanical energy, the energy equation may be written in cylindrical coordinates, Fig. 1,

$$\frac{\partial t}{\partial \tau} + u\frac{\partial t}{\partial r} + \frac{v}{r}\frac{\partial t}{\partial \theta} + w\frac{\partial t}{\partial z} = a\left\{\frac{\partial^2 t}{\partial r^2} + \frac{1}{r}\frac{\partial t}{\partial r} + \frac{1}{r^2}\frac{\partial^2 t}{\partial \theta^2} + \frac{\partial^2 t}{\partial z^2}\right\} \quad (1)$$

The solution of the problem requires steady state, $\partial/\partial\tau = 0$, two-dimensional flow, $w = \partial t/\partial z = 0$, and the additional assumptions:

(a) Conduction of heat in θ direction is negligible, $\partial^2 t/\partial\theta^2 = 0$.

(b) The radial velocity is everywhere zero, $u = 0$, and the angular velocity is a constant, $v = V$.

(c) The surface temperature of the cylinder is a constant.

Introducing a dimensionless temperature, $\vartheta = (t - t_w)/(t_0 - t_w)$, and making use of the above assumptions, Eq. (1) becomes

$$\frac{V}{r}\frac{\partial \theta}{\partial \theta} = a\left\{\frac{\partial^2 \vartheta}{\partial r^2} + \frac{1}{r}\frac{\partial \vartheta}{\partial r}\right\} \quad (2)$$

Boundary conditions applicable to continuum or slip flows may be considered. In the continuum-flow case the fluid adjacent to the cylinder surface has the same temperature as the surface; thus, $\vartheta = 0$, while the fluid far away from the cylinder has a temperature t_0 and $\vartheta = 1$. The point $\theta = 0$, $r = r_1$ provides some difficulty, inasmuch as ϑ has two values there—0 and 1. This is best seen if the problem is visualized in the r-θ plane. However, at distances along $\theta = 0$ somewhat greater than r_1, the cylinder radius, the oncoming flow has the same characteristics as the free-stream flow; thus, for $r > r_1$ along $\theta = 0$, $\vartheta = 1$. For the slip-flow case, the above arguments apply except at the surface, $r = r_1$, where there exists a temperature discontinuity between the surface and the adjacent gas which is proportional to the heat rate. Making this change, the boundary conditions may be written as:

Continuum Flow

$$\vartheta = 0, \quad r = r_1, \quad 0 < \theta < \pi$$
$$\vartheta = 1, \quad r > r_1, \quad \theta = 0$$

Slip Flow

$$\frac{\partial \vartheta}{\partial r} = L\vartheta, \quad r = r_1, \quad 0 < \theta < \pi$$
$$\vartheta = 1, \quad r > r_1, \quad \theta = 0$$

where

$$\frac{1}{L} = 1.996\left(\frac{\gamma}{\gamma + 1}\right)\left(\frac{2 - \alpha}{\alpha}\right)\frac{\lambda}{\sigma}$$

SOLUTION ON THE DIFFERENTIAL EQUATION

Introducing a new independent variable $y = \sqrt{r}$, Eq. (1) has the form

$$\frac{\partial^2 \vartheta}{\partial y^2} + \frac{1}{y}\frac{\partial \vartheta}{\partial y} - \frac{1}{K}\frac{\partial \vartheta}{\partial \theta} = 0 \quad (3)$$

where $K = a/4V$ and the boundary conditions become:

Continuum Flow

$$\vartheta = 0, \quad y = \sqrt{r_1}, \quad 0 < \theta < \pi$$
$$\vartheta = 1, \quad y > \quad r_1, \quad \theta = 0$$

Slip Flow

$$\frac{\partial \vartheta}{\partial y} = \xi\vartheta, \quad y = \sqrt{r_1}, \quad 0 < \theta < \pi$$
$$\vartheta = 1, \quad y > \quad r_1, \quad \theta = 0$$

where $\xi = 2L\sqrt{r_1}$.

Eq. (3) is identical with the equation for the transient radial conduction of heat into an infinite region bounded internally by a circular cylinder. The slip-flow boundary condition is identical with the "radiation" boundary condition. The solutions are well known and have been found by the Laplace transform method by Carslaw and Jaeger[4] among others. Each case will be presented separately.

CONTINUUM FLOW

The solution of Eq. (2), transforms from the solution of Eq. (3), is the following:

$$\vartheta = -\frac{2}{\pi}\int_0^\infty e^{-Ku^2\theta}\,\frac{J_0(u\sqrt{r})\,Y_0(u\sqrt{r_1}) - Y_0(u\sqrt{r})\,J_0(u\sqrt{r_1})}{J_0^2(u\sqrt{r_1}) + Y_0^2(u\sqrt{r_1})}\,\frac{du}{u} \quad (4)$$

where u is an arbitrary parameter of integration.

The local heat-transfer coefficient at the surface is given by

$$h = k\,(\partial\theta/\partial r)_{r=r_1} \tag{5}$$

Performing the necessary differentiation, the local Nusselt Number becomes

$$\frac{hD}{k} = \frac{4}{\pi^2}\int_0^\infty \frac{e^{-Ku^2\theta}}{J_0^2(u\sqrt{r_1}) + Y_0^2(u\sqrt{r_1})}\,\frac{du}{u} \tag{6}$$

Let $U = u\sqrt{r_1}$ and $x = K\theta/r_1 = a\theta/2VD$; Eq. (6) becomes

$$\frac{hD}{k} = \frac{4}{\pi^2}\int_0^\infty \frac{e^{-xU^2}}{J_0^2(U) + Y_0^2(U)}\,\frac{dU}{U} = \frac{4}{\pi^2}\,[I(0,1;x)] \tag{6a}$$

Jaeger and Clark[5] give an excellent tabulation of the function $I(0,1;x)$. The same reference gives a series valid for small values of x, $(x << 1)$.

$$I(0,1;x) = \frac{\pi^2}{4}\left[(\pi x)^{-1/2} + \frac{1}{2} - \frac{1}{4}\left(\frac{x}{\pi}\right)^{1/2} + \frac{1}{8}x - 0.1469x^{3/2} + 0.203x^2 - 0.315x^{5/2} + 0.536x^3 + \ldots\right] \tag{7}$$

The average heat-transfer coefficient will be calculated over the region $0 < \theta < \pi$.

$$\left(\frac{hD}{k}\right)_{\text{av.}} = \frac{1}{x_\pi}\int_0^{x_\pi} I(0,1;x)\,dx \tag{8}$$

where x_π corresponds to the value of x at $\theta = \pi$.

For small values of x_π, using Eq. (7),

$$(hD/k)_{\text{av.}} = 1.128x_\pi^{-1/2} + 0.500 - 0.0941x_\pi^{1/2} + 0.0625x_\pi - 0.0588x_\pi^{3/2} + 0.0677x_\pi^2 \ldots \tag{9}$$

For the region $x < 0.1$, $(hD/k)_{\text{av.}}$ was calculated from Eq. (9); for $x > 0.1$, the average heat-transfer coefficient was found by numerical integration of Eq. (8) by means of the tabulated values of Jaeger and Clark.

The value of V has been left arbitrary up to this point. Let $V = V_0/n$ and $\sigma = 0.70$ for air;

$$x_\pi = \frac{n\pi a}{2V_0D} = \frac{n\pi}{2\,Re\sigma} = \frac{2.24n}{Re}$$

The calculated solution may be compared with the recommended curve of McAdams[6] for forced convection of air flowing normal to cylinders. If $n = 3$, the curves are nearly coincident in the region of Re less than 100 as seen on Fig. 2. The calculated values of Re with $n = 3$ are shown in Table 1.

For $Re > 300$ and σ representative of air, Eq. (9) reduces to

$$(hD/k)_{\text{av.}} = 0.500 + 0.435Re^{1/2} \tag{9a}$$

TABLE 1

x	$\left(\frac{hD}{k}\right)_{\text{av.}}$	Re
0.01	12.8	672.0
0.10	4.04	67.2
1.0	1.57	6.72
2.0	1.22	3.36
10.0	0.740	0.672
100.0	0.431	0.0672
200.0	0.379	0.0336

Eq. (9a) may be compared with the empirical Eq. (4) of McAdams based on the experiments of many investigators,

$$(hD/k)_{\text{av.}} = 0.32 + 0.43Re^{0.52}$$

Slip Flow

The solution of Eq. (2) with the temperature jump boundary condition is

$$\vartheta = -\frac{2\xi}{\pi}\int_0^\infty \frac{J_0(u\sqrt{r})\,[uY_1(u\sqrt{r_1}) + \xi\,Y_0(u\sqrt{r_1})] - Y_0(u\sqrt{r})\,[uJ_1(u\sqrt{r_1}) + \xi J_0(u\sqrt{r_1})]e^{-Ku^2\theta}}{[uJ_1(u\sqrt{r_1}) + \xi\,J_0(u\sqrt{r_1})]^2 + [uY_1(u\sqrt{r_1}) + \xi Y_0(u\sqrt{r_1})]^2}\,\frac{du}{u} \tag{10}$$

Note that Eq. (4) is a special case of Eq. (10)—i.e. $\xi \to \infty$.

Differentiating Eq. (10) and substituting into Eq. (5), the local Nusselt Number is found to be

$$\frac{hD}{k} = \frac{4\xi^2}{\pi^2}\int_0^\infty \frac{e^{-Ku^2\theta}}{[uJ_1(u\sqrt{r_1}) + \xi\,J_0(u\sqrt{r_1})]^2 + [uY_1(u\sqrt{r_1}) + \xi Y_0(u\sqrt{r_1})]^2}\,\frac{du}{u} \tag{11}$$

As before, let $U = u\sqrt{r_1}$. After some rearrangement Eq. (11) can be written in the dimensionless form,

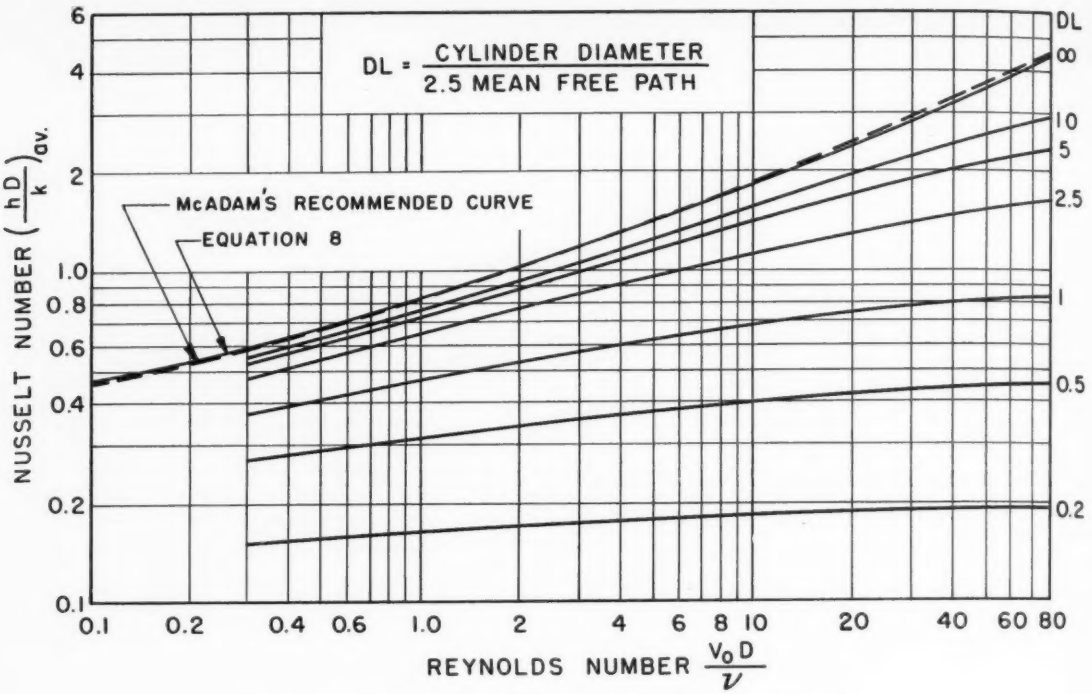

FIG. 2. Heat-transfer coefficient for horizontal circular cylinders in air.

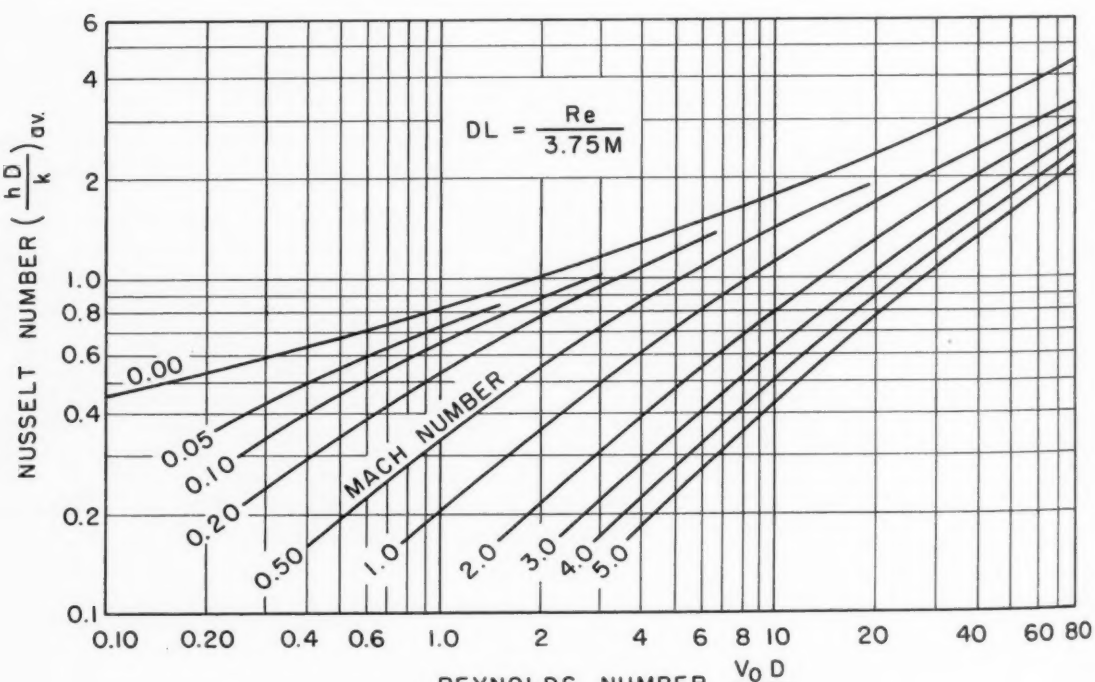

FIG. 3. Heat-transfer coefficient for horizontal circular cylinders in air showing variation with Mach and Reynolds Numbers.

TABLE 2

DL	0.2	0.5	1	2.5	5.0	10
Re			$(hD/k)_{av.}$			
0.672	0.160	0.304	0.435	0.583	0.651	0.679
1.344	0.167	0.329	0.488	0.690	0.780	0.824
6.72	0.180	0.392	0.650	1.03	1.24	1.35
67.2	0.192	0.453	0.837			
672			0.932	2.12		
6,720					4.38	7.15
67,200					4.81	9.30
∞	0.2	0.5	1.0	2.5	5.0	10.0

$$\frac{hD}{k} = DL \int_0^\infty \frac{e^{-xU^2}}{\left[\frac{\pi}{2}(DL)^{-1/2}UJ_1(U) + \frac{\pi}{2}(DL)^{1/2}J_0(U)\right]^2 + \left[\frac{\pi}{2}(DL)^{-1/2}UY_1(U) + \frac{\pi}{2}(DL)^{1/2}Y_0(U)\right]^2} \frac{dU}{U} = DL[I(DL;x)] \quad (11a)$$

where $x = K\theta/r_1 = a\theta/2VD$ and DL = const. (D/λ).

For small values of x, the integral

$$I(p, q, x) = \int_0^\infty \frac{e^{-xU^2}}{[pUJ_1(U) + qJ_0(u)]^2 + [pUY_1(U) + qY_0(U)]^2} \frac{dU}{U} \quad (12)$$

is approximated by the series

$$I(p, q, x) = (\pi^2/2pq)\,[1 - 2p^{-1}q\pi^{-1/2}x^{1/2} + (1/2)p^{-2}\,q(p + 2q)x + \ldots\,]$$

For $p = (\pi/2)\,(DL)^{-1/2}$ and $q = \pi/2\,(DL)^{1/2}$, Eq. (12) becomes

$$I(DL, x) = [1 - (2/\pi^{1/2})x^{1/2} + (1/2)\,(DL)\,(1 + 2DL)x + \ldots\,] \quad (13)$$

For larger values of x, $I(p,q;x)$ is plotted in reference 7, p. 226, and also in reference 8, p. 283, from which curve values were read and replotted to larger scale.

As before, the average heat-transfer coefficient is found in the region $0 < \theta < \pi$. For small values of x_π,

$$\left(\frac{hD}{k}\right)_{av.} = DL\left[1 - \frac{4}{3\pi^{1/2}}(DL)\,x_\pi^{1/2} + \frac{DL}{4}(1 + 2DL)\,x_\pi + \ldots\right] \quad (14)$$

For $x_\pi > 1$, the average value was found by graphical and numerical integration of the curves of Eq. (8). Values for $V = 1/3\ V_0$ are shown in Table 2.

Assigning values of $\alpha = 0.80$, $\gamma = 1.4$, and $\sigma = 0.70$ for air,

$$DL = D/2.5\,\lambda$$

For conditions peculiar to rarefied gases, there exists a relationship[9] between the molecular mean free path to body dimension ratio and the Mach and Reynolds Numbers, which is for air,

$$\lambda/D = 1.5\,(M/Re)$$

thus,

$$DL = 0.267\,Re/M$$

A plot of $(hD/k)_{av.}$ versus (V_0D/ν) with DL as a parameter is shown on Fig. 2. Curves with Mach Number as a parameter were obtained by cross plotting from Fig. 2, and these are shown on Fig. 3 as the desired solutions for the average heat-transfer coefficients.

COMPARISON WITH EXPERIMENT

The results of the analysis as shown graphically in Figs. 2 and 3 may be compared with experimental data of heat transfer from cylinders in cross flow as reported by Kovásznay and Törmarck[3] and Stalder, Goodwin and Creager.[10] The data of reference 3 were taken under conditions of supersonic flow at normal pressures with very small wires, and the data in reference 10 were taken in supersonic flow under very low pressures with somewhat larger cylinders. The data so obtained cover a range $0.07 < M/\sqrt{Re} < 5.5$. On the basis of the presently defined flow region limits, these data are considered to extend from the near slip region into the free-molecule flow region.[1] The experimental data are shown in terms of Nusselt and Reynolds Numbers, wherein the velocity and density are taken as the free-stream values while the viscosity and thermal conductivity are evaluated at the stagnation temperature. The data are considered herein on that same basis, al-

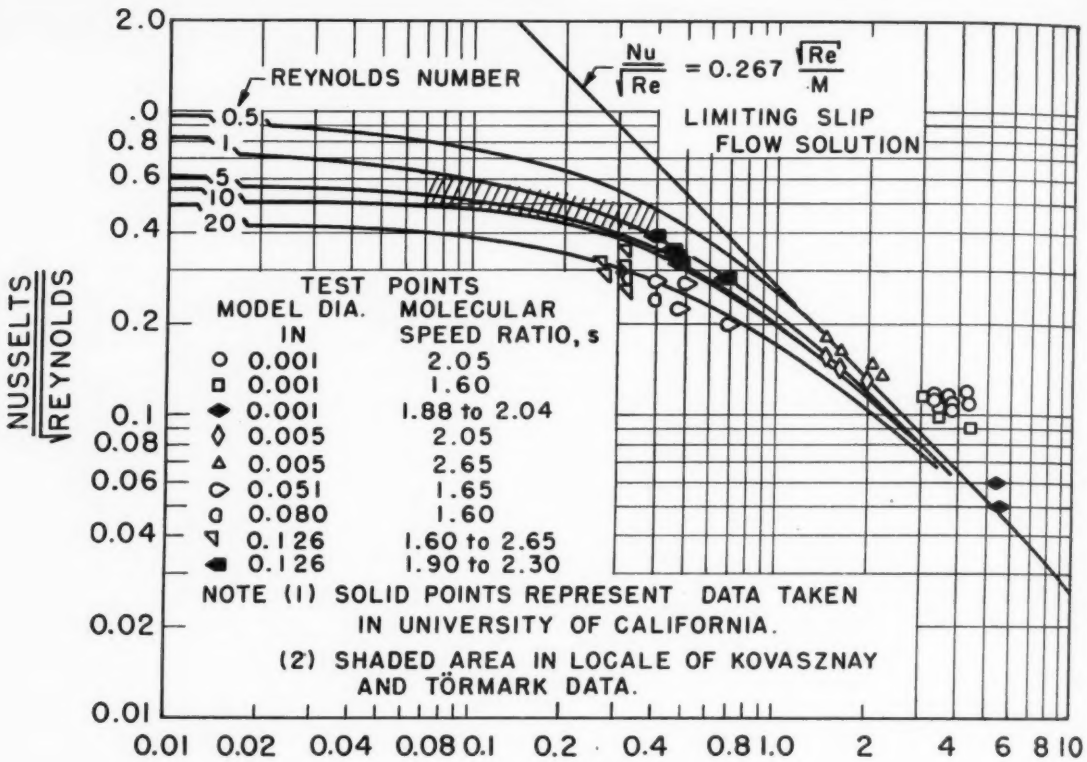

FIG. 4. Comparison of analysis and experiment for heat transfer from horizontal circular cylinders to rarefied gas (air).

though it is realized that this particular selection of property values tends to suppress the Mach Number effect.

In order to compare the analysis with the experimental data, Fig. 3 was replotted as shown in Fig. 4. In this plot the intercept for $M/\sqrt{Re} = 0$ represents the Hilpert continuum experimental data as represented by Eq. (4) in reference (6) and by Eq. (9a) herein. As the $M/\sqrt{Re}$ ratio increases for greater rarefaction, this effect is shown on the $Nu/\sqrt{Re}$ ratio. The limiting solution is for the case of infinite $M/\sqrt{Re}$ ratio. It may be seen that the analysis predicts correctly the trend of the experimental data, although some question remains with regard to the representative magnitudes, since for the most part the data of Kovásznay and Törmarck are higher than the values predicted by the theory. The selection of the fluid property values would greatly influence the correspondence between the experimental data and the analytical results in any case.

SUMMARY

An analytical treatment has been presented which yields a specification of the average heat-transfer coefficients for right circular cylinders arranged horizontally in a gas stream for flow conditions characteristic of both continuum and slip flow conditions. This solution of the energy equation was effected for boundary conditions incorporating a temperature discontinuity between the cylinder surface and the gas by virtue of a simplifying assumption concerning the nature of the free-stream velocity distribution around the cylinder. The solution is approximate in this respect.

The solution obtained closely represents the continuum heat-transfer results for horizontal cylinders to air; and, when compared with experimental data for horizontal cylinders in the slip-flow region, it was seen to predict the trend of the data satisfactorily, though some question remains regarding the representative magnitudes. The disagreement here may be in part a result of the selection of the fluid property values as were used in the reduction of the experimental data.

REFERENCES

[1] Tsien, H. S., *Superaerodynamics, The Mechanics of Rarefied Gases*, Journal of the Aeronautical Sciences, Vol. 13, No. 12, pp. 653–664, December, 1946.

(*Concluded on page 209*)

Inelastic Instability and Incremental Theories of Plasticity*

E. T. ONAT† AND D. C. DRUCKER‡
Brown University

SUMMARY

A most troublesome paradox has existed for a number of years with respect to buckling in the plastic range. Theoretical considerations and all direct experimental evidence show conclusively that an incremental or flow type of mathematical theory of plasticity is valid. However, the results of plastic buckling tests are well correlated by a simple total or deformation theory[1–4] and bear no resemblance to published predictions of incremental theory.[5, 6]

The suggestion was made[7] that initial imperfections of shape or loading might well explain this most peculiar result. However, subsequent investigations by several authors seem to have given the impression that excessively large imperfections would be needed and that the answer would be overly sensitive to the magnitude of such imperfections.[6, 7, 8]

It is the purpose of this paper to demonstrate that extremely small, and therefore unavoidable, imperfections of shape do account for the paradox in a simple manner. The buckling load is shown to be extremely insensitive to the amount of imperfection. The example chosen is a simplified version of the long rectangular plate hinged along one edge and free on the other under uniform compressive stress at the ends. This is the equivalent of the case of the cruciform column, which has been so disturbing in the past because incremental theory applied to a perfect cruciform column did lead to an entirely incorrect result.[5]

STRESS-STRAIN RELATION

THE EXACT FORM OF THE incremental stress-strain relation used is not especially significant. Any reasonable isotropic loading function will lead to essentially the same result, so that the simplest one, the Mises function J_2, will be chosen. For plastic straining, $dJ_2 > 0$ and

$$d\epsilon_{ij} = d\epsilon_{ij}^{e} + d\epsilon_{ij}^{p} = \frac{(1+\nu)}{E}\, d\sigma_{ij} - \frac{\nu}{E}\, d\sigma_{kk}\delta_{ij} + F(J_2)s_{ij}dJ_2 \quad (1)$$

where

$$J_2 = (1/2)s_{ij}s_{ij}$$
$$s_{ij} = \sigma_{ij} - (1/3)\sigma_{kk}\delta_{ij}$$

ν is Poisson's ratio, E is Young's modulus, and δ_{ij} is the Kronecker delta. Repetition of an index in a term indicates summation.

If the only stresses present are a normal stress σ and a shearing stress τ on the same plane plus its cross-shear, the two important components of the relation (1) may be written

$$d\epsilon = \frac{d\sigma}{E} + F(J_2)\,\frac{4}{3}\,\sigma\left(\frac{\sigma d\sigma}{3} + \tau d\tau\right) \quad (2)$$

$$d\gamma = 2d\epsilon_{\text{shear}} = \frac{2(1+\nu)}{E}\,d\tau + F(J_2)\,4\tau\left(\frac{\sigma d\sigma}{3} + \tau d\tau\right) \quad (3)$$

where $d\epsilon$ is the normal strain increment in the σ direction, $d\gamma$ is the (engineering) shear strain increment corresponding to τ, $d\sigma$ and $d\tau$ are the increments of normal stress and shearing stress, and $E/2(1+\nu)$ is the shear modulus G,

$$J_2 = (1/3)\sigma^2 + \tau^2$$
$$dJ_2 = 2[(\sigma d\sigma/3) + \tau d\tau] \quad (4)$$

$F(J_2)$ can be determined from a simple tension test for which

$$d\epsilon = (d\sigma/E) + F(J_2)(4/9)\sigma^2 d\sigma$$
$$\frac{d\epsilon}{d\sigma} = \frac{1}{E_t} = \frac{1}{E} + F(J_2)\,4\,\frac{J_2}{3}$$

or

$$F(J_2) = (3/4J_2)[(1/E_t) - (1/E)] \quad (5)$$

where E_t is the ordinary tangent modulus and J_2 is given by Eq. (4) in the special case of combined normal and shearing stress only.

PREVIOUS DIFFICULTY

Although the paradox described in the Summary occurs for all problems studied, it appears at its worst in the torsional buckling of a cruciform in the plastic range. If a cruciform, Fig. 1, is loaded uniformly in compression, failure by twisting is likely. The kinematics is particularly simple if the ends are not restrained (Fig. 2). Each straight line parallel to the axis becomes a helix. The state of stress and strain is the same at each cross section. For a perfectly straight column at the instant of buckling, shearing stress and strain are added to the existing state of simple compression, point B of the curve J_2 = constant, Fig. 3. Whether or not the Shanley concept of increasing

Received September 10, 1952.
* The results presented in this paper were obtained in the course of research sponsored by the Office of Naval Research under Contract N7onr-35801 with Brown University.
† Frank B. Jewett Research Fellow.
‡ Chairman, Division of Engineering.

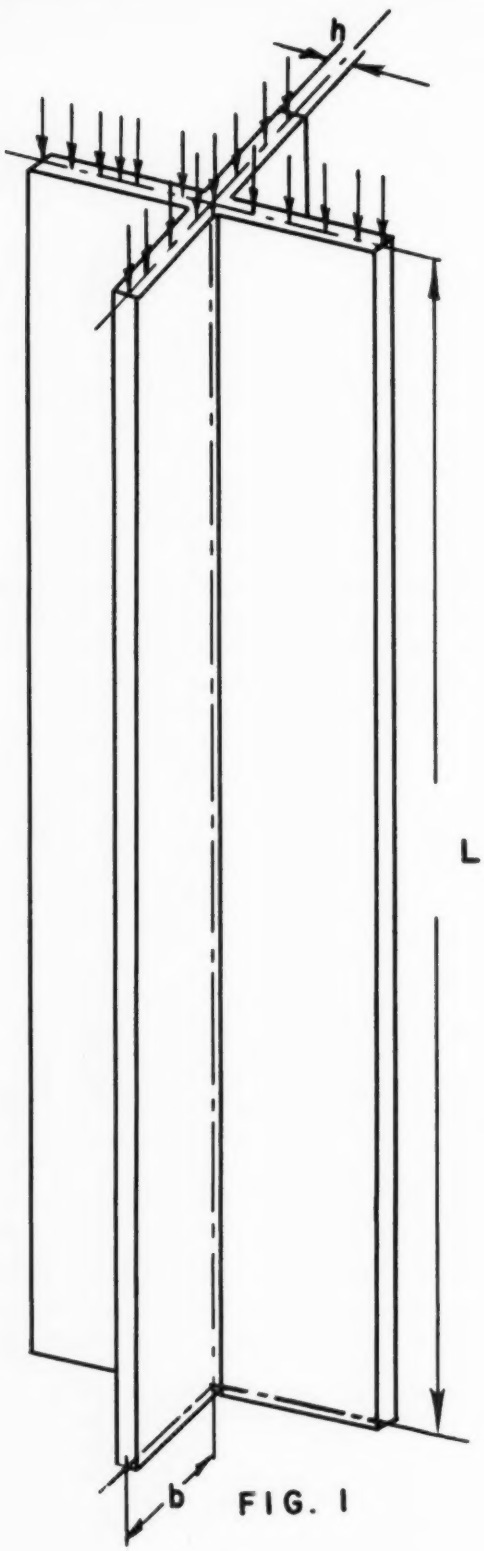

FIG. 1

FIG. 2

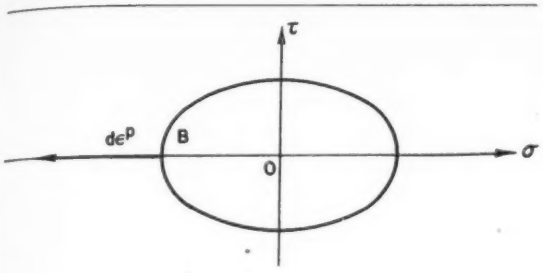

FIG. 3

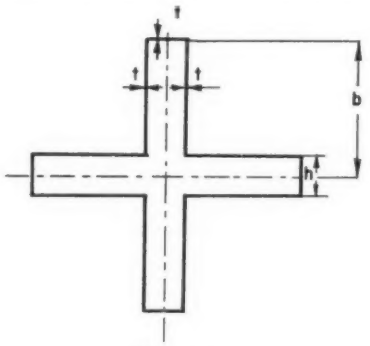

FIG. 4

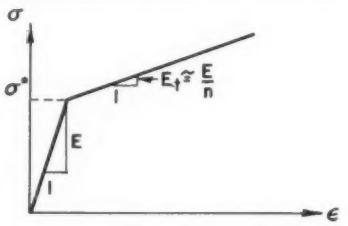

FIG. 5

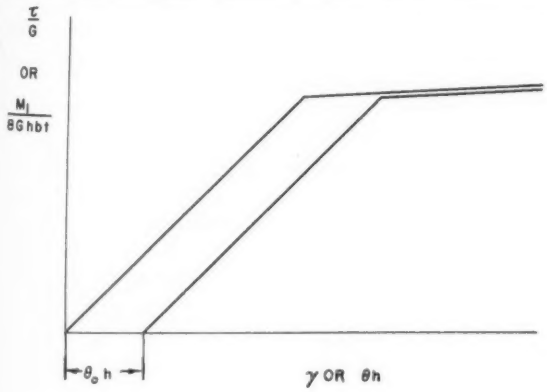

FIG. 6

TWIST OF THE CRUCIFORM WITHOUT AXIAL STRESS

the compression is followed and no matter what smooth symmetric loading function is assumed, the normal to the loading surface and therefore the plastic strain increment vector at B points along the negative σ-axis. This means that all incremental theories of plasticity which do not have a corner at B predict a purely elastic response to a shearing stress increment from point B regardless of how large a normal stress increment is applied simultaneously. The critical compressive stress σ_c predicted in this way is therefore given by

$$\sigma_c I_p \theta = GC\theta \tag{6}$$

or

$$\sigma_c = Gh^2/b^2 \tag{7}$$

where θ is the angle of twist per unit length, G is the elastic shear modulus, GC is the torsional rigidity, I_p is the polar moment of inertia, h is the thickness of each leg, and b is the width, Fig. 1. Simple J_2 deformation theory,[3] on the other hand, predicts $G_s h^2/b^2$, where G_s is the secant modulus in shear. This latter result is in excellent agreement with experiment.[4]

It is well recognized now that a physically valid theory must be of the incremental type. Furthermore, direct tests on circular tubes under compression and torsion verify the elastic response to torsion.[10,11] Therefore, when the agreement of buckling tests with deformation theory was so prominent in technical discussion, the suggestion was advanced that initial imperfection might well provide the explanation of the paradox.[7] More confusion than enlightenment seems to have resulted from several subsequent investigations that were interpreted as proving that excessively large imperfections would be needed and that the answer would be overly sensitive to the magnitude of such imperfections.

A Simplified Model

Considerably clearer understanding of the physical behavior involved is obtained by a simplified model and a simplified stress-strain diagram. The cruciform cross section ($h \ll b$) will be taken as a thin shell of constant thickness t, Fig. 4, instead of a solid plate; but the cross-sectional shape will still be supposedly maintained under twist. As a consequence, the shear stress on the cross section follows the contour and is constant in magnitude, and the shear strain γ is given by

$$\gamma = h\theta \tag{8}$$

where θ is the angle of twist per unit length.

The elastic buckling load, Eq. (6), is

$$\sigma_c' = \frac{GC}{I_p} = \frac{8Gh^2bt}{8tb^3/3} \text{ (approximately)}$$
$$= 3Gh^2/b^2 \tag{9}$$

under the assumption $h \ll b$. Deformation theory would substitute the secant modulus for the elastic modulus.

As the paradox and its explanation are not linked to any particular stress-strain relation, the simplified two sloping lines of Fig. 5 will be chosen for clarity of exposition.

A Qualitative Picture of the Buckling Process

The basic physical picture depends upon the shear stress-shear strain relation for the test piece, which may be translated directly into the moment-angle of twist per unit length relation. If there is no axial force acting on the shell cruciform, the M-θ relation is simply the stress-strain curve to a different scale, Fig. 6. The moment is

$$M_1 = 8\tau hbt \tag{10}$$

and $\gamma = \theta h$ if the cruciform is perfect to start. If the cruciform is initially twisted by a small amount, θ_0 per unit length, the lines are just shifted to the right as shown. The presence of appreciable axial compressive stress changes the picture completely. Designating the magnitude of the compressive stress by σ and employing Wagner's concept of the stress following the fiber, the axial force produces a twisting moment

$$M_2 = \sigma I_p \theta \tag{11}$$

The external twisting moment needed to maintain the twist is now

$$M = M_1 - M_2 \tag{12}$$

Should M_2 equal or exceed M_1, no external moment is needed, and the column will fail by twisting. Equating M_1 to M_2 for an initially untwisted column gives the elastic result of Eq. (6) for the critical load. It can also be readily seen that the maximum load for a completely elastic column is not appreciably influenced by initial twist (location of point A, Fig. 7). M_1 increases more than M_2, for a given increase in θ, until σ reaches the elastic buckling stress.

If the shell column is loaded in axial compression only, so that there is no external moment, $M_1 = M_2$ and (approximately)

$$\sigma(8/3)tb^2\theta = 8\tau hbt = M_1$$

or

$$\sigma = \left(\frac{3h}{b^2}\right)\left(\frac{\tau}{\theta}\right) = \frac{M_1}{(8/3)tb^3\theta} \tag{13}$$

The important physical point here is that the shearing stress and the twisting moment increase as σ increases and also as θ increases. From Eq. (13),

$$d\sigma = \frac{3h}{b^2}\left(\frac{d\tau}{\theta} - \frac{\tau d\theta}{\theta^2}\right) = \frac{3h^2}{b^2}\left(\frac{d\tau}{\gamma} - \frac{\tau}{\gamma}\frac{d\gamma}{\gamma}\right) = \frac{\sigma}{\tau}d\tau - \sigma\frac{d\gamma}{\gamma} \tag{14}$$

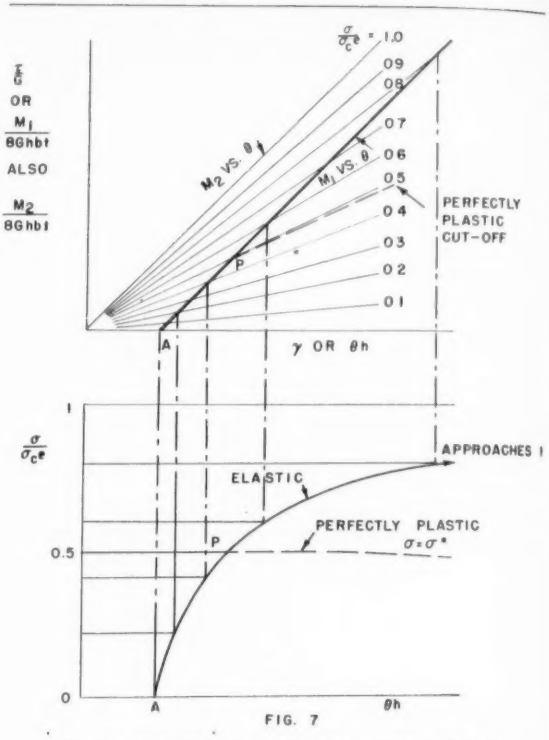

FIG. 7

INITIAL IMPERFECTION HAS LITTLE EFFECT ON THE ULTIMATE LOAD OF A COMPLETELY ELASTIC COLUMN WHICH FAILS BY TWISTING

It is somewhat more convenient to work in τ and γ notation rather than M_1 and θ, which are proportional, respectively, Eqs. (10) and (8).

Substituting Eqs. (5), (13), and (14) in the shear strain relation, Eq. (3), which applies in the plastic range, and rearranging

$$\frac{d\tau}{Gd\gamma} = \frac{1}{n} + \frac{[1 - (1/n)](\tau/G\gamma)}{1 + 3(\tau/\sigma)^2} \tag{15}$$

where $n = (3G/E_t) + 1 - (3G/E)$ is approximately the ratio of the elastic shear modulus to the tangent shear modulus. In terms of M_1 and θ,

$$\tau/G\gamma = M_1/8Gh^2bt\theta$$

Consider again the idealized stress-strain diagram of Fig. 5. Eq. (15) is valid as soon as the yield point is reached, which for all practical purposes requires $\sigma = \sigma^*$ because τ is zero or very small. The enormous importance of extremely small imperfections in shape is immediately apparent when the plastic line is flat; n is infinite. Upon reaching yield, the slope of the τ-γ or M_1-θ curve immediately goes from the elastic slope to the value τ/γ or M_1/θ. No matter how small the initial imperfection, no further increase in σ is required to continue twisting. In fact, the τ/σ term in the denominator of Eq. (15) makes the process instable; the column will twist to complete collapse

at $\sigma = \sigma^*$. In Fig. 7, if $\sigma^* = (1/2)\sigma_c^e$, σ will increase from point A to point P and then stay almost constant, as shown by the dashed line.

If n is reasonably large but not infinite, say 20, the slope of τ/G vs. γ or $M_1/8Ghbt$ vs. θh, which is unity in the elastic range, drops to a value that is larger than the slope of the radial line from the origin by about 1/40 in Fig. 8. Therefore, some increase in σ is required to continue the twisting of the column. Until the τ/σ term in the denominator of Eq. (15) becomes important, the τ/G vs. γ curve is fairly close to a logarithmic spiral centered at the origin. However, the tangent to the spiral is so nearly a radial line that a very small increase in σ over the value σ^* is sufficient to produce a large enough twist for τ/σ to take over and produce collapse.

As an example, if σ^* is one-half of the elastic buckling stress

$$\sigma^* = (3/2)(Gh^2/b^2)$$

or

$$\sigma^* I_p \theta = 4Gh^2 bt\theta$$

the equation of the spiral is approximately

$$r = r_0 e^{50\varphi} \tag{16}$$

where φ is the angular coordinate. This means that before σ exceeds σ^* by 20 per cent, the radius will be e^1 or 50 times the radius when plastic action began. Initial twists that are extremely small compared with maximum possible elastic twists therefore require stresses only a little higher than σ^* to cause collapse. Furthermore, large differences in initial imperfection change the maximum or buckling stress only a little.

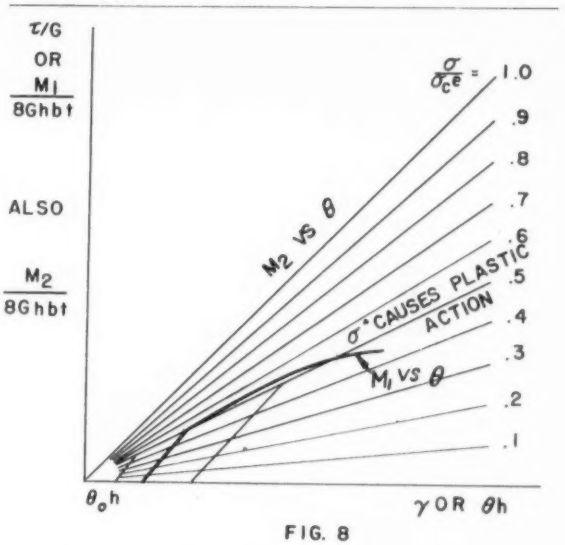

FIG. 8

INITIAL IMPERFECTION IS THE ANSWER

Quantitative Solution for the Maximum Load and the Load Twist Relation

The preceding discussion gives a physical picture of plastic buckling and explains why the buckling stress cannot exceed the yield strength of structural metals by a large amount. Detailed calculations are obtained in more useful form, however, from an equation in σ rather than τ. In terms of $\gamma = \theta h$,

$$\gamma \frac{d\sigma}{d\gamma} + \sigma \left[\frac{\frac{1}{n} + 3\left(\frac{b^2}{3h^2}\right)^2 \gamma^2}{1 + 3\left(\frac{b^2}{3h^2}\right)^2 \gamma^2} \right] = \frac{3h^2}{b^2} \frac{G}{n} \tag{17}$$

when the material is in the plastic range, or

$$2\Psi \frac{d\sigma}{d\Psi} + \sigma \left[\frac{(1/n) + \Psi}{1 + \Psi} \right] = \frac{\sigma_c^e}{n} \tag{18}$$

where $\Psi = (b^4/3h^2)\theta^2$ and $\sigma_c^e = (3h^2/b^2)G$.

The equation for the elastic range is obtained by setting $n = 1$. Any initial twist will be magnified as the compressive stress is increased from 0 to σ^*. For convenience however, the twist at σ^* will be designated by θ_0 and the corresponding value of Ψ by Ψ_0. The smaller true initial twist can be computed if desired, but it is not especially important here.

The solution of Eq. (17) may be written as

$$\sigma = \sigma^* \left(\frac{\Psi_0}{\Psi}\right)^{1/2n} \left(\frac{1 + \Psi_0}{1 + \Psi}\right)^{(n-1)/2n} + \frac{\sigma_c}{2n} \frac{\int_{\Psi_0}^{\Psi} (1 + \zeta)^{(n-1)/2n} \zeta^{(1-2n)/2n} d\zeta}{\Psi^{1/2n}(1 + \Psi)^{(n-1)/2n}} \tag{19}$$

Because Ψ is small compared with unity and Ψ_0 is extremely small, a good approximation to Eq. (19) is

$$\sigma = \frac{\sigma^* \left(\frac{\Psi_0}{\Psi}\right)^{1/2n} + \sigma_c^e \left[1 - \left(\frac{\Psi_0}{\Psi}\right)^{1/2n}\right]}{1 + [(n-1)/2n](\Psi - \Psi_0)} \tag{20}$$

If $\Psi_0 = 0$, $\sigma = \sigma_c^e$; but, for $n = 20$ if $\Psi_0 \neq 0$, then $(\Psi_0/\Psi)^{1/2n}$ is close to unity for extremely large ratios of Ψ/Ψ_0. Large twists therefore occur for small increase of σ over σ^*. The denominator of Eq. (20) then becomes appreciable, and σ decreases as the twist continues to increase.

Fig. 9 is a plot of σ/σ^* vs. Ψ for various Ψ_0 under the same assumption used for illustration in Figs. 7 and 8, $\sigma^*/\sigma_c^e = 1/2$. The value of $n = 20$ has been chosen as reasonable for an aluminum alloy. Interpretation of the results is aided by noting that $\Psi = b^2/12h^2(2b\theta)^2$, of the relative angular rotation of two cross sections a distance apart equal to the approximate overall depth of section, $2b$, is

$$2b\theta = 3.46(h/b)\Psi^{1/2} \text{ rad.} = 20\Psi^{1/2} \text{ deg.}$$

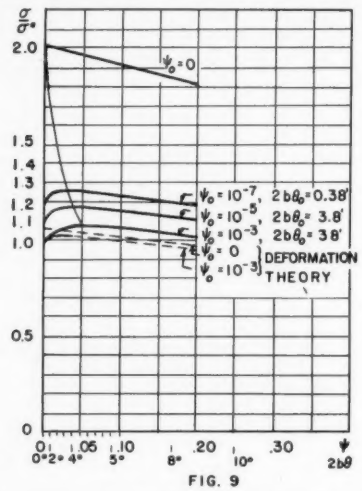

FIG. 9

$2b\theta_0$ IS THE ANGLE OF TWIST IN A LENGTH $2b$ AT $\sigma = \sigma^*$ THE ACTUAL INITIAL TWIST IS THEREFORE ONLY HALF AS LARGE

for h/b close to 1/10. An initial $\Psi_0 = 10^{-3}$ or $2b\theta_0 = 3.8$ min. is small indeed and certainly will exist. The actual initial twist is only half of the magnified value of 3.8 min. As shown in Fig. 9, a change in θ by a factor of 10 produces a change of less than 10 per cent in the critical load. Comparison with deformation theory is also included to show that initial imperfection can, and in all likelihood does, account for the experimental data.

Concluding Remarks

Many practical problems involving maximum compressive loading of actual columns and plates in the linear elastic range can be treated as static buckling problems for perfect elements. A static stability criterion may not be useful, however, for nonlinear problems. This seems to be especially true when the system is nonconservative as well. Apparently a solution of the boundary value problem for an initially imperfect member is often required to obtain the physically proper result. In some cases, however, a dynamic type of criterion may be needed to analyze the effect of lateral or other disturbance.

In this paper it has been shown by use of a simplified cruciform and a simplified stress-strain relation that incremental plasticity theory does lead to proper results when unavoidable initial imperfection of shape is considered. Detailed consideration of the actual cruciform and a more realistic curved stress-strain relation is left for a later paper. However, it is clear that failure by twisting will occur before the yield strength of the material is appreciably exceeded.

Although the predictions of deformation and incremental theory now agree fairly well, it should be noted that it is a somewhat involved function of the tangent modulus which is significant rather than the secant modulus of deformation theory. Special and possibly unrealizable stress-strain curves therefore do exist for which predictions of the two theories would differ widely.

References

[1] Bijlaard, P. P., *Theory and Tests on the Plastic Stability of Plates and Shells*, Journal of the Aeronautical Sciences, Vol. 16, No. 9, pp. 529–541, September, 1949.

[2] Stowell, E. Z., *A Unified Theory of Plastic Buckling of Columns and Plates*, N.A.C.A. T.N. No. 1556, April, 1948.

[3] Stowell, E. Z., *Critical Shear Stress of an Infinitely Long Plate in the Plastic Region*, N.A.C.A. T.N. No. 1681, August, 1948.

[4] Pride, R. A., and Heimerl, G. J., *Plastic Buckling of Simply Supported Compressed Plates*, N.A.C.A. T.N. No. 1817, April, 1949.

[5] Handelmann, G. H., and Prager, W., *Plastic Buckling of a Rectangular Plate Under Edge Thrusts*, N.A.C.A. T.N. No. 1530, 1948.

[6] Pearson, C. E., *Bifurcation Criterion and Plastic Buckling of Plates and Columns*, Journal of the Aeronautical Sciences, Vol. 17, No. 7, pp. 417–424, July, 1950.

[7] Drucker, D. C., *A Discussion of the Theories of Plasticity*, Readers' Forum, Journal of the Aeronautical Sciences, Vol. 16, No. 9, p. 567, September, 1949.

[8] Cicala, P., *On Plastic Buckling of a Compressed Strip*, Readers' Forum, Journal of the Aeronautical Sciences, Vol. 17, No. 6, p. 378, June, 1950.

[9] Cicala, P., *On Plastic Buckling of Plates and a Theory of Plastic Slip*, Readers' Forum, Journal of the Aeronautical Sciences, Vol. 18, No. 4, p. 285, April, 1951.

[10] Peters, R. W., Dow, N. F., and Batdorf, S. B., *Preliminary Experiments for Testing Basic Assumptions of Plasticity Theories*, Proceedings of the Society for Experimental Stress Analysis, Vol. 7, No. 2, pp. 127–140, 1950.

[11] Budiansky, B., Dow, N. F., Peters, R. W., and Shepherd, R. P., *Experimental Studies of Polyaxial Stress-Strain Laws of Plasticity*, Proceedings of the First U.S. National Congress of Applied Mechanics, A.S.M.E., June, 1951.

Thermal Distributions in Jeffery-Hamel Flows Between Nonparallel Plane Walls*

KNOX MILLSAPS† AND KARL POHLHAUSEN‡
Flight Research Laboratory, U.S.A.F.

ABSTRACT

The authors give the exact solution for the thermal distributions for the steady laminar flow of a viscous incompressible fluid between nonparallel plane walls held at a constant temperature. The velocity profiles are determined with the aid of Jacobian elliptic functions by using the Jeffery-Hamel solution of the hydrodynamic problem. It is shown that in this special case the energy equation giving the temperature profiles can be reduced to an ordinary linear differential equation with variable coefficients. After the introduction of dimensionless parameters, numerical solutions are given for diverging and converging channels with total openings of 10° for the possible combinations of three Reynolds Numbers and five Prandtl Numbers.

INTRODUCTION

IT IS WELL KNOWN that the flow of a viscous incompressible fluid between plane parallel plates, the so-called plane Poiseuille flow, is governed by a parabolic velocity distribution. This flow is easily shown to be an exact solution of the Navier-Stokes equations because of the fact that the nonlinear terms vanish identically. For the case of nonparallel plane walls where such fortuitous circumstances do not occur, the exact solution has been found by Jeffery[1] and, independently, by Hamel.[2]

It is the purpose of this paper to give the exact solution and a numerical discussion of the thermal distribution for the Jeffery-Hamel flow under the assumptions of constant fluid density and constant wall temperature.

(1) FORMULATION OF THE HYDRODYNAMICAL PROBLEM

In polar coordinates (r, ϑ) the equations for the velocity components (u, v) for the steady $(\partial/\partial t = 0)$ flow of an incompressible (density ρ = constant) fluid are: continuity,

$$\frac{\partial(ru)}{\partial r} + \frac{\partial v}{\partial \vartheta} = 0 \tag{1.1}$$

momentum,

$$u\frac{\partial u}{\partial r} + \frac{v}{r}\frac{\partial u}{\partial \vartheta} - \frac{v^2}{r} = -\frac{1}{\rho}\frac{\partial p}{\partial r} + \nu\left(\nabla^2 u - \frac{2}{r^2}\frac{\partial v}{\partial \vartheta} - \frac{u}{r^2}\right) \tag{1.2}$$

and momentum,

$$u\frac{\partial v}{\partial r} + \frac{v}{r}\frac{\partial v}{\partial \vartheta} + \frac{uv}{r} = -\frac{1}{\rho r}\frac{\partial p}{\partial \vartheta} + \nu\left(\nabla^2 v + \frac{2}{r^2}\frac{\partial u}{\partial \vartheta} - \frac{v}{r^2}\right) \tag{1.3}$$

where

$$\nabla^2 = \frac{\partial^2}{\partial r^2} + \frac{1}{r}\frac{\partial}{\partial r} + \frac{1}{r^2}\frac{\partial^2}{\partial \vartheta^2}$$

and p and ν denote the pressure and kinematic viscosity, respectively.

If the flow is purely radial, then one may put

$$u = \nu F(\vartheta)/r, \qquad v = 0 \tag{1.4}$$

where $F(\vartheta)$ is termed the dimensionless velocity profile, and one then notes that the terms in Eq. (1.1) vanish identically and that Eqs. (1.2) and (1.3) become, respectively,

$$-\frac{\nu^2 F^2}{r^3} = -\frac{1}{\rho}\frac{\partial p}{\partial r} + \frac{\nu^2 F''}{r^3} \tag{1.5}$$

$$0 = -\frac{1}{\rho r}\frac{\partial p}{\partial \vartheta} + \frac{2\nu^2 F'}{r^3} \tag{1.6}$$

If Eq. (1.5) is multiplied by $r^3\nu^{-2}$, a rearrangement gives

$$(r^3/\rho\nu^2)\,(\partial p/\partial r) = F^2 + F'' \tag{1.7}$$

A partial integration of Eq. (1.6) with respect to ϑ gives

$$p = (2\nu^2\rho F/r^2) + S(r) \tag{1.8}$$

where $S(r)$ is an arbitrary function of r, and a partial differentiation of the resulting Eq. (1.8) with respect to r gives

$$\frac{r^3}{\nu^2\rho}\frac{\partial p}{\partial r} = -4F + \frac{S'r^3}{\rho\nu^2} \tag{1.9}$$

Paper presented before the Eighth International Congress of Theoretical and Applied Mechanics held at Istanbul, Turkey, in August, 1952. Received July, 1952.

* The authors wish to express their gratitude to Mrs. Olga Kay Francis for performing the major portion of the numerical computations on desk calculators; to Capt. Brian T. Hastings for checking some of the calculations with IBM equipment; and to Col. L. B. Williams, Chief, Flight Research Laboratory, Wright Air Development Center, for his active encouragement during the entire period required for this study.

† Consultant in Applied Mechanics.

‡ Research Specialist.

One sees that p as given in Eq. (1.8) is a proper functional relation, provided that $S(r)$ is chosen so that $S'r^3$ is a constant; hence,

$$S(r) = K\rho\nu^2/2r^2 \tag{1.10}$$

where K is a constant.

It is now clear from Eqs. (1.9) and (1.10) that Eqs. (1.5) and (1.6) will be simultaneously satisfied and that a solution to the flow between nonparallel plane walls, $\vartheta = \pm\alpha$, will be obtained, provided that

$$F^2 + 4F + F'' + K = 0 \tag{1.11}$$

with the boundary conditions,

$$F(\pm\alpha) = 0 \tag{1.12}$$

expressing the imperviousness of the walls.

Thus the partial differential equations that formulate the conservation of mass and momentum have been reduced to an ordinary nonlinear differential equation of the second order whose solutions must satisfy in the physical problem under consideration two boundary conditions of vanishing velocity at the walls.

(2) Solution of the Hydrodynamic Problem

After multiplying Eq. (1.11) by $6F'$, an obvious integration yields

$$2F^3 + 12F^2 + 3(F')^2 + 6KF + 2H = 0 \tag{2.1}$$

where $2H$ denotes the integration constant. Solving Eq. (2.1) for $(F')^2$, one gets

$$(F')^2 = (2/3)\,(H - 3KF - 6F^2 - F^3) \tag{2.2}$$

or

$$\vartheta = \left(\frac{3}{2}\right)^{1/2} \int \frac{dF}{(H - 3KF - 6F^2 - F^3)^{1/2}} \tag{2.3}$$

where the integration limits must be determined later from the boundary condition. Thus, it is clear that ϑ is given by an elliptic integral. An evaluation is given by Hamel[2] in terms of the Weierstrassian functions, but, if numerical results are desired, it seems to be more convenient to use Jacobian elliptic functions because of the present availability of a suitable table.[13] The unavailability of an extensive table of elliptic functions appears to be the principal reason that—although the incomplete theoretical solution has been known since 1915—numerically calculated velocity profiles for assigned Reynolds Numbers have been published only for singularly selected values.[6,10,11] Furthermore, Goldstein[10] remarks, "The discussion is hardly yet complete," but, since completing this paper, the authors' attention has been called to a penetrating theoretical analysis of the problem by Rosenhead.[11] However, a direct comparison between his results and those of the present paper is rather difficult because of the different definitions of the Reynolds Number, the use of different notations for elliptic functions, and his use of the convergence and divergence of the channel as a parameter.

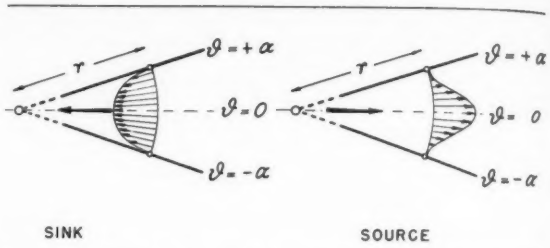

Fig. 1. Schematic diagram of flows in converging and diverging channels.

Assuming that the trinomial in Eq. (2.3) has real roots $e_1 \geqslant e_2 \geqslant e_3$ (the remaining case of one real root is discussed later), one can factor the denominator so that

$$\vartheta = \left(\frac{3}{2}\right)^{1/2} \int \frac{dF}{[(e_1 - F)\,(e_2 - F)\,(e_3 - F)]^{1/2}} \tag{2.4}$$

where

$$e_1 + e_2 + e_3 = -6 \tag{2.5}$$

and the roots are related to the integration constants H and K by

$$e_1e_2 + e_2e_3 + e_1e_3 = 3K \tag{2.6}$$

$$e_1e_2e_3 = H \tag{2.7}$$

It is now necessary to distinguish two different types of flow that are described by Eq. (2.4). The first type is the flow in diverging channels in which it is assumed that a line source with a positive efflux velocity is present at the origin of the diverging channel walls; the second type is the flow in converging channels in which it is assumed that a line sink with a negative influx velocity is located at the intersection of the converging channel walls. Schematic diagrams of these flows are given in Fig. 1. It is convenient to follow the treatment by Hamel,[2] and its excellent review by Goldstein,[10] in the subsequent discussion of the flows in diverging and converging channels.

Case (A) Flows in Diverging Channels

It is clear that in this case $F \geqslant 0$, $e_1 \geqslant 0$, $e_3 \leqslant e_2 \leqslant 0$, $H \geqslant 0$, and $0 \leqslant F \leqslant e_1$ and that

$$\vartheta = \left(\frac{3}{2}\right)^{1/2} \int_F^{e_1} \frac{dF}{[(e_1 - F)\,(F - e_2)\,(F - e_3)]^{1/2}} \tag{2.8}$$

The reduction of this integral to a Jacobian elliptic function is given by

$$\int_F^{e_1} \frac{dF}{[(e_1 - F)\,(F - e_2)\,(F - e_3)]^{1/2}} = \frac{2}{(e_1 - e_3)^{1/2}}\, sn^{-1}\left[\left(\frac{e_1 - F}{e_1 - e_2}\right)^{1/2}, k\right] \tag{2.9}$$

where

$$k^2 = (e_1 - e_2)/(e_1 - e_3) \tag{2.10}$$

Thus,

$$\vartheta = \left(\frac{6}{e_1 - e_3}\right)^{1/2} sn^{-1}\left[\left(\frac{e_1 - F}{e_1 - e_2}\right)^{1/2}, k\right] \tag{2.11}$$

After denoting $[(e_1 - e_3)/6]^{1/2}$ by m, an inversion yields

$$F = e_1 - (e_1 - e_2)\, sn^2(m\vartheta, k) \tag{2.12}$$

The roots may be expressed in terms of m and k, and these expressions are

$$\left.\begin{aligned} e_1 &= 2[m^2(1 + k^2) - 1] \\ e_2 &= 2[m^2(1 - 2k^2) - 1] \\ e_3 &= 2[m^2(k^2 - 2) - 1] \end{aligned}\right\} \tag{2.13}$$

Now, if the velocity along the axial stream line, $\vartheta = 0$, is prescribed to be u_0 and if the Reynolds Number, $R_0 = F_0 = u_0 r/\nu$, is introduced (the case of asymmetric back-flow patterns requires a slight modification), then the fact that $sn(0, k) = 0$ enables one to conclude from Eqs. (2.12) and (2.13) that

$$R_0 = e_1 = 2[m^2(1 + k^2) - 1] \tag{2.14}$$

or

$$m = \{[1 + (R_0/2)]/(1 + k^2)\}^{1/2} \tag{2.15}$$

Thus, the velocity profile is given by

$$F(\vartheta) = R_0 - 6m^2k^2sn^2(m\vartheta, k) \tag{2.16}$$

and, since the boundary condition (1.12) must be satisfied, it follows that

$$R_0 = 6m^2k^2sn^2(m\alpha, k) \tag{2.17}$$

It is clear that the elimination of m from Eqs. (2.15) and (2.17) yields an equation determining k; this transcendental equation is

$$\frac{1 + k^2}{3k^2[1 + (2/R_0)]} = sn^2\left\{\left[\frac{1 + (R_0/2)}{1 + k^2}\right]^{1/2}\alpha, k\right\} \tag{2.18}$$

which is most easily solved by graphical means.

Thus, if the divergence α and the Reynolds Number R_0 are specified, k may be found as a root of the transcendental Eq. (2.18), and m may be obtained from Eq. (2.15). The velocity profile may then be calculated from Eq. (2.16).

As was previously noted in Eq. (2.4), it is possible that the trinomial in the denominator on the right side of Eq. (2.3) has one real root e_1 and that the remaining two roots, e_2 and e_3, are conjugate complex numbers,

$$e_2 = a + bi, \qquad e_3 = a - bi$$

In this case Eq. (2.4) becomes

$$\vartheta = \left(\frac{3}{2}\right)^{1/2} \int_F^{e_1} \frac{dF}{[(e_1 - F)\,(F^2 - 2aF + a^2 + b^2)]^{1/2}} \tag{2.19}$$

Now, since $e_1 + e_2 + e_3 = -6$, it follows that

$$a = -[3 + (e_1/2)] \tag{2.20}$$

If one introduces the following notations,

$$e_1^2 - 2ae_1 + a^2 + b^2 = q^2 \tag{2.21}$$

$$\frac{q + e_1 - a}{2q} = \frac{3 + q + (3e_1/2)}{2q} \equiv k^2 \tag{2.22}$$

then a familiar transformation of elliptic integrals gives

$$\int_F^{e_1} \frac{dF}{[(e_1 - F)\,(F^2 - 2aF + a^2 + b^2)]^{1/2}} = \frac{1}{q^{1/2}}\, cn^{-1}\left(\frac{q - e_1 + F}{q + e_1 - F}, k\right) \tag{2.23}$$

The combination of Eqs. (2.19) and (2.23) yields

$$\frac{q - e_1 + F}{q + e_1 - F} = cn\left[\left(\frac{2q}{3}\right)^{1/2}\vartheta, k\right] \tag{2.24}$$

If, as in the case with real roots, one prescribes that $F(0) = R_0$, then, since $cn(0, k) = 1$, it follows that

$$e_1 = R_0 \tag{2.25}$$

Since the boundary conditions require $F(\alpha) = 0$, one has

$$\frac{q - R_0}{q + R_0} = cn\left[\left(\frac{2q}{3}\right)^{1/2}\alpha, k\right] \tag{2.26}$$

The substitution of Eq. (2.25) into Eq. (2.22) gives

$$q = 3[1 + (R_0/2)]/(2k^2 - 1) \tag{2.27}$$

The determination of k can now be made by introducing q from Eq. (2.27) into Eq. (2.26) and solving the resulting transcendental equation,

$$\frac{6 + R_0(5 - 4k^2)}{6 + R_0(1 + 4k^2)} = cn\left[\left(\frac{2 + R_0}{2k^2 - 1}\right)^{1/2}\alpha, k\right] \tag{2.28}$$

If a solution for k is known, then q may be calculated from Eq. (2.27). Subsequently, the velocity profile may be calculated from Eq. (2.24), and it is found to be

$$F(\vartheta) = \frac{R_0 - q + (R_0 + q)\, cn\,[(2q/3)^{1/2}\vartheta, k]}{1 + cn\,[(2q/3)^{1/2}\vartheta, k]} \tag{2.29}$$

At this point it is interesting to consider several particular examples of diverging flows.

Example (1): Flows with Low Reynolds Number in Channels of Small Divergence.—In this instance the elliptic function sn in Eq. (2.16) reduces to its argument, and the velocity profile is given by

$$F(\vartheta) = R_0 - 6m^4k^2\vartheta^2$$

The boundary condition yields

$$R_0 = 6m^4k^2\alpha^2$$

hence,

$$F(\vartheta) = R_0[1 - (\vartheta^2/\alpha^2)]$$

which is the familiar parabolic velocity distribution for plane Poiseuille flow.

Example (2): Flows Having Unitary Elliptic Modularity.—If $k = 1$, it follows from Eq. (2.15) that

$$m = \left[\frac{2 + \bar{R}_0}{4}\right]^{1/2} \approx \frac{\bar{R}_0^{1/2}}{2}$$

Moreover, it is well known that for unitary modulus the elliptic function $sn(m\vartheta, 1)$ degenerates into tanh $m\vartheta$ so that

$$F(\vartheta) = \bar{R}_0\left(1 - \frac{\tanh^2 m\vartheta}{\tanh^2 m\alpha}\right) \approx \bar{R}_0\left(1 - \frac{\tanh^2 \frac{\bar{R}_0^{1/2}\vartheta}{2}}{\tanh^2 \frac{\bar{R}_0^{1/2}\alpha}{2}}\right)$$

where from Eq. (2.18)

$$\bar{R}_0 = \frac{4}{\alpha^2}\left[\tanh^{-1}\left(\frac{2}{3}\right)^{1/2}\right]^2 \approx \frac{5.232}{\alpha^2}$$

Example (3): Flows with Vanishing Inclination at the Channel Walls.—It is easily seen from Eq. (2.2) that

$$F'(\alpha) = \left(\frac{2H}{3}\right)^{1/2} = \left(\frac{2e_1e_2e_3}{3}\right)^{1/2}$$

and, if this is to vanish, then at least one of the roots must be zero. It is convenient to take $e_2 = 0$, and with this choice Eq. (2.13) shows that

$$m = [1/(1 - 2k^2)]^{1/2}$$

Since $0 \leqslant k \leqslant 1$, a critical comparison with Eq. (2.15) enables one to conclude that

$$k^2 \approx 1/2, \qquad m \approx (\bar{R}_0/3)^{1/2}$$

In this example it is clear that Eq. (2.12) reduces to

$$sn^2(m\alpha, k) = 1$$

Since sn is a periodic function, this equation is satisfied when

$$m\alpha = nK(k) \approx \alpha(\bar{R}_0/3)^{1/2}$$

where $K(k)$ denotes the complete elliptic integral of the first kind and n is an odd integer. When $k^2 = 1/2$, $K(k) = 1.85407$, and therefore for $n = 1$ one has

$$\alpha(\bar{R}_0)^{1/2} \approx 3^{1/2}K \approx 3.211$$

From these considerations it follows that the first Reynolds Number having zero slope at the walls is given by

$$\bar{R}_0 \approx (3.211/\alpha)^2 \approx 2\bar{R}_0$$

where $\bar{R}_0$ denotes the Reynolds Number of the flow having unitary elliptic modularity. The velocity profile is easily calculated by appropriate substitution in Eq. (2.16).

Example (4): Flows with Large Reynolds Numbers.—As the Reynolds Number of the diverging flow becomes larger than the Reynolds Number corresponding to zero slope at the walls, the computation of the corresponding velocity profiles for the larger Reynolds Numbers shows that a region of back flow appears along each wall. As the Reynolds Number increases to still larger values, positive jets, in addition to the back-flow regions, will appear along each wall. This process continues with an increasing number of back-flow regions and positive jets appearing in a symmetrical distribution about the main flow. However, it should be noted that, since between each forward jet and each back-flow region there is a point in the profile with zero velocity, at this point a wall could be placed leading to asymmetrical velocity profiles with the possible number of asymmetrical configurations increasing in the directly obvious manner with increasing Reynolds Number.

Moreover, at sufficiently large Reynolds Numbers it is found that the transcendental Eq. (2.18) has multiple roots. Each member of the set of solutions corresponding to a definite Reynolds Number leads to a possible symmetrical profile with back-flow regions and positive jets. As the Reynolds Numbers increase, so do the number of solutions of Eq. (2.18), although it should be noted that the number remains finite. The asymmetrical profiles may be constructed by the previously outlined procedure.

Case (B) Flows in Converging Channels

In this case it is easily seen that $F \leqslant 0$ and that the roots are real with $e_1 \geqslant 0$ and $0 \geqslant e_2 \geqslant e_3$. Further, one notes that $0 \geqslant F \geqslant e_2$, and, consequently, from Eq. (2.4) it follows that

$$\vartheta = \left(\frac{3}{2}\right)^{1/2}\int_{e_3}^{F} \frac{dF}{[(e_1 - F)(F - e_2)(F - e_3)]^{1/2}} \tag{2.30}$$

An application of a standard reduction formula for elliptic integrals gives

$$\vartheta = \frac{1}{m}\,dn^{-1}\left[\left(\frac{e_2 - e_3}{F - e_3}\right)^{1/2}, k\right] \tag{2.31}$$

The reduction for F gives

$$F = e_3 + (e_2 - e_3)\,dn^{-2}(m\vartheta, k) \tag{2.32}$$

or, in terms of m and k, one has

$$F = 2[m^2(k^2 - 2) - 1] + 6m^2(1 - k^2)\,dn^{-2}(m\vartheta, k) \tag{2.33}$$

If one introduces the Reynolds Number R_0 as the velocity along the axial streamline, one sees that

$$R_0 = F_0 = e_2 \tag{2.34}$$

$$m^2 = [1 + (R_0/2)]/(1 - 2k^2) \tag{2.35}$$

The imposition of the boundary condition $F(\pm\alpha) = 0$ yields a transcendental determination of k,

$$dn^2(m\alpha, k) = 1 - R_0/e_3 \tag{2.36}$$

TABLE 1
Diverging Flows

R_0	k^2	m^2	e_1	e_2	e_3	$F'(\alpha)$
684	1.000	171.5	684	−345	−345	−7,367
1,342	0.4989	448.3	1,342	0	−1,348	0
5,000	0.745	1,393.3	5,000	−1,646	−3,360	135.8×10^3

or, since $dn^2x = 1 - k^2sn^2x$, a substitution for e_3 from Eq. (2.13) gives

$$sn^2(m\alpha, k) = \frac{R_0(1 - 2k^2)}{2k^2[3k^2 - 3 + (R_0/2)(k^2 - 2)]} \quad (2.37)$$

For extremely large Reynolds Numbers, Eq. (2.37) reduces to

$$sn^2(m\alpha, k) \approx \frac{1 - 2k^2}{k^2(k^2 - 2)} \quad (2.38)$$

If the value of k which is determined by solving either Eq. (2.37) or (2.38) is inserted into Eq. (2.35) and if this value of m and the value of k are substituted into Eq. (2.33), the velocity profile for a prescribed Reynolds Number may easily be calculated.

It is interesting to consider several particular examples of flow in converging channels.

Example (1): Flows at Low Reynolds Numbers in Channels of Small Convergence.—For small R_0 and α, the series development for $dn(x, k)$ shows that

$$dn(x, k) \approx 1 - (k^2x^2/2) \quad (2.39)$$

$$dn^{-2}(x, k) \approx 1 + k^2x^2 \quad (2.40)$$

The substitution of approximation (2.39) into Eq. (2.36) gives

$$e_3 \approx R_0/m^2\alpha^2k^2 \quad (2.41)$$

and the further substitutions of Eq. (2.34) and approximations (2.40) and (2.41) into Eq. (2.32) give

$$F = R_0[1 - (\vartheta^2/\alpha^2)] \quad (2.42)$$

which is the familiar parabolic velocity distribution of plane Poiseuille flow.

Example (2): Flows with Large Reynolds Numbers.—For large R_0, a critical study of Eq. (2.35) and approximation (2.38) shows that $k \approx 1$ and $m^2 \approx R_0/2$; hence $e_2 \approx e_3$, and the integral in Eq. (2.30) can then be evaluated in terms of hyperbolic functions. If this evaluation is made, one obtains a familiar result due to Pohlhausen:[4]

$$F = R_0\left\{3\tanh^2\left[\left(\frac{R_0}{2}\right)^{1/2}(\alpha - \vartheta) + \tanh^{-1}\left(\frac{2}{3}\right)^{1/2}\right] - 2\right\} \quad (2.43)$$

Example (3): Profiles with Back Flows.—The transcendental Eq. (2.37) that determines the elliptic modularity of the converging flows has multiple roots—in fact, a denumerable infinitude. The largest value of k leads to the normal symmetrical profile, and each of the remaining values leads to a symmetrical profile with jets and back-flow regions. It should also be noted that asymmetrical profiles may be constructed for converging in exactly the same manner as in the case of diverging flows. This infinitude of possible profiles was first noted by Rosenhead.[11]

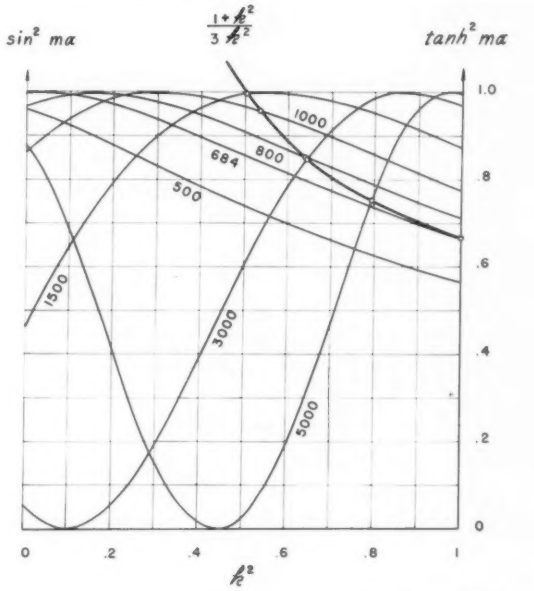

FIG. 2. Graphical solution of the transcendental equation for k.

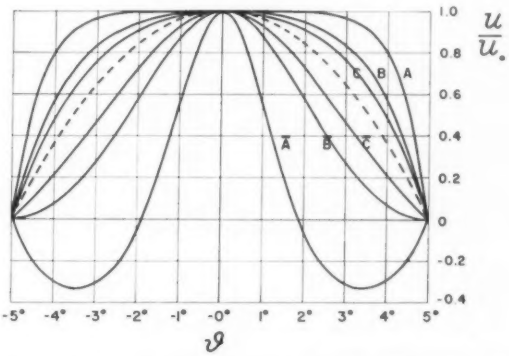

FIG. 3. Numerical values for the velocity profiles. The broken line is the Poiseuille parabola. The convex profiles are converging flows with (A): $R = 5{,}000$, (B): $R = 1{,}342$, and (C): $R = 684$; the concave profiles are diverging flows with ($\bar{A}$): $R = 5{,}000$, ($\bar{B}$): $R = 1{,}342$, and ($\bar{C}$): $R = 684$.

TABLE 2
Converging Flows

R_0	k^2	m^2	e_1	e_2	e_3	$F'(\alpha)$
−684	0.9457	382.5	1,486.5	−684	−808.5	$2{,}341 \times 10$
−1,342	0.9835	692.8	2,746	−1,342	−1,410	$5{,}887 \times 10$
−5,000	0.9998	2,500	9,997	−5,000	−5,003	$4{,}083 \times 10^2$

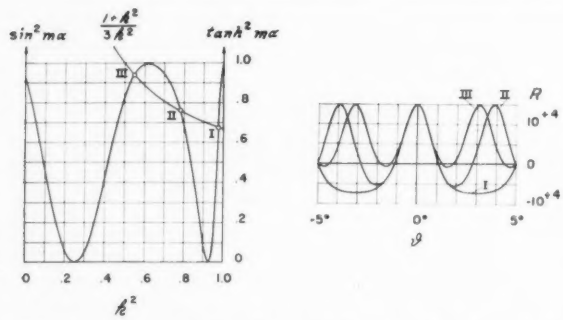

FIG. 4. A numerical example for a diverging flow with R = 15,000 showing the determination of the three possible values for k and the complete set of associated profiles.

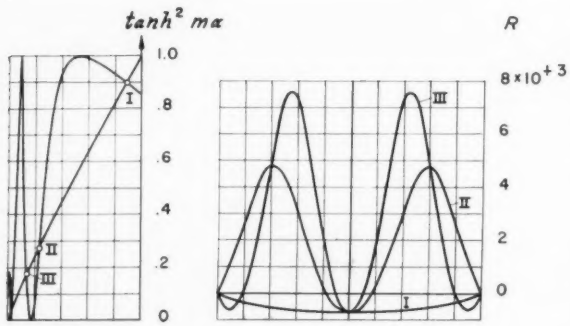

FIG. 5. A numerical example for a converging flow with R = 684 showing the determination of k and the associated profiles for the first three of the infinite number of possible solutions.

Numerical Examples

In addition to the general examples previously considered in this section, it is instructive to consider a few specific examples of the procedure for obtaining numerical values for the velocity profiles. In the following numerical examples, a total angle of 10° has been chosen for the divergence or convergence of the fixed walls.

With the prescribed divergence and for the diverging solution, the Reynolds Number that corresponds to unitary elliptic modularity is 684. One also finds that the Reynolds Number corresponding to a profile with zero slope at the walls is 1,342. As a third case, a velocity profile that has back-flow phenomena is given; a sufficiently large Reynolds Number to illustrate these phenomena is 5,000. Fig. 2 is a graph showing the transcendental determination of k—i.e., Eq. (2.18) One sees that the $sn^2(m\alpha, k)$ curve intersects the curve

$$\frac{1 + k^2}{3k^2[1 + (2/R_0)]}$$

at $k = 1$ when $R_0 = 684$. From this value, k decreases (as R_0 increases) until k^2 reaches approximately 0.5 when $R_0 = 1{,}342$. For still larger Reynolds Numbers, k again increases. The pertinent data for the three chosen examples are contained in Table 1.

Fig. 3 gives the velocity profiles F/R_0 or, equivalently, u/u_0. An obvious inspection shows that each of these profiles is more sharply curved in the middle of the channel than the Poiseuille parabola, which is valid for parallel flows. It is to be noted that all of the profiles have inflection points. The velocity profile for the highest Reynolds Number is particularly interesting, since it exhibits two back-flow regions. Further, one sees that F vanishes at four points across the profile and that walls may be placed at any of these points giving flows with two symmetrical back-flow regions with a total divergence of 10° or an asymmetrical flow (or its mirror image) with one back-flow region with a total divergence of 6.9°.

In order that comparisons may be made, velocity profiles for flows in converging channels have been calculated for the same set of Reynolds Numbers and the same amount of convergence as divergence in the numerical examples that were previously discussed. The pertinent data for these converging flows are given in Table 2. The corresponding velocity profiles are given in Fig. 3. It should be noted that the profiles are flatter in the middle than the Poiseuille parabola and that the profiles have no inflection points.

As numerical examples of flows with a multiplicity of possible profiles, the three possible profiles for a diverging flow with Reynolds Number of 15,000 are given in Fig. 4, together with a graph showing the transcendental determination of k in this case, and the first three profiles of the possible infinitude for the converging flow with a Reynolds Number of 684 are given in Fig. 5, together with the associated determination of k for this case. It should be noted that in some cases of converging channels considered here the total flow is an efflux.

In concluding this section on the hydrodynamic problem of the flow between nonparallel walls, many important conjectures can be made and many interesting questions can be asked on the bearing of the existence of jets and back-flow regions on the problem of hydro-

dynamic stability and on the possibilities of studying turbulence by examining in greater detail the multiplicity of possible solutions of the Navier-Stokes equations.

(3) Formulation of the Thermodynamic Problem

The continuity Eq. (1.1) and the two Eqs. (1.2) and (1.3) for the momenta formulate the hydrodynamic problem of the flow through diverging or converging channels. To determine the thermal distribution within the channels it is necessary to solve the equation resulting from the substitution of the solution of the hydrodynamic problem into the energy equation. Expressing the differential equation in terms of the previously used symbolism and denoting the temperature of the fluid by t, the energy equation is known to be

$$c_v\left(u\frac{\partial t}{\partial r}+\frac{v}{r}\frac{\partial t}{\partial \vartheta}\right)=\frac{\kappa}{\rho}\left(\frac{\partial^2 t}{\partial r^2}+\frac{1}{r}\frac{\partial t}{\partial r}+\frac{1}{r^2}\frac{\partial^2 t}{\partial \vartheta^2}\right)+ \nu\left(2e_{rr}^2+2e_{\vartheta\vartheta}^2+e_{r\vartheta}^2\right) \quad (3.1)$$

where c_v is the specific heat expressed in mechanical mass units, κ is the thermal conductivity, and the components of the strain tensor are given by

$$\left.\begin{aligned} e_{rr} &= \partial u/\partial r \\ e_{\vartheta\vartheta} &= \frac{1}{r}\frac{\partial v}{\partial \vartheta}+\frac{u}{r} \\ e_{r\vartheta} &= \frac{1}{r}\frac{\partial u}{\partial \vartheta}+\frac{\partial v}{\partial r}-\frac{v}{r} \end{aligned}\right\} \quad (3.2)$$

In a closely analogous manner to the analysis used by Jeffery and Hamel in obtaining the hydrodynamic solution, it is found that the partial differential equation, Eq. (3.1), can be reduced to an ordinary differential equation by using the Jeffery-Hamel transformation, Eq. (1.4), together with a transformation

$$t=[g(\vartheta)/r^2]+t_w \quad (3.3)$$

where t_w is the constant temperature of the walls. This reduction yields

$$-2\nu c_v Fg=\frac{\kappa}{\rho}(4g+g'')+\nu^3(4F^2+F'^2) \quad (3.4)$$

and, upon introducing the Prandtl Number, $\sigma = \rho\nu c_v/\kappa$, and the dimensionless function, $G = c_v g/\nu^2$, a further reduction gives

$$G''+(4+2\sigma F)G+\sigma(4F^2+F'^2)=0 \quad (3.5)$$

If one wishes to determine the thermal distributions within a channel of total opening 2α, then the solution of Eq. (3.5) must satisfy the boundary conditions

$$G(\pm\alpha)=0 \quad (3.6)$$

and it is clear that the dimensionless temperature, $T = (c_v/u_0^2)t$, is given by

$$T=(G/R_0^2)+T_w \quad (3.7)$$

where R_0 is the previously defined Reynolds Number and T_w is the dimensionless wall temperature. In the case of symmetrical profiles, it is advantageous in performing numerical calculations to replace the boundary conditions (3.6) by

$$G'(0)=0, \qquad G(\alpha)=0 \quad (3.8)$$

(4) Solutions of the Thermodynamic Problem

Eq. (3.5) is an ordinary linear differential equation of the second order in normal form; it is an example of the generalized Lamé equation that is usually treated in studies on ellipsoidal harmonics. However, since the homogeneous part has a variable coefficient containing the square of an elliptic function and since the excitation is a complicated combination of elliptic functions, the analytical integration is not simple even in the exceptionally solvable instances due principally to Lamé, Hermite, and Halphen.[12] Although the analytical solution is known only for certain cases, some special instances are treated to illustrate nontrivial solutions of the energy equation in finite form.

In accordance with the general theory of linear differential equations, it is possible to obtain the solution for the homogeneous equation and then to treat the problem of the inhomogeneous equation by the method of the variation of parameters. Following this procedure, it is convenient to consider the case of diverging flows in some detail and then to indicate the result for converging flows. It is easily seen from Eqs. (2.16) and (3.5) that the homogeneous Lamé equation for diverging flows is

$$G''+[4+12\sigma m^2k^2sn^2(m\alpha,k)- 12\sigma m^2k^2sn^2(m\vartheta,k)]G=0 \quad (4.1)$$

The most general instance of this equation which has been treated is the case when

$$12\sigma m^2=n(n+1) \quad (4.2)$$

where n is a positive integer. In this case the solution given by Hermite[12] is

$$\left.\begin{aligned} G &= A\prod_{r=1}^{n}\left\{\frac{\mathrm{H}(\vartheta+\vartheta_r)}{\Theta(\vartheta)}\exp\left[-\vartheta Z(\vartheta_r)\right]\right\}+ \\ &\quad B\prod_{r=1}^{n}\left\{\frac{\mathrm{H}(\vartheta-\vartheta_r)}{\Theta(\vartheta)}\exp\left[\vartheta Z(\vartheta_r)\right]\right\} \\ &= AG_1+BG_2 \end{aligned}\right\} \quad (4.3)$$

provided that the solutions are not doubly periodic, that $\mathrm{H}(\vartheta)$, $\Theta(\vartheta)$, and $Z(\vartheta)$ are the principal Jacobian functions, and that the ϑ_r are determined from the $n+1$ independent equations comprised in the system:

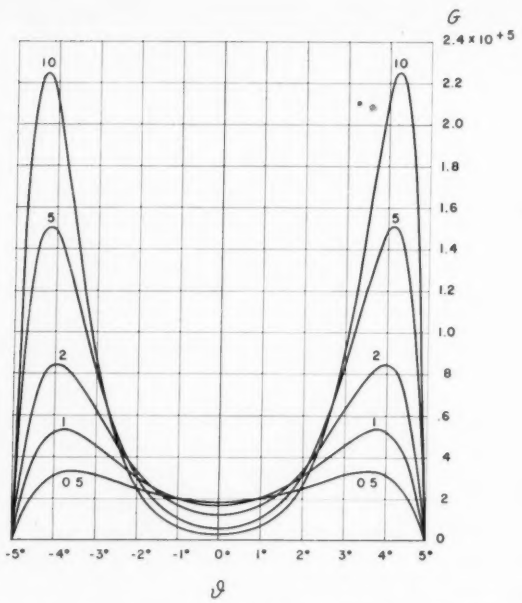

FIG. 6. The thermal distributions in a converging channel of total opening of 10° for a flow with $R = 684$ for parametric values of the Prandtl Number. Only the normal solution is shown.

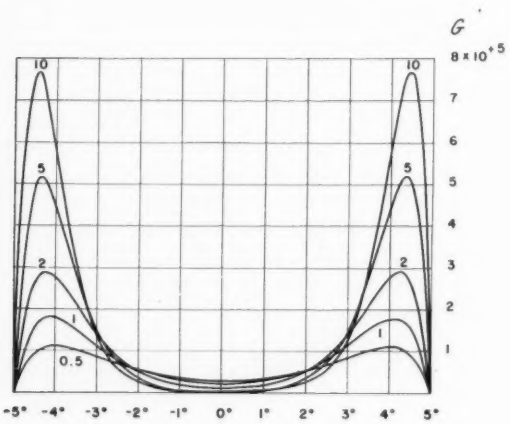

FIG. 7. The thermal distributions in a converging channel of total opening of 10° for a flow with $R = 1{,}342$ for parametric values of the Prandtl Number. Only the normal solution is shown.

for $i = 1,2, \ldots, n$,

$$\left.\begin{aligned} &\sum_{r=1}^{n}{}' \frac{sn\vartheta_r\, cn\vartheta_r\, dn\vartheta_r + sn\vartheta_i\, cn\vartheta_i\, dn\vartheta_i}{sn^2\vartheta_r - sn^2\vartheta_i} = 0 \\ &\left[\sum_{r=1}^{n} cn\vartheta_r\ \ ds\vartheta_r\right]^2 - \\ &\sum_{r=1}^{n} ns^2\vartheta_r + 4 + n(n+1)k^2sn^2(m\alpha, k) = 0 \end{aligned}\right\} \quad (4.4)$$

where $\sum_r{}' f(i)$ denotes summation excluding the term $r = i$. Having the solution for the homogeneous equation, one uses the method of the variation of parameters to obtain the general solution,

$$G = \sigma G_2 \int \frac{G_1(4F^2 + F'^2)}{G_1G_2' - G_1'G_2}\, d\vartheta - \sigma G_1 \int \frac{G_2(4F^2 + F'^2)}{G_1G_2' - G_1'G_2}\, d\vartheta + AG_1 + BG_2 \quad (4.5)$$

An almost completely similar analysis may be made for the case of converging flows after a standard transformation from *dn* to *sn* functions and a change of modulus have been made in Eq. (2.33) so that the associated energy equation has been reduced to an ordinary Lamé equation.

The case when $[-2 \pm m(3\sigma)^{1/2}]/2$ is integral may also be treated for certain specific Reynolds Numbers.[12]

Although a general analytical solution has been given for certain specific parametric values of the Reynolds and Prandtl Numbers, the result is so complicated and involves so much additional computation in the solution of the auxiliary equations that it appears advisable to use numerical methods *ab initio*.

One of the more desirable procedures appears to be the method of finite differences. In using this method, Eq. (3.5) is rewritten in the abbreviated form,

$$-y'' + P(\vartheta)y = Q(\vartheta) \quad (4.6)$$

One then approximates this equation with the following finite difference scheme:[14]

$$Y_{i+1} - 2Y_i + Y_{i-1} - \frac{h^2}{12}(Y_{i+1}'' + 10Y_i'' + Y_{i-1}'') = 0 \quad (4.7)$$

where

$$Y_i'' = PY_i - Q_i \quad (4.8)$$

h is the interval width, and i is a free index varying over

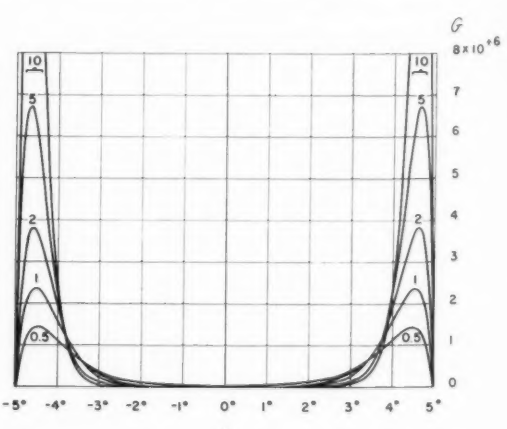

FIG. 8. The thermal distribution in a converging channel of total opening of 10° for a flow with $R = 5{,}000$ for parametric values of the Prandtl Number. Only the normal solution is shown.

the range $1,2, \ldots, n-1$, and a subscript denotes the value of the indicated functions at $\vartheta = \alpha i/2n$ for symmetrical profiles (obvious adjustments can be made in the case of asymmetrical profiles). This difference scheme is not the usual one, but it is a more refined method where the first neglected term in the Taylor expansion has a magnitude $h^4 Y_0^{vi}/20$. The substitution of Eq. (4.8) into Eq. (4.7) gives

$$Y_{i+1}\left[1 - \frac{h^2}{12} P_{i+1}\right] - Y_i\left[2 + \frac{5h^2}{6} P_i\right] + Y_{i-1} \times \left[1 - \frac{h^2}{12} P_{i-1}\right] = -\frac{h^2}{12}\left[Q_{i+1} + 10Q_i + Q_{i-1}\right] \quad (4.9)$$

for $i = 1, \ldots, n-1$, and the boundary conditions (3.6) become

$$Y_n = 0 \quad (4.10)$$

Since each ordinate is a function of the ordinates adjacent to it, the successive numerical evaluations of Eq. (4.9) lead to the following set:

$$Y_{i+1} = a_{i+1} + b_{i+1} Y_i \quad (4.11)$$

for $i = 1,2, \ldots, n-1$, and the imposition of Eq. (4.10) on the member of set (4.11) for which $i = n-1$ leads to the complete determination of the Y_i and the numerical solution of the energy equation.

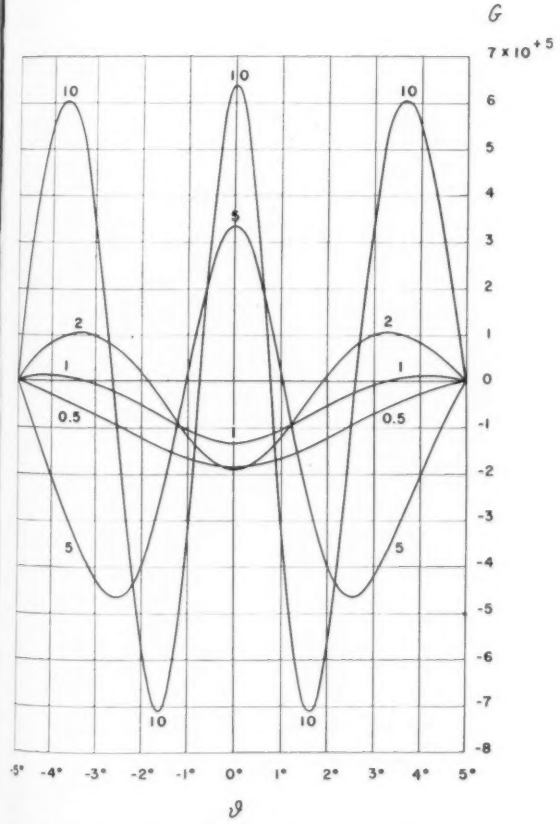

FIG. 9. The thermal distribution in a diverging channel of total opening of 10° for a flow with $R = 684$ for parametric values of the Prandtl Number.

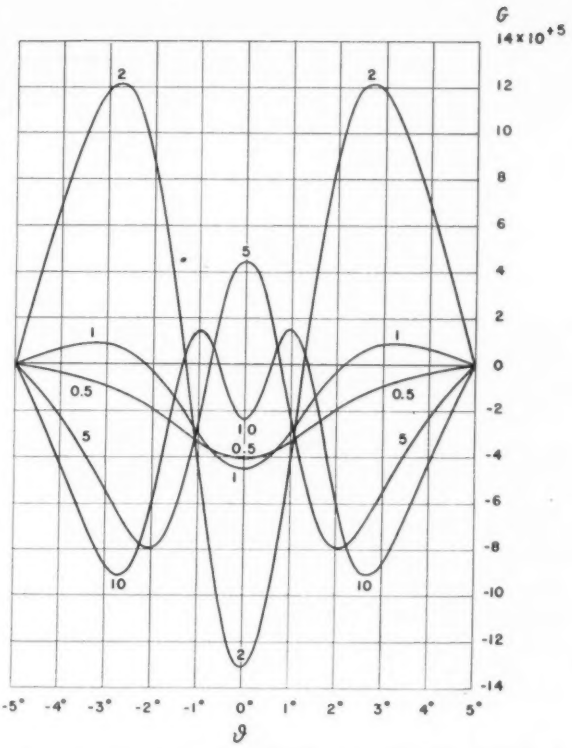

FIG. 10. The thermal distributions in a diverging channel of total opening of 10° for a flow with $R = 1{,}342$ for parametric values of the Prandtl Number.

Eq. (3.5) has been solved by the outlined method of finite differences for five Prandtl Numbers (0.5, 1, 2, 5, and 10) and for the normally symmetrical profiles for three Reynolds Numbers (684, 1,342, and 5,000). The numerical results are given in Figs. 6–11.

The thermal profiles for the normal solutions of converging flows in Figs. 6–8 have similiar properties—a definite thermal boundary-layer behavior with rapid increases to a maximum temperature occurring near the walls and an almost constant distribution across the remainder of the channel with a minimum temperature along the channel axis.

The characteristic behavior in diverging channels, Figs. 9–11, is quite different. The thermal distributions contain oscillations with maxima and minima above and below the wall temperature and with their number depending on the Prandtl Number of the fluid and the number of fundamental flow regions in the hydrodynamic profiles. For certain critical Prandtl Numbers, there exist points within the channel where the temperature becomes infinite with the sign of the temperature changing upon passing through the critical Prandtl Numbers. The variation of the profiles with Prandtl Number is similiar to the stability phenomena in solutions of the Mathieu equation. The reader

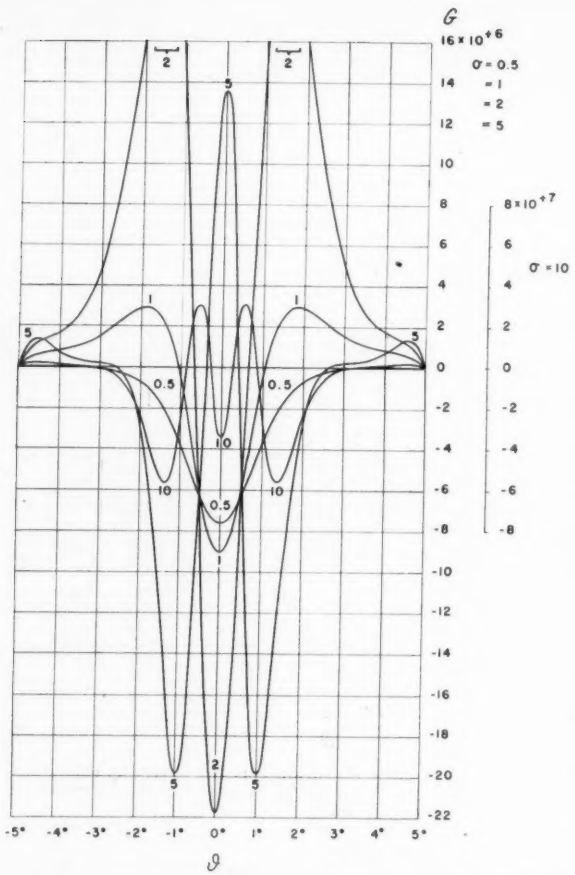

FIG. 11. The thermal distribution in a diverging channel of total opening of 10° for a flow with $R = 5{,}000$ for parametric values of the Prandtl Number.

should note the incompatibility of the assumed incompressibility of the fluid and the extreme values of temperature in the profiles.

In view of these theoretical conclusions, a comparison between the theoretical predictions and experimental data obtained from interferograms of the real behavior of the laminar flow in channels with a constant wall temperature should prove to be highly interesting.

REFERENCES

[1] Jeffery, G. B., *Steady Motion of a Viscous Fluid*, Phil. Mag., Ser. 6, Vol. 29, p. 455, 1915.

[2] Hamel, G., *Spiralförmige Bewegungen zäher Flssigükeiten*, Jahresbericht der Deutschen Math. Vereinigung, Vol. 25, p. 34, 1916.

[3] Harrison, W. J., *The Pressure in a Viscous Liquid Moving Through a Channel with Diverging Boundaries*, Proc. Camb. Phil. Soc., Vol. 19, p 307, 1919.

[4] Pohlhausen, K., *Zur näherungsweisen Integration der Differentialgleichung der Grenzschicht*, Zeitschrift für angew. Math. u. Mech., Vol. 1, p. 252, 1921.

[5] von Kármán, Th., *Vorträge aus dem Gebiet der Hydro- und Aerodynamik, Innsbruck 1922*, p. 150; Julius Springer, Berlin, 1924.

[6] Tollmien, W., *Handbuch der Experimentalphysik*, Vol. 4, p. 257; Akademische Verlagsgesellschaft, Leipzig, 1931.

[7] Noether, F., *Handbuch der physikalischen und technischen Mechanik*, Vol. 5, p. 733; Ambrosius Barth, Leipzig, 1931.

[8] Rosenblatt, A., *Sur certains mouvements plans des liquides visqueux*, Bulletin des sciences math., Vol. 55, p. 175, 1931.

[9] Dean, W. R., *Note on the Divergent Flow of Fluids*, Phil. Mag., Ser. 7, Vol. 18, p. 759, 1934.

[10] Goldstein, S., *Modern Developments in Fluid Dynamics*, Vol. 1, p. 105; Oxford, 1938.

[11] Rosenhead, L., *The Steady Two-Dimensional Radial Flow of Viscous Fluid Between Two Inclined Walls*, Proc. Roy. Soc. London, Vol. 175, p. 436, 1940.

[12] Whittaker, E. T., and Watson, G. N., *A Course of Modern Analysis*, 4th Ed., Chapt. XXIII, pp. 536–578; Cambridge, 1935.

[13] Milne-Thomson, L. M., *Jacobian Elliptic Function Tables*; Dover, New York, 1950.

[14] Collatz, L., *Numerische Behandlung von Differentialgleichungen*, p. 122; Julius Springer, Berlin, 1951.

Quadruple Velocity Correlations and Pressure Fluctuations in Isotropic Turbulence*†

MAHINDER S. UBEROI‡
The Johns Hopkins University

SUMMARY

It is shown that the correlation of fluctuating static pressure (in an incompressible and homogeneous turbulence) with any fluctuating quantity in the flow field can be expressed in terms of the correlation of the same quantity with two or more components of the velocity.

The correlations of pressure with itself are investigated in detail for the case of isotropic turbulence. These correlations can be expressed in terms of correlations involving two velocity components at a point and two velocity components at another point. A postulated relation between the fourth-order and second-order correlations is investigated. This relation is satisfied, for example, if the joint probability density of the four components of velocity is Gaussian. The consequences of this relation are compared with the measurements of the fourth-order correlations.

The root mean square (r.m.s.) pressure and pressure gradients are computed from second-order correlation for a range of turbulence Reynolds Numbers. Since the pressure gradient is related to diffusion of marked particles from a source, the computed pressure gradient level is compared with that calculated from a set of diffusion measurements.

INTRODUCTION

ALTHOUGH in isotropic turbulence the dynamical (correlation) equation does not contain any pressure correlations, the correlation of pressure with itself is of interest in turbulent diffusion and in the study of sound generation by turbulence (for very low Mach Numbers of turbulence velocities when there is little effect of sound on the turbulent field—i.e., only a slight amount of energy is drained away from the turbulent energy in the form of sound waves). The static pressure fluctuations are also intimately connected with the onset of cavitation in turbulent flow of liquids.

The pressure gradient fluctuation, in connection with diffusion in isotropic turbulence, was first considered by Taylor.[1] He postulated that $(1/\rho^2)\,\overline{(\partial p/\partial x_1)^2}$ is of the order $\overline{U_1^2(\partial U_1/\partial x_1)^2}$, independent of Reynolds Number of turbulence. Heisenberg[2] later derived, from detailed spectral considerations, an expression for $\overline{(\partial p/\partial x_1)^2}$,

$$\frac{1}{\rho^2}\overline{\left(\frac{\partial p}{\partial x_1}\right)^2} \cong \overline{U_1^2}\,\overline{\left(\frac{\partial U_1}{\partial x_1}\right)^2}\Big/0.13R_\lambda$$

where $R_\lambda = \overline{U_1^2}/\nu\sqrt{\overline{(\partial U_1/\partial x_1)^2}}$ is the Reynolds Number of turbulence and the symbols have the usual meaning.

Obukhov[3] derived an expression for the pressure correlation for distances between two points whose spacing is within the Kolmogoroff's "inertial subrange." Batchelor[4] considered the pressure correlation in isotropic turbulence. These investigators have, from the very beginning, assumed a simple relation between the fourth-order and the second-order correlations. In order to compare the primary result with experiment, it is necessary to have the results in terms of the fourth-order correlation.

Before taking up pressure correlation, we shall consider correlations involving static pressure in general and show that these correlations can be expressed in terms of correlations involving more than two velocity components. This is convenient from the theoretical point of view, since it may then be possible to express higher order correlations in terms of second-order correlations on the basis of some plausible hypothesis, such as those used by other investigators. It may be also noted that Heisenberg's[2] expression for the spectral transfer term is a hypothesis for the triple correlation in terms of the second-order correlations. The fact that correlations involving static pressure can be expressed in terms of correlations involving more than two components of velocity is also convenient from an experimental point of view, since at present there exists no technique for the measurement of static pressure fluctuations. On the other hand, the standard hot-wire technique can be extended to correlations involving more than two velocity components.

GENERAL RELATIONS

Consider a statistically homogeneous and incompressible turbulence with no mean velocity (i.e., a "box turbulence"). The equations of motion for an arbitrary point $\boldsymbol{x}$ are: momentum,

$$\frac{\partial U_i}{\partial t} + U_j\frac{\partial U_i}{\partial x_j} = -\frac{1}{\rho}\frac{\partial p}{\partial x_i} + \nu\Delta U_i \qquad (1)$$

continuity,

$$\partial U_i/\partial \boldsymbol{x}_i = 0 \qquad (1a)$$

Received July 31, 1952.

* This is a part of the report, "On Correlations Involving Pressure Fluctuations in Homogeneous Turbulence" submitted to the National Advisory Committee for Aeronautics under Contract NAw-6093. The National Advisory Committee for Aeronautics has kindly granted permission to publish this part.

† The author wishes to thank Drs. S. Corrsin, L. S. G. Kovásznay, and F. H. Clauser for their helpful criticism and Mr. A. Kistler for his help in conducting the experiments reported here.

‡ Department of Aeronautics.

where the symbols have the usual meaning and repeated index means summation over the index. Taking the divergence of Eq. (1) and making use of Eq. (1a), we get the well-known relation,

$$\frac{1}{\rho}\frac{\partial^2 p}{\partial x_i \partial x_i} = -\frac{\partial U_i U_j}{\partial x_i \partial x_j} \tag{2}$$

The fact that the pressure in an incompressible viscous fluid satisfies Poisson's equation means that it is not a primary variable, since by using the well-known solution for Poisson's equation we can express the pressure in terms of the velocity derivatives.

Multiply Eq. (2) with q', any quantity at another point $\boldsymbol{x}'$, and taking a statistical average, we get

$$\frac{1}{\rho}\overline{q'\frac{\partial^2 p}{\partial x_i \partial x_i}} = -\overline{q'\frac{\partial^2 U_i U_j}{\partial x_i \partial x_j}}$$

Making use of the fact that the turbulence is statistically homogeneous and interchanging the order of differentiation and averaging, we have

$$\frac{1}{\rho}\frac{\partial^2 \overline{pq'}(\boldsymbol{\xi})}{\partial \xi_i \partial \xi_i} = -\frac{\partial^2 \overline{U_i U_j q'}(\boldsymbol{\xi})}{\partial \xi_i \partial \xi_j} \tag{3}$$

where $\boldsymbol{x}' = \boldsymbol{x} + \boldsymbol{\xi}$ and

$$\overline{p(\boldsymbol{x})q'(\boldsymbol{x}')} = \overline{pq'}(\boldsymbol{\xi})$$

An overbar denotes statistical average. Eq. (3) is just the Poisson equation for $\overline{pq'}$, and its solution can be written immediately as

$$\frac{1}{\rho}\overline{pp'}(\boldsymbol{\xi}') = \frac{1}{4\pi}\int \frac{\partial^2 \overline{U_i U_j q'}(\boldsymbol{y})}{\partial y_i \partial y_j}\frac{dV(\boldsymbol{y})}{|y - \xi|} \tag{4}$$

where $dV(\boldsymbol{y})$ is a volume element. Let

$$q' = \frac{1}{\rho}\frac{\partial^2 p'}{\partial x_j' \partial x_j'} = -\frac{\partial^2 U_k' U_l'}{\partial x_k' \partial x_l'}$$

Substituting this into Eq. (3), interchanging the order of differentiation, and averaging, we get

$$\frac{1}{\rho^2}\frac{\partial^4 \overline{pp'}}{\partial \xi_i \partial \xi_i \partial \xi_j \partial \xi_j} = \frac{\partial^4 \overline{U_i U_j U_k' U_l'}}{\partial \xi_i \partial \xi_j \partial \xi_k \partial \xi_l} \tag{5}$$

For the isotropic case

$$\frac{\partial^4(\,)}{\partial \xi_i \partial \xi_i \partial \xi_j \partial \xi_j} = \frac{1}{r}\frac{\partial^4[r(\,)]}{\partial r^4}$$

and the bilaplacian equation, Eq. (5), simplifies to

$$\frac{1}{\rho^2 r}\frac{\partial^4 \overline{rpp'}(r)}{\partial r^4} = \frac{\partial^4 \overline{U_i U_j U_k' U_l'}}{\partial \xi_i \partial \xi_j \partial \xi_k \partial \xi_l} \tag{6}$$

After four repeated integrations, for any fixed l, we get

$$\frac{1}{\rho^2}\overline{pp'}(r) = \frac{1}{6r}\int_r^\infty y(y - r)^3 \frac{\partial \overline{U_i U_j U_k' U_l'}}{\partial y_i \partial y_j \partial y_k \partial y_l}\, dy \tag{7}$$

$\overline{U_i U_j U_k' U_l'}$ is a fourth-order isotropic tensor and its form can be derived using some simple results of the invariant theory.[5] Thus,

$$\overline{U_i U_j U_k' U_l'} = \frac{R_{ll}{}^{ll}(r) - R_{nn}{}^{nn}(r) - 2R_{nn}{}^{ll}(r) - 4R_{nl}{}^{nl}(r)}{r^4}\xi_i\xi_j\xi_k\xi_l + R_{nn}{}^{mm}(r)\delta_{ij}\delta_{kl} + \frac{1}{2}[R_{nn}{}^{nn}(r) - R_{nn}{}^{mm}(r)][\delta_{ik}\delta_{jl} + \delta_{il}\delta_{jk}] + \frac{1}{r^2}[R_{nn}{}^{ll}(r) - R_{nn}{}^{mm}(r)][\xi_i\xi_j\delta_{kl} + \xi_k\xi_l\delta_{ij}] + \frac{1}{2r^2}[2R_{nl}{}^{nl}(r) - R_{nn}{}^{nn}(r) - R_{nn}{}^{mm}(r)][\xi_i\xi_k\delta_{lj} + \xi_j\xi_k\delta_{il} + \xi_j\xi_l\delta_{ki} + \xi_i\xi_l\delta_{kj}] \tag{8}$$

The various fourth-order correlations are shown in Fig. 1.

Some investigators[3, 4] have assumed that joint probability density of U_i, U_j, U_k', and U_l' is Gaussian; under this assumption the quadruple correlations are related to the double correlations by the following:

$$\overline{U_i U_j U_k' U_l'} = \overline{U_i U_k'}\cdot\overline{U_j U_l'} + \overline{U_i U_l'}\cdot\overline{U_j U_k'} + \overline{U_i U_j}\cdot\overline{U_k' U_l'} \tag{9}$$

and, in particular,

$$\left.\begin{aligned} R_{ll}{}^{ll}(r) &= 2R_l{}^{l2}(r) + R_{ll}{}^2 \\ R_{nn}{}^{nn}(r) &= 2R_n{}^{n2}(r) + R_{nn}{}^2 \\ R_{nl}{}^{nl}(r) &= R_l{}^l(r)R_n{}^n(r) \\ R_{nn}{}^{ll}(r) &= R_{ll}R_{nn} \\ R_{nn}{}^{mm}(r) &= R_{nn}R_{mm} \end{aligned}\right\} \tag{10}$$

These relations and the expression for $\overline{U_i U_j U_k' U_l'}$ for the case $k = l = i$ were first given by Millionshtchikov.[6] The second-order correlations $R_l{}^l$ and $R_n{}^n$ [essentially the von Kármán-Howarth $g(r)$ and $f(r)$] are connected by the continuity equation of incompressible flow.[7]

$$R_n{}^n(r) = R_l{}^l(r) + \frac{r}{2}\frac{\partial}{\partial r}R_l{}^l(r) \tag{11}$$

The hypothesis of Gaussian joint probability density makes all odd moments (e.g., triple correlations) zero. However, the above relations are only integral conditions on the joint probability density, and the hypothesis of Gaussian probability density is not strictly necessary for their validity. Without making any such hypothesis about the probability density, we simply take Eq. (9) as a plausible hypothesis. Substituting Eq. (8) in Eq. (7) and carrying out some algebraic simplifications and integrations by parts, we get

$$\frac{1}{\rho^2}\overline{pp'}(r) = R_{ll}{}^{ll}(r) - R_{ll}{}^2 - 4\int_r^\infty \left[2R_{nl}{}^{nl} + R_{nn}{}^{ll} - R_{nn}{}^{nn} + \frac{r^2}{y^2}(R_{nn}{}^{nn} + R_{ll}{}^{ll} - 2R_{nn}{}^{ll} - 4R_{nl}{}^{nl})\right]\frac{dy}{y} \tag{12}$$

The pressure gradient is of special interest since it is related to the diffusion of marked fluid particles from a fixed source (see next section on "Pressure Gradient and Diffusion Measurements"). Now,

$$\overline{(\partial p/\partial x_1)^2} = \lim_{r\to 0}\overline{[\partial p(x_1)/\partial x_1]\cdot[\partial p(x_1')/\partial x_1']}$$

where $x_1' = x_1 + r$. Interchanging the order of integration and averaging, we have

$$\overline{(\partial p/\partial x_1)^2} = -(\partial^2\overline{pp'}(r)/\partial r^2)_{r=0}$$

Substituting for $\overline{pp'}$ from Eq. (12), we get

$$\frac{1}{\rho^2}\overline{\left(\frac{\partial p}{\partial x_1}\right)^2} = -\left[\frac{d^2}{dr^2}2R_{ll}{}^{ll}(r) - R_{nn}{}^{nn}(r)\right]_{r=0} + 8\int_0^\infty (R_{nn}{}^{nn} + R_{ll}{}^{ll} - 2R_{nn}{}^{ll} - 4R_{nl}{}^{nl})\frac{dy}{y^3} \tag{13}$$

In order for the above integrals to converge, it is necessary that the series expansion of

$$(R_{nn}{}^{nn} + R_{ll}{}^{ll} - 2R_{nn}{}^{ll} - 4R_{nl}{}^{nl})$$

at the origin begin with terms of order r^4; therefore,

$$\left[\frac{d^2}{dr^2}(R_{nn}{}^{nn} - R_{ll}{}^{ll} - 2R_{nn}{}^{ll} - 4R_{nl}{}^{nl})\right]_{r=0} = 0$$

We have made use of this fact in deriving the expression (13). Under the assumption of Eq. (9), Eqs. (12) and (13) become

$$\frac{1}{\rho^2}\overline{pp'}(r) = 2\int_r^\infty\left(y - \frac{r^2}{y}\right)\left[\frac{d}{dy}R_l{}^l(y)\right]^2 dy \tag{12a}$$

$$\frac{1}{\rho^2}\overline{(\partial p/\partial x_1)^2} = 4\int_0^\infty\left[\frac{d}{dy}R_l{}^l(y)\right]^2\frac{dy}{y} \tag{13a}$$

For vanishing turbulence Reynolds Number,

$$R_\lambda \to 0 (R_\lambda = \sqrt{\overline{U_1^2}}\,\lambda/\nu)$$

where

$$\lambda^2 = \overline{U_1^2}/\overline{(\partial U_1/\partial x_1)^2}$$

$R_l{}^l(r)$ can be calculated neglecting the inertia terms of the equations of motion,[8]

$$R_l{}^l(r) = \overline{U_1^2}\exp[-r^2/2\lambda^2]$$

Substituting this result in Eqs. (12a) and (13a) we get

$$\overline{pp'}(r) = \rho^2\overline{U_1^2}^2\exp[-r^2/\lambda^2] = \rho^2(R_l{}^l)^2 \tag{14}$$

$$\overline{(\partial p/\partial x_1)^2} = 2\rho^2\overline{U_1^2}^2/\lambda^2 \tag{15}$$

On the basis of Kolmogoroff's hypothesis of local isotropy, for large Reynolds Numbers and r with the "inertial subrange" we have[9]

$$\overline{(U - U')^2} = 2[\overline{U^2} - R_l{}^l(r)] = C_1(\nu\epsilon)^{1/2}\left(\frac{r}{\zeta}\right)^{2/3} \tag{16}$$

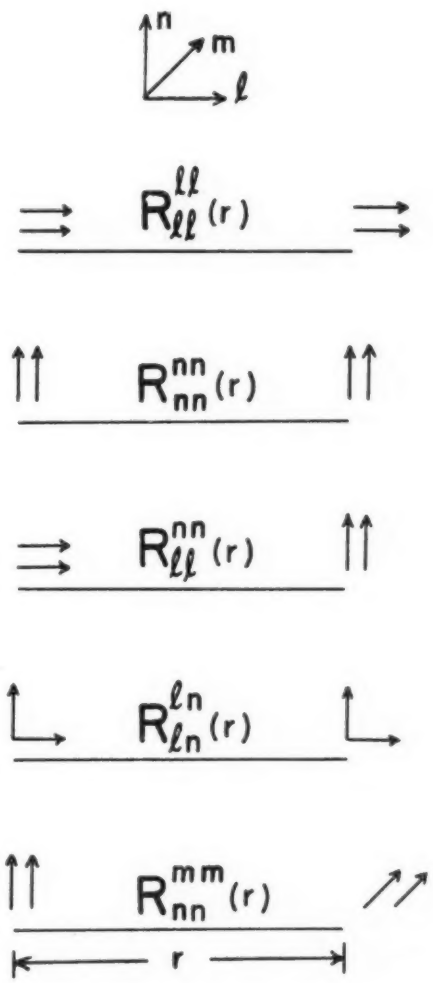

FIG. 1. The fourth-order correlations.

where U is the velocity along the displacement vector, $\xi = x' - x'$,

$$r^2 = \xi_i \xi_i, \quad \epsilon \left(= \frac{1}{2} \frac{d\overline{U_i U_i}}{dt} \right)$$

is the energy dissipation per unit mass of the fluid, the length $\zeta = \nu^{3/4}\epsilon^{1/4}$, and C_1 is an absolute constant. ϵ and λ are connected by Taylor's decay equation,[1]

$$(1/2)\ (d\overline{U_i U_i}/dt) = -15\nu\ \overline{U_1^2}/\lambda^2$$

Hence, for values of r within the inertial subrange,

$$\frac{1}{2\rho^2}\ (p^2 - \overline{pp'}) = \int_0^r \left[\frac{d}{dy}\ R_l{}^l(y)\right]^2 y\ dy + r^2 \int_r^\infty \left[\frac{d}{dy}\ R_l{}^l(y)\right]^2 \frac{dy}{y} \tag{17}$$

The integrals in Eq. (17) can be evaluated by using Eq. (16). The result is

$$\frac{1}{\rho^2}\ (p^2 - \overline{pp'}) = \frac{C_1^2}{2}\ \epsilon\nu \left(\frac{r}{\zeta}\right)^{4/3}$$

or

$$(1/\rho)^2\ \overline{(p - p')^2} = \overline{(U - U')^2}{}^2 \tag{18}$$

This relation was first given by Obukhov,[3] and Eqs. (12a) and (13a) were given by Batchelor.[4]

Pressure Gradient and Diffusion Measurements

In reference 10, the "Lagrangian" microscale λ_η was related to the acceleration in isotropic turbulence without the neglect of viscosity. A brief résumé follows:

$$\frac{2}{\lambda_\eta{}^2} = \frac{1}{V'^4}\left[\overline{\left(\frac{dV}{dt}\right)^2} - \overline{\left(\frac{dV'}{dt}\right)^2}\right] \tag{19}$$

where V' is the r.m.s. velocity in the y-direction. Squaring and averaging the v-component equation of motion, we get

$$\overline{\left(\frac{dV}{dt}\right)^2} = \frac{1}{\rho^2}\ \overline{\left(\frac{\partial p}{\partial y}\right)^2} + \nu^2\overline{(\Delta V)^2} \tag{20}$$

The term $\overline{(\partial p/\partial y\ \Delta V)} = 0$ because of isotropy. All terms in the expansion of $\overline{(\Delta V)^2}$ can be expressed in terms of the derivatives of $R_l{}^l(r)$ by making use of the relations given by von Kármán and Howarth.[7] Thus,

$$\overline{(\Delta V)^2} = \frac{33}{2}\left[\frac{\partial^4 R_l{}^l(r)}{\partial r^4}\right]_{r=0}$$

Townsend[11] has made measurements of

$$[\partial^4 R_l{}^l(r)/\partial r^4]_{r=0}$$

his result is

$$\overline{(\Delta V)^2} = \frac{33}{2}\left[\frac{\partial^4 R_l{}^l(r)}{\partial r^4}\right]_{r=0} = \frac{33}{2}\ \frac{V'^2}{\lambda^4}\left[\frac{30}{7} + 0.2R_\lambda\right] \tag{21}$$

For the isotropic turbulence

$$dV'^2/dt = -10\nu\ (V'^2/\lambda^2)$$

(the "decay equation," due to Taylor[1]). Thus,

$$(\lambda^2/V'^4)\ (dV'/dt)^2 = 25/R_\lambda \tag{22}$$

Substituting Eqs. (20), (21), and (22) in Eq. (19), we get*

$$\frac{\rho^2 V'^4}{\lambda^2\overline{(\partial p/\partial y)^2}} = \left[\frac{2\lambda^2}{\lambda_\eta{}^2} - \frac{20.7}{R_\lambda{}^2} - \frac{2.1}{R_\lambda}\right]^{-1} \tag{23}$$

Heisenberg[2] has calculated an expression for pressure gradient using the hypothesis that various Fourier components of the velocity field are statistically independent. As far as the fourth-order correlations are concerned, the consequences of this hypothesis can be shown to be equivalent to Eq. (9).[4] His result is

$$\frac{\rho^2 V'^4}{\lambda^2\overline{(\partial p/\partial y)^2}} = 0.038\kappa R_\lambda \tag{24}$$

Instead of Heisenberg's original extrapolation formula for the stationary velocity spectrum, Chandrasekhar's solution[13] was used to calculate Eq. (24). κ is a "universal" constant that must be determined from experimental data. Heisenberg found from turbulence decay that $\kappa = 0.85$. Lee[14] gives its value as 0.13, based on skewness of the probability density of $(\partial U_1/\partial x_1)$ as

* This is the first step toward the establishment of a possible relation between Lagrangian and Eulerian correlations. If we consider nondecaying isotropic turbulence, then the Lagrangian correlation

$$\overline{U_1(t)U_1(t+\tau)} = R_1(\tau) = \overline{U_1}^2 + \sum_{n=0}^{\infty}(-1)^n\left(\overline{\frac{d^n U_1}{dt^n}}\right)^2 \frac{\tau^{2n}}{(2n)!}$$

We can express each term of this series in terms of the Eulerian correlations by using equations of motion. The first nonconstant term involves pressure or fourth-order velocity correlations. The next term will involve still higher order correlations. It may be possible to relate higher order correlations with second-order correlations by making a further hypothesis about the joint probability density of the velocities at two points. We have just carried out the first step of this computation. The next step will involve many more calculations. This is probably not the best method of attack of the problem of relating the Lagrangian and the Eulerian correlations. Frenkiel[12] has related Lagrangian and Eulerian microscales under some assumptions.

measured by Townsend.[11] Proudman[15] has calculated double and triple correlations from Chandrasekhar's solution of Heisenberg's self-preserving spectrum. He has estimated its value as 0.45 from comparison of theoretical correlations with measured correlation. Heisenberg's results are only approximate, and the value of κ depends on the range of spectrum (or correlation) which is made to fit the experimental data. We have taken $\kappa = 0.45$ as a compromise value.

Experimental Observations

The measurement of various correlations was made in isotropic turbulence at $R_\lambda = 60$. The correlations $R_{ll}{}^{ll}(r)$, $R_{nn}{}^{nn}(r)$, $R_{nn}{}^{mm}(r)$, and two independent combinations

$$(R_{ll}{}^{ll} + R_{nn}{}^{nn} + 2R_{nn}{}^{ll} - 4R_{nl}{}^{nl})$$
$$(R_{ll}{}^{ll} + R_{nn}{}^{nn} + 2R_{nn}{}^{ll} + 4R_{nl}{}^{nl})$$

were measured. The measurements are compared with the hypothesis of Eq. (9) in Figs. 2, 3, 4, 5, and 6. While measuring the fourth-order correlation, the corresponding second-order correlation was also measured simultaneously. For sufficiently large distance, the correlation between U_i^2 and U_j^2 disappears and $\overline{U_i^2 U_j^2}$ tends to a constant value $\overline{U_i^2}\cdot\overline{U_j^2}$, which is equal to $\overline{U_1^2}^2$ for isotropic turbulence. If we assume that the probability density of U_1 is Gaussian, then $\overline{U_1^2}^2/\overline{U_1^4} = 1/3$. This is indicated by a dashed line in Figs. 2, 3, and 6. This assumption is less restrictive than the hypothesis of Eq. (9) and is fairly well satisfied in prac-

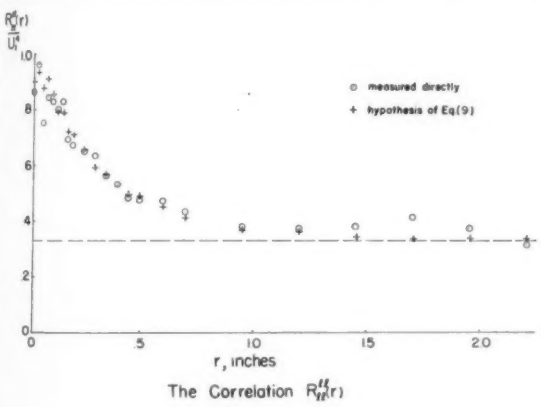

Fig. 2.

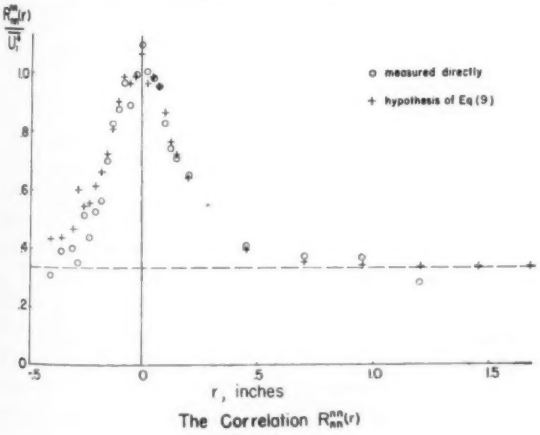

Fig. 3.

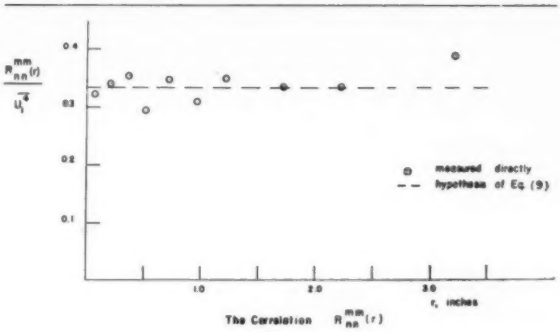

Fig. 4.

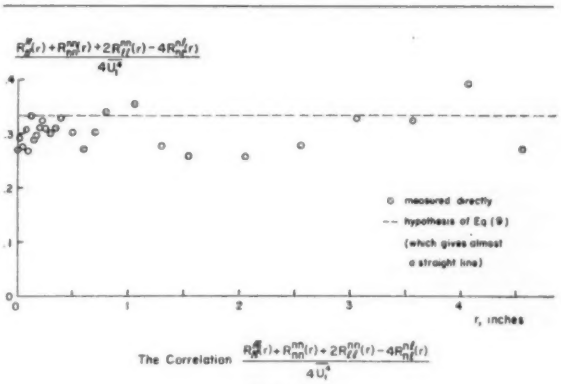

Fig. 5.

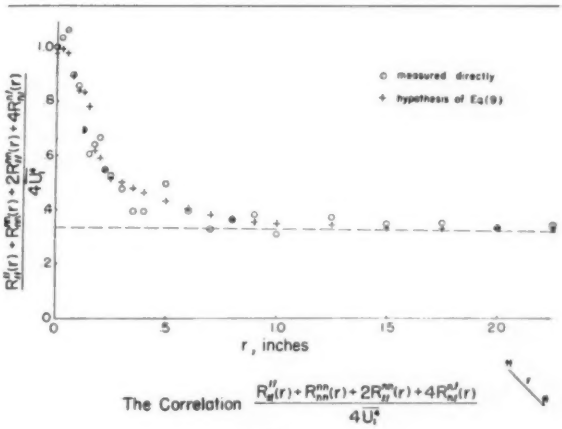

Fig. 6.

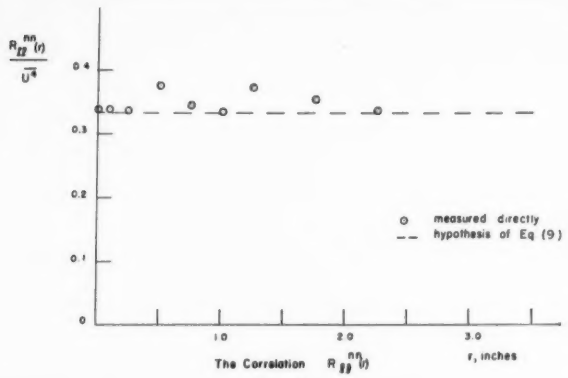

FIG. 7.

tice. The correlation R_{ll}^{nn} (Fig. 7) was also measured; this is not independent of the above five correlations. Since the hypothesis of Eq. (9) gives it a constant value, it is of interest to see whether the measured value deviates from this constant. Within the experimental accuracy, all the fourth-order correlations are close to those computed from corresponding second-order correlations using Eq. (9).

Batchelor[4] has presented R. W. Stewart's measurement of

$$\overline{(U_1 - U_1')^4}/\overline{(U_1 - U_1')^2}^2$$

in support of the hypothesis of Gaussian joint probability density of the four velocity components entering in Eq. (5).

$$\overline{(U_1 - U_1')^4}/\overline{(U_1 - U_1')^2}^2 = 3.0$$

if this hypothesis is satisfied. For the purpose of relating pressure correlation with second-order velocity correlation, it is only necessary to assume the hypothesis of Eq. (9) for the fourth-order correlations involving two velocity components at one point and two velocity components at another point. The quantity

$$\overline{(U_1 - U_1')^4}/\overline{(U_1 - U_1')^2}^2$$

includes fourth-order correlations involving three velocity components at one point and one velocity component at another point, and these correlations do not enter in the pressure correlation Eq. (5). In passing, we mention that, if the fourth-order correlations entering in Eq. (5) are related to second-order correlation by Eq. (9) and if these new fourth-order correlations are related to the second-order correlations by the relation

$$\overline{U_iU_jU_kU_l'} = \overline{U_iU_k}\cdot\overline{U_jU_l'} + \overline{U_iU_l'}\cdot\overline{U_jU_k} + \overline{U_iU_j}\cdot\overline{U_kU_l'}$$

then

$$\overline{(U_1 - U_1')^4}/\overline{(U_1 - U_1')^2}^2 = 3.0$$

This is similar to the hypothesis of Eq. (9) and is less restrictive than the hypothesis of Gaussian joint distribution of the four velocity components. The fourth-order correlations $\overline{U_iU_jU_kU_l'}$ have been measured. The results and further discussion on this point are presented in reference 5.

Let R_1, R_2, and R_3 denote the correlations R_{ll}^{ll}, R_{nn}^{nn} and the combination

$$\frac{1}{4}(R_{ll}^{ll} + R_{nn}^{nn} + 2R_{nn}^{ll} + 4R_{nl}^{nl}$$

respectively. This set of correlations, among other possible sets, suffices to determine the pressure correlation. In terms of the above notation, the Eq. (12) becomes

$$\frac{1}{\rho^2}\overline{pp'}(r) = R_1(r) - \overline{U_1^2}^2 + 2\int_r^\infty \left[3R_2 + R_1 - 4R_3 - \frac{4r^2}{y^2}(R_1 + R_2 - 2R_3)\right]\frac{dy}{y}$$

R_2 was measured for both positive and negative values of r (see Fig. 3) and the point $r = 0$ was determined from the fact that it is an even function of r. R_1 and R_3 were measured for positive values of r, and there is some uncertainty ($= 0.025$ in.) in the determination of the point $r = 0$ for these two correlations. This uncertainty, the experimental scatter, and the fact that small differences between relatively large quantities are required to compute the pressure correlation have made the results extremely uncertain.

Two widely different sets of curves were drawn for each measured correlation, taking into account the experimental scatter and the uncertainty in the determination of the point $r = 0$. Two pressure correlations were computed from these two different sets of fourth-order correlations. The result of these computations and those from the second-order correlation are compared in Table 1 and Fig. 8.

It appears that for the computation of pressure correlation one should measure directly the differences $(3R_2 + R_1 - 4R_3)$ and $(R_1 + R_2 - 2R_3)$ instead of the individual correlations. This involves the difficult problem of measuring small correlation between relatively large quantities.

TABLE 1

	$p^2/\rho^2\,\overline{U_1^2}^2$	$\overline{\left(\frac{\partial p}{\partial x_1}\right)^2}\Big/\rho^2\,\overline{U_1^2}^2$	$\left[2\bar{p}^2\Big/\overline{\left(\frac{\partial p}{\partial x_1}\right)^2}\right]^{+1/2}$
Two extreme values computed from fourth-order correlation	3.3	85	0.28
	0.45	11	0.20
Computed from second-order correlation	0.50	12	0.20

In view of the fact that hypothesis of Eq. (9) is approximately satisfied we may use double-correlation to compute r.m.s. pressure and pressure gradient. However, we must not overlook one unfortunate circumstance. It is possible that hypothesis of Eq. (9) is approximately satisfied but the r.m.s. pressure and pressure gradient computed from using this hypothesis are still in error, because the r.m.s. pressure and pressure gradient depend on the difference of various fourth-order correlations.

Eqs. (12a) and (13a) express the desired quantities in terms of the longitudinal second-order correlation $R_l{}^l$. $R_l{}^l$ and $R_n{}^n$ are connected by Eqs. (11). We need to express $(\partial/\partial r)R_l{}^l$ in terms of $R_n{}^n$. Since

$$\frac{\partial}{\partial r} R_n{}^n = \frac{1}{2r^2}\frac{\partial}{\partial r}\left[r^3 \frac{\partial}{\partial r} R_l{}^l\right]$$

therefore,

$$\frac{\partial}{\partial r} R_l{}^l = \frac{2}{r^3}\int_0^r \frac{\partial}{\partial y} R_n{}^n(y) y^2\, dy$$

using this result, Eqs. (12a) and (13a) become

$$\left(\overline{\frac{p^2}{\rho^2}}\right)\Big/\overline{U_1^2}^2 = \frac{8}{U_1^2}\int_0^\infty \left[\int_0^r \frac{d}{dy} R_n{}^n(y) y^2\, dy\right]^2 \frac{dr}{r^5}$$

$$\overline{\left(\frac{\partial p}{\partial x_1}\right)^2}\Big/\rho^2\,\overline{U_1^2}^2 = \frac{16}{\overline{U_1^2}}\int_0^\infty \left[\int_0^r \frac{d}{dy} R_n{}^n(y) y^2\, dy\right]^2 \frac{dr}{r^7}$$

Root mean square pressure and pressure gradient were computed from measured $R_n{}^n(r)$ for various Reynolds Numbers. The results of the computation are shown in Figs. 9 and 10. The data for the two highest Reynolds Numbers were taken from reference 16. The data in reference 16 are given in terms of grid Reynolds Numbers. Turbulence Reynolds Numbers, R_λ and λ/M (where M is the mesh spacing) were estimated from grid Reynolds Numbers by assuming that $U_0^2/\overline{U_1^2} \sim t^{-1}$ in the initial period. U_0 is the mean velocity.

Eq. (23) relates the "Lagrangian micro-scale," λ_η, with the r.m.s. pressure gradients. Measurements of λ_η have been made by Simmons[17] and Collis,[18] and an extensive set of measurements is given in reference 10. The experimental data (Table 2) are used to compute the pressure gradient [Eq. (23)], and the results are compared with Heisenberg's analysis [Eq. (24)] in Fig. 10.

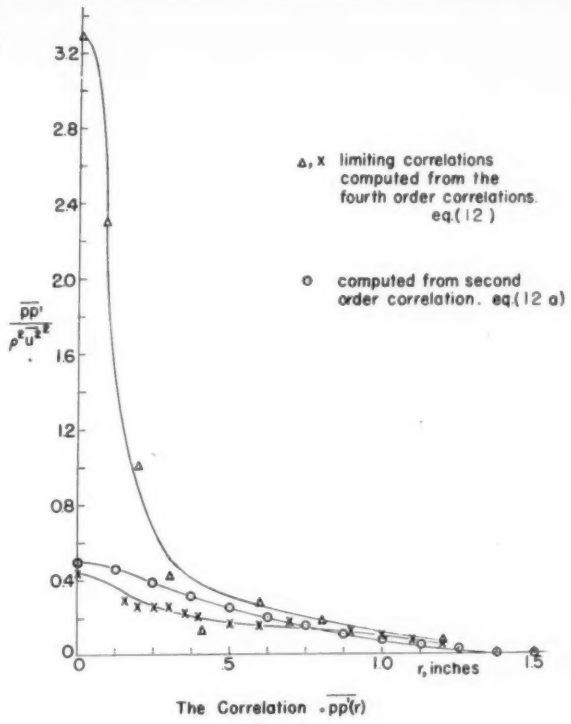

The Correlation $= \overline{pp'}(r)$

FIG. 8.

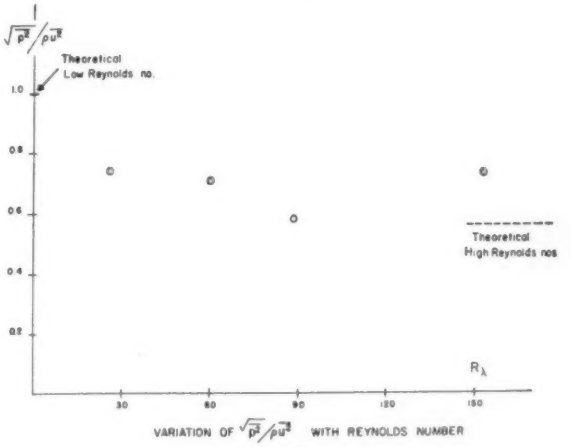

FIG. 9.

REFERENCES

[1] Taylor, G. I., *Statistical Theory of Turbulence, IV Diffusion in Turbulent Air Stream*, Proc. Roy. Soc., Ser. A, Vol. 151, 1935.

[2] Heisenberg, W., *Zur. Statistischen Theory der Turbulenz*, Z. Phy., Vol. 124, 1948.

[3] Obukhov, A. M., *The Pressure Fluctuations in Turbulent Flow*, C.R. Acad. Sci., U.S.S.R., Vol. 37, No. 4, 1949.

(*Concluded on page 204*)

TABLE 2

	R_λ	λ, In.	λ_η, In.	$\frac{2\lambda^2}{\lambda_\eta^2}$	$\frac{20.7}{R_\lambda^2}+\frac{2.1}{R_\lambda}$	$\frac{\lambda^2\left(\frac{\partial p}{\partial y}\right)^2}{\rho^2 V'^4}$	$\sqrt{\frac{\rho^2 V'^4}{\lambda^2\left(\frac{\partial p}{\partial y}\right)^2}}$
Simmons, 1935	37.0	0.16	0.08	8.00	0.072	7.930	0.356
Collis, 1948	23.0	0.14	0.20	1.00	0.130	0.870	1.070
Collis, 1948	38.0	0.14	0.20	1.00	0.070	0.930	1.030
Reference 10, 1951	29.0	0.17	0.11	4.78	0.097	4.680	0.463
Reference 10, 1951	32.0	0.12	0.12	2.00	0.086	1.914	0.725
Reference 10, 1951	36.0	0.41	0.36	2.60	0.074	2.530	0.629
Reference 10, 1951	42.5	0.23	0.235	1.92	0.061	1.860	0.735
Reference 10, 1951	43.5	0.165	0.245	0.910	0.059	0.851	1.084
Reference 10, 1951	49.0	0.35	0.22	5.04	0.052	4.990	0.448
Reference 10, 1951	61.0	0.23	0.34	0.914	0.040	0.874	1.070
Reference 10, 1951	67.0	0.34	0.22	4.76	0.036	4.720	0.461
Reference 10, 1951	74.0	0.19	0.27	0.990	0.032	0.958	1.022

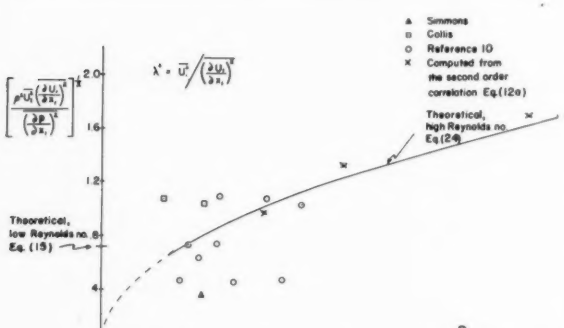

FIG. 10.

[4] Batchelor, G. K., *Pressure Fluctuations in Isotropic Turbulence*, Proc. Cambridge Phil. Soc., Vol. 47, 1951.

[5] Uberoi, M. S., *On the Correlations Involving Static Pressure Fluctuations in Homogeneous Turbulence*, Report submitted to N.A.C.A. under Contract NAw-6093.

[6] Millionshtchikov, M. D., *On the Theory of Homogeneous Isotropic Turbulence*, C. R. Acad. Sci., U.S.S.R., Vol. 32, 1941.

[7] von Kármán, T., and Howarth, L., *On the Statistical Theory of Turbulence*, Proc Roy. Soc., Ser. A, Vol. 164, 1938.

[8] Loitsiansky, L. G., *Some Basic Laws of Isotropic Turbulence*, C.A.H.T., Moscow Report, No. 440, Translated as N.A.C.A. T.M. No. 1079, September, 1945.

[9] Batchelor, G. K., *Kolmogoroff's Theory of Local Isotropic Turbulence*, Proc. Cambridge Phil. Soc., Vol. 43, 1947.

[10] Uberoi, M. S., and Corrsin, S., *Diffusion of Heat from a Line Source in Isotropic Turbulence*, N.A.C.A. T.N. No. 2710, June, 1952.

[11] Batchelor, G. K., and Townsend, A. A., *Decay of Vorticity in Isotropic Turbulence*, Proc. Roy. Soc., Ser. A, Vol. 190, 1947.

[12] Frenkiel, F. N., *Comparison Between Theoretical and Experimental Results on the Decay of Turbulence*, Proc. Seventh International Congress for Applied Mechanics, Vol. II, 1948.

[13] Chandrasekhar, S., *On Heisenberg's Elementary Theory of Turbulence*, Proc. Roy. Soc., Ser. A, Vol. 200, 1949.

[14] Lee, T. D., *Note on the Coefficient of Eddy Viscosity in Isotropic Turbulence*, Phy. Rev., Vol. 77, 1950.

[15] Proudman, I., *Comparison of Heisenberg's Spectrum of Turbulence with Experiment*, Proc. Cambridge Phil. Soc., Vol. 47, 1951.

[16] Liepmann, H. W., Laufer, J., and Liepmann, K., *On the Spectrum of Isotropic Turbulence*, N.A.C.A. T.N. No. 2473, November, 1951.

[17] Simmons, L. F. G., Experiments reported by Taylor in reference 1.

[18] Collis, D. C., *The Diffusion Process in Turbulent Flow*, Com. Sci. Industr. Res. Aust. Div., Aero. Rep. No. A55, 1948.

A Field-Mapping Method for Analysis and Synthesis of Linear Closed-Loop Systems

MIKE W. FOSSIER* AND HAROLD A. ROSEN†

Raytheon Manufacturing Company

SUMMARY

A field mapping method that is an extension of the usual steady-state transfer function methods of analyzing closed-loop systems is presented. It is shown that, for such a system, the open-loop transfer function may be represented as a potential flow field in the complex plane (either the s-plane or, better, log s-plane) in which sources and sinks are placed at the locations of the poles and zeros of this open-loop transfer function. The values of the open-loop transfer function along the imaginary axis of this plane represent the steady-state (frequency) response of the open loop, and from their knowledge the flow field in the vicinity of closed-loop roots may be determined graphically by means of analytic continuation. The closed-loop roots occur at those points s for which the open-loop transfer function achieves the value -1. The method allows a quick determination of the closed-loop roots for any value of loop gain and further shows the dependency of the roots on additionally introduced phase shifts.

LIST OF SYMBOLS

- s = Laplace transform operator
- θ = direction of fuselage centerline in space
- δ = deflection angle of control surface
- Φ = complex potential function ($\varphi + j\psi$)
- φ = potential function
- ψ = stream function
- j = $\sqrt{-1}$
- E = angle of radial line in s-plane
- db. = decibels, measure of amplitude ratio
- r = magnitude of radial line in s-plane; undamped frequency
- ω = angular frequency, rad. per sec.; $\omega = r \sin E$
- ζ = damping factor, expressed as a proportion of critical damping

INTRODUCTION

THE CLOSED-LOOP DYNAMICAL SYSTEM is one in which the output of the system is fed back into the system as an additional input. Any closed-loop system may be pictured schematically as in Fig. 1. If the elements represented by the symbols μ and β in Fig. 1 can be represented by a set of linear differential equations with constant coefficients, then the analysis of these elements by the method of the Laplace transformation yields general rational algebraic fractions as the representation of these elements in terms of the Laplace transform operator, s.[1] These functions are termed "transfer functions," and their multiplication by any general input (in operational form) yields the response to that input (also in operational form).

The transfer function for the closed loop may be seen from Fig. 1 to be given by Eq. (1).

$$\theta_0/\theta_i = \mu/(1 + \mu\beta) \qquad (1)$$

The poles of θ_0/θ_i (i.e., the roots of the equation obtained by setting the denominator equal to zero) give the decay time constants and frequencies of the various modes of the system. The poles of θ_0/θ_i from Eq. (1) are those values of s for which $\mu\beta$ is -1. Since μ and β are general rational algebraic fractions, it follows that these values of s either will be real or will occur in complex conjugate pairs. For the system to be stable, these values of s must have negative real parts; a pair of pure imaginary roots results in a neutrally stable system.

The complex value of a transfer function for an imaginary value of s is the ratio (amplitude and phase) of the output to the input of the corresponding element for a steady-state sinusoidal input. A compilation of the ratios for various input frequencies is termed the "frequency response" of the element. In the usual methods of frequency analysis, the degree of stability of the closed-loop system is inferred from the margins with which the complex values of the open loop $\mu\beta$ miss being -1 for the imaginary values of s, since this corresponds to neutral stability. In the field-mapping method, presented herein, the complex value of s for which $\mu\beta$ is actually -1 is obtained from the frequency response of $\mu\beta$ by means of analytic continuation. There have recently been published a number of papers on this subject,[9,10] and a summary of these and other recent developments in the field of automatic control may be found in reference 11.

THE POTENTIAL ANALOGY

The field-mapping method is based on the consideration of the transfer function representing any linear element as a two-dimensional potential field. This relationship is known as the potential analogy,[2,3] and the manner in which it comes about may be seen by considering the general rational algebraic fraction $F(s)$, which arises in the solution of the equations representing the dynamics of this element by operational means,

Received April 29, 1952. Revised and received December 17, 1952.

* Staff Aerodynamicist, Missile Flight Test Department, Missile and Radar Division.

† Senior Staff Engineer, Missile Flight Test Department, Missile and Radar Division.

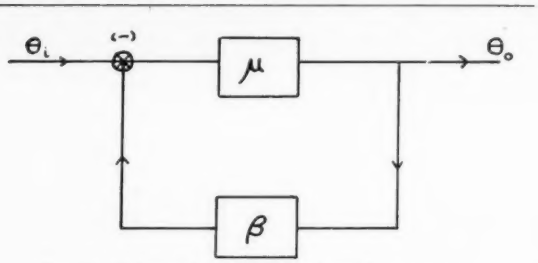

FIG. 1. Schematic drawing of closed-loop system.

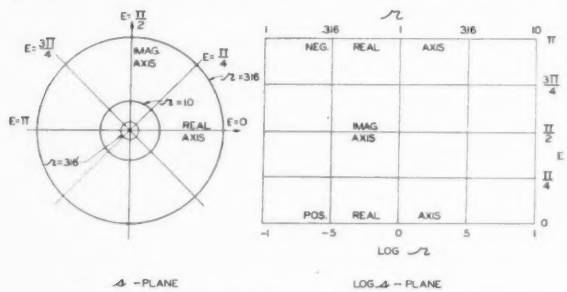

FIG. 2. Transformation of s-plane into log s-plane.

$$F(s) = \frac{P(s)}{Q(s)} = K \frac{s^p + \alpha_{p-1} s^{p-1} + \ldots + \alpha_1 s + \alpha_0}{s^q + \beta_{q-1} s^{q-1} + \ldots + \beta_1 s + \beta_0} \tag{2}$$

If the roots of $P(s) = 0$ are $-a_i$ and those of $Q(s) = 0$ are $-b_i$, then the fraction may be written (where a_i and b_i are, in general, complex numbers)

$$F(s) = K \frac{\prod_{i=1}^{p} (s + a_i)}{\prod_{i=1}^{q} (s + b_i)} \tag{3}$$

It follows that

$$\log [F(s)] = \log K + \sum_{i=1}^{p} \log (s + a_i) - \sum_{i=1}^{q} \log (s + b_i) \tag{4}$$

Consider now the complex potential function $\Phi(s)$ representing radial source flow at the points $-c_i$ (where c_i is, in general, a complex number).[4]

$$\Phi(s) = \varphi(s) + j\psi(s) = -C \log (s + c_i) \tag{5}$$

Comparing Eqs. (4) and (5), it is seen that $\log [F(s)]$ may be considered to be the complex potential function for a flow field in which the poles of $F(s)$ act as sources and the zeros of $F(s)$ act as sinks (i.e., negative sources). Since $F(s)$ may be considered to have an amplitude A and phase B, then

$$F(s) = A(s)e^{jB(s)}$$

and so

$$\log [F(s)] = \log[A(s)] + jB(s) \tag{6}$$

Comparing Eqs. (5) and (6), it is seen that the potential function φ corresponds to the logarithmic amplitude of the transfer function $F(s)$ and that the stream function ψ corresponds to the phase of $F(s)$.

Method of Mapping

The (logarithmic) amplitude and phase functions of $F(s)$ were shown to be analogous to the potential and stream functions of a flow field determined by sources and sinks placed at the locations of the poles and zeros of $F(s)$. If the values of the complex potential function of such a field are known along a line of finite length within this field, then the flow field may be uniquely determined except in small regions enclosing the singularities within the field.[5] This process is known as analytic continuation. In its application to the field-mapping method, it shall be assumed that the frequency response of $F(s)$ is known [i.e., the phase and amplitude of $F(s)$ are known along the imaginary axis of the s-plane], and the flow field shall be constructed by flux plotting,[6] which is the graphical equivalent to analytic continuation.

In order to increase the convenience in application of the method in the frequency range of interest, the field shall be developed in the plane log s.[7] Since s is a complex variable, expressible in the vector form $s = re^{jE}$, it is seen that

$$\log s = \log r + j E \tag{7}$$

The log s-plane is thus one in which the abscissa is the logarithm of the length of the radial line drawn from the origin to any point in the s-plane, and the ordinate is the counterclockwise angle between this line and the positive real axis. Since this angle repeats itself every 2π rad. it is seen that the log s-plane will consist of a series of horizontal strips 2π high and that the flow field will be identical in each strip. Thus only one such strip need be considered. In addition, it may be noted that all singularities either lie along the real axis or occur in conjugate pairs. Thus the flow field in the s-plane is symmetrical about the real axis, and in the log s-plane only a strip between 0 and π need be considered. The positive real axis transforms into the base of this strip, the negative real axis transforms into the top of the strip, and radial lines from the origin transform into horizontal lines in the strip, the vertical coordinate E being the angle that the radial line makes with the real axis, as shown in Fig. 2.

In the application of the method to closed-loop systems, the information available as a result of the usual frequency analysis is assumed to be known. This means that the amplitude and phase of $F(j\omega)$ are known [where $F(j\omega)$ represents the steady-state open-loop transfer function], and, hence, the potential and stream functions of the flow field are known along the imaginary s-axis (i.e., along the line $E = 90°$ in the log s-plane). From this information the flow field in the log

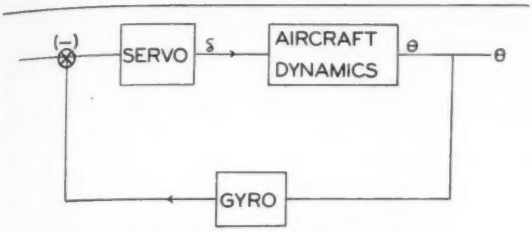

FIG. 3. Block diagram for numerical example.

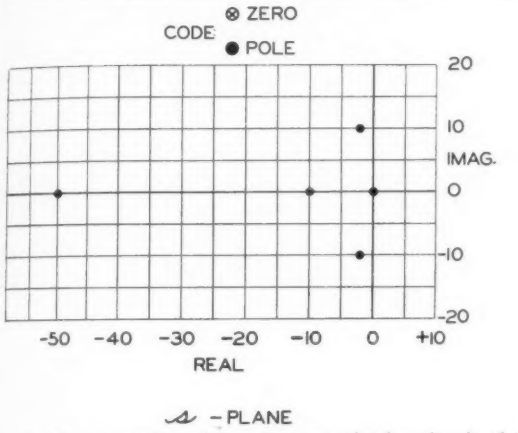

FIG. 4. Representation of open-loop transfer function in the s-plane.

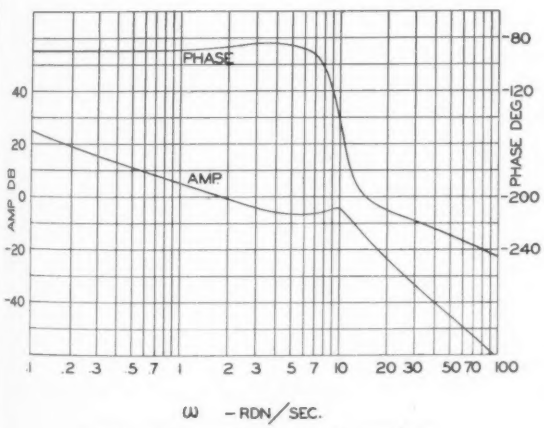

FIG. 5. Frequency response of open loop.

strip can be constructed by making use of the fact that the potential and stream functions are orthogonal functions, provided the same scale is used for ordinate and abscissa. From Eq. (7) it may be seen that the horizontal length of one decade must be log 10, which is 2.303. The total height of the strip is π, or 3.1416. Three-cycle semilogarithmic graph paper of these dimensions may be obtained from the Raytheon Manufacturing Company, Oxnard, Calif. The size of the mesh is determined from similar considerations, and it may be shown that 20° of phase corresponds in size to 3.03 db. The procedure followed in constructing the field is as follows. From the known amplitude and phase curves of the steady-state open-loop transfer function, spacings of, e.g., 3 db. in amplitude and 20° of phase are noted along the line $E = 90°$ in the log s-plane. Through these points are sketched lines with such a slope that the lines through the amplitude and phase curves form curvilinear squares. The resulting mesh is uniquely determined from the values along the line $E = 90°$, and the sketching may be done by eye with reasonable accuracy. The size of the mesh is arbitrary so long as the relative lengths along the potential and stream lines are maintained; a mesh size of 10° versus 1.5 db. usually provides sufficient accuracy combined with ease of plotting.

Numerical Example

As an example of the use of the method, the case of a small high-speed aircraft stabilized to fly a level course by means of a free gyro shall be considered. The block diagram for such a system is shown in Fig. 3. The aerodynamics of the aircraft may be represented by a transfer function of the following type:

$$\left[\frac{\theta}{\delta}\right] = \frac{10\ (s + 10)}{s(s^2 + 4s + 104)} \tag{8}$$

The servo transfer function is assumed to be given by Eq. (9).

$$[s] = K_s/(1 + 0.02s) \tag{9}$$

The gyro is assumed to have unity response. The open-loop transfer function may thus be obtained from Eqs. (8) and (9) as

$$\mu\beta = \frac{10K_s(s + 10)}{s(s^2 + 4s + 104)\ (s + 50)} \tag{10}$$

This function may be represented in the s-plane by a zero at $s = -10$ and poles at $s = 0$, $s = -50$, and $s = -2 \pm j10$, as shown in Fig. 4. To obtain the frequency response of the open loop, the substitution $s = j\omega$ is made in Eq. (10). The resulting amplitude and phase curves may be seen in Fig. 5 for an assumed value of $K_s = 89$. Fig. 6 shows the complete flow field in the log s-plane, constructed as discussed in the preceding section from the known amplitude and phase values along the imaginary s = axis (determined from Fig. 5) and from the knowledge of symmetry along the top and bottom of the strip. In this particular example, the locations of the singularities are known, and thus additional aid in drawing the field may be had. However, such information is not necessary except to determine the field in a small area around the singularity. From Fig. 6, the following characteristics of the system may be easily determined:

(1) The closed-loop roots—namely, the locations of the intersections of the 180° phase stream lines and the

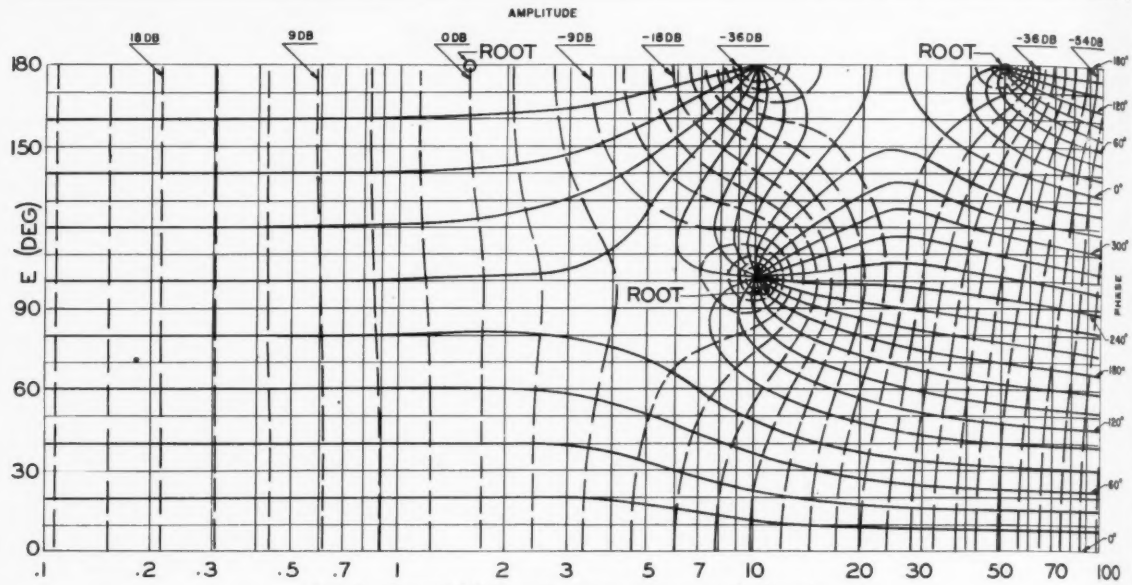

FIG. 6. Potential field analog to open-loop transfer function.

unity gain potential lines. These in turn determine (a) the damping factors of the oscillatory modes [if the vertical coordinate on which a root lies has the value E_1, then $\zeta = \sin(E_1 - 90°)$]; (b) the damped natural frequency ω of the oscillation, from $\omega = r \sin E_1$.

(2) The effects on the locations of the roots of small changes in gain or phase shift of the open loop.

It should be noted that it is not necessary to develop the entire flow field to determine roots corresponding to less than critically damped modes. Rather, just the region in the vicinity of the 180° phase lines and 0-db. amplitude lines need be developed. For poorly damped roots, this was seen to be near the imaginary axis, and thus the location of the root may be determined quickly with good accuracy. For well-damped roots, the root lies near the real axis, and it becomes more difficult to determine its location accurately. However, in such cases great accuracy is not usually required. For the problem investigated above, only the region shown in Fig. 7 would have had to be developed, a job requiring only a few minutes. The construction of the field may be made with any desired accuracy, the only restrictions being the effort put in by the operator and the accuracy with which the basic data are known.

Another advantage of the method is that the effects of shaping networks in improving the stability of the system may be determined by the direct superposition of the flow field of the shaping network on the flow field of the open loop, since potential fields are directly additive. In particular, the fields representing various combinations of one and two singularities may be drawn for standard spacings of the singularities, thus enabling

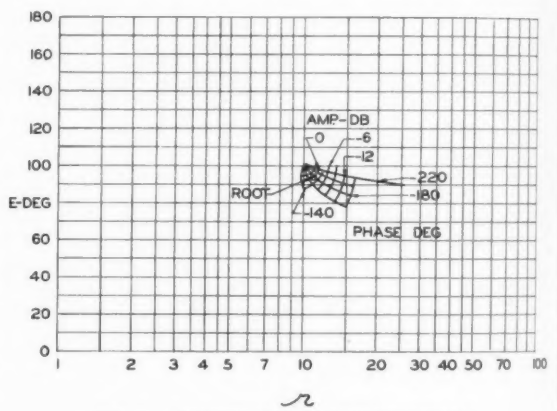

FIG. 7. Determination of oscillatory mode.

the operator to know at a glance the effects of the standard networks, such as low-pass filters, bridged-T filters, etc. The logarithmic abscissa is particularly useful in this respect, since such fields may be positioned at any frequency without changing the shape of the potential or stream lines. The concept of regarding the zeros and poles of the open-loop transfer function as the singularities of a flow field is a useful one in this respect,[1] in that a physical feeling may be developed for the proper positioning of zeros and poles of the shaping networks to reduce the effects from undesirable singularities in the original function or to provide desired effects on the final field.

REFERENCES

[1] Brown, G. S., and Campbell, D. P., *Principles of Servomechanisms*, p. 96; John Wiley & Sons, Inc., New York, 1948.

[1] Hansen, W. W., and Lundstrom, O. C., *Experimental Determination of Impedence Functions by the Use of an Electrolytic Tank;* Proc. of I.R.E., August, 1945.

[2] Rosen, H. A., *Applications of the Potential Analogy in Network Analysis*, Ph.D. Thesis, California Institute of Technology, 1951.

[4] Lamb, H., *Hydrodynamics*, p. 64; Dover Publications, New York, 1945.

[5] Pipes, L. A., *Applied Mathematics for Engineers and Physicists*, p. 457; McGraw-Hill Book Company, Inc., New York, 1946.

[6] Weber, E., *Electromagnetic Fields, Theory and Applications; Volume I—Mapping of Fields*, p. 202; John Wiley & Sons, Inc., New York, 1950.

[7] Huggins, W. W., *A Note on Frequency Transformations for Use with the Electrolytic Tank;* Proc. of I.R.E., March, 1948.

[8] Gardner, M. F., and Barnes, J. L., *Transients in Linear Systems; Volume I, Lumped-Constant Systems*, p. 153; John Wiley & Sons, Inc., New York, 1942.

[9] Profos, P., *A New Method for the Treatment of Regulation Problems*, Sulzer Technical Review (Winterthur, Switzerland), No. 2, 1945.

[10] Evans, W. R., *Servo Analysis by Locus of Roots Method*, North American Aviation, Inc., Aerophysics Laboratory Report 787, November 1, 1948.

[11] Bollay, W., *Aerodynamic Stability and Automatic Control*, Fourteenth Wright Brothers Lecture, Journal of the Aeronautical Sciences, Vol. 18, No. 9, pp. 569–617, September, 1951.

Forced Convection Heat Transfer from Horizontal Cylinders in a Rarefied Gas

(*Concluded from page 180*)

[2] Drake, R. M., Jr., and Kane, E. D., *Heat Transfer Problems in Rarefied Gases*—General Discussion of Heat Transfer, London, 1951.

[3] Kovásznay, L. S. G., and Törmarck, S. I. A., *Heat Loss of Hot Wires in Supersonic Flow*, Bumblebee Report 127, The Johns Hopkins University, April, 1950.

[4] Carslaw, and Jaeger, J. C., *Some Problems in the Conduction of Heat*, Proc. London Math. Soc. (2), Vol. 46, p. 361, 1940

[5] Jaeger and Clark, *A Short Table of* $\int_0^\infty \frac{e^{-xu^2}}{J_0^2(u) + Y_0^2(u)} \frac{du}{u}$, Proc. Royal Soc. of Edinburgh (A), Vol. 61, p. 229, 1941–1943.

[6] McAdams, W. H., *Heat Transmission*, 2nd Ed., p. 221, McGraw-Hill Book Company, Inc., New York, 1942.

[7] Jaeger, J. C., *Heat Flow in a Region Bounded Internally by a Circular Cylinder*, Proc. Royal Soc. of Edinburgh (A), Vol. 61, p. 223, 1941–1943.

[8] Carslaw and Jaeger, *Conduction of Heat in Solids*, Oxford University Press, London, 1947.

[9] Kennard, E. H., *Kinetic Theory of Gases;* McGraw-Hill Book Company, Inc., New York, 1938.

[10] Stalder, J. R., Goodwin, Glen, and Creager, M. O., *Heat Transfer to Bodies in a High Speed Rarefied Gas Stream*, General Discussions on Heat Transfer, London, 1951.

[11] Hilpert, R., *Wärmeagabe von geheizten Drahten und Rohren im Luftstrom*, Forschung Ingenieurwesens, Vol. 4, pp. 215–224, 1933. (See also reference 6.)

Readers' Forum

BRIEF REPORTS of investigations in the aeronautical sciences and discussions of papers published in the JOURNAL are presented in this special department. Publication will be completed as soon as possible after receipt of the material. The Editorial Committee does not hold itself responsible for the opinions expressed by the correspondents. Contributions should not exceed 800 words in length.

The Equations for Pressure and Momentum Using Linearized Theory for Compressible Flow

Lee S. Wasserman
Wright Air Development Center, Wright-Patterson Air Force Base, Ohio
November 7, 1952

THE PROBLEM OF COMPUTING DRAG by the momentum theorem for linearized compressible flow requires the use of expressions for the pressure and the momentum. These expressions are given in the Russian literature by Gurevich, but I have not seen them published in this country.

The pressure expression is derived as follows:

$$-dP/\rho = (U_0 + u)\,du + v\,dv \tag{1}$$

According to the linear theory $\rho = \rho_0[1 - (U_0 u/a_0^2)]$ so that by substitution of the expression for ρ and integration we obtain:

$$\frac{P_0 - P}{\rho_0} = U_0 u + \frac{u^2}{2}(1 - M_0^2) + \frac{v^2}{2} \tag{2}$$

where only terms up to second order are retained, $M_0 = U_0/a_0$ is the Mach Number of the free stream and P_0 is the free-stream static pressure.

The rate of change of momentum (I) is of the form

$$dI/d\tau = \int \rho u(u_0 + u)\,dy + \int \rho uv\,dx \tag{3}$$

making the substitution for ρ given above yields

$$(1/\rho_0)\,(dI/dt) = \int U_0 u\,dy + (1 - M_0^2)\int u^2\,dy + \int uv\,dx \tag{4}$$

where the terms up to second order are retained.

Note on a Method of Root Area Analysis for Swept Wings

John C. Bowman
Research Engineer, Special Weapons Division, Northrop Aircraft, Inc., Hawthorne, Calif.
October 27, 1952

IN A RECENT SUMMARY of swept-wing analysis methods,[1] mention was made of an approximate method by Hall[2] with apparently limited applicability. Mr. Hall's method has been the basis of an analysis[3] conducted at Northrop in which the following extensions and refinements have been made in an effort to increase its usefulness:

(1) The analysis is extended from a four-spar system to include any number of spars. This was accomplished by means of a simplified equivalent structure developed from a suggestion by H. Wagner.

(2) An alternative exponential spanwise distribution of root effect is evaluated.

(3) A simplifying concept regarding a first estimate of initial root effects is made on the basis of empirical information.

(4) An improved method of torque box analysis is introduced.

(5) Warping as a result of external torque loading, assumed negligible in Mr. Hall's work, is found important and is considered.

(6) Clarification of notation is made.

(7) Application of the method to a typical multispar thick-skin sweptback wing is made, including a tab form solution suitable for desk calculator techniques.

(8) Comparison with Northrop test results[4,5] is introduced. Agreement is good in most respects. General analytical results appear consistent with those from the large number of less approximate methods[1] applying to rather different structure.

Basically, the analysis method is one of consistent deformations in which an elementary stress system is selected which satisfies statical requirements and which provides calculable elementary deformations, including warpage of sections out of their planes. These deformations are not necessarily compatible initially in all parts of the structure. Additional self-equilibrating, or redundant, stresses are then applied which produce corrective deformations so that the final deformations are consistent. Several simplifying assumptions are utilized in evaluating the redundant stress system.

REFERENCES

[1] Williams, M. L., *A Review of Certain Analysis Methods for Swept-Wing Structures*, Journal of the Aeronautical Sciences, Vol. 19, No. 9, p. 615, September, 1952.

[2] Hall, D. B., *Method of Stress Analysis of a Swept Back Wing*, The Glenn L. Martin Company, Report No. SDR-37, October, 1947.

[3] Bowman, J. C., *Method of Root Area Analysis for a Swept Back Wing*, Northrop Aircraft, Inc., Report No. MSRD-6, February, 1952.

[4] Cole, D. M., Jr., *Static Test of Wing*, Northrop Aircraft, Inc., Report No. GM-409, June, 1949.

[5] Simms, M. S., and Benson, A. S., *Evaluation of Wing Static Test Results*, Northrop Aircraft, Inc., Report No. GM325, March, 1950.

Lift of Highly Swept Wings

Harold Mirels
Cornell University, Ithaca, N. Y.
December 17, 1952

THE TWO-DIMENSIONAL CROSS-FLOW CONCEPTS of Munk[1] and Jones[2] have been widely used to obtain the aerodynamic coefficients of low aspect ratio pointed wings, bodies, and wing-body combinations. Relatively few investigations have been made, however, when the cross flow contains a free vortex sheet.

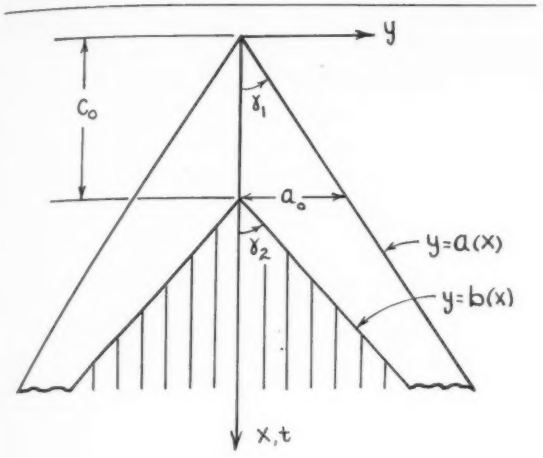

FIG. 1.

This arises, for example, in studies of highly swept wings (Fig. 1). For $x > c_0$, the cross flow contains a shed vortex sheet whose strength depends on the spanwise variation of lift. Thus the cross flow is no longer independent of upstream conditions, and the solution is thereby considerably complicated. A special family of swept wings was considered in reference 3. More recently, Robinson[4] has presented an elegant general solution for the lift of highly swept wings. The solution is expressed in terms of an unknown function, $A(x)$, whose value depends on the wing plan form and is determined from an integral equation. Unfortunately, Robinson's work contains an error that makes his integral equation incorrect. It may therefore be of interest to summarize the lift properties of a highly swept wing, indicating the corrected integral equation and some limiting solutions.

The notation of reference 4 will be used. Only chordwise stations $x \geq c_0$ are considered. The spanwise lifting pressure distribution is

$$\Delta p = 2\rho V \left(\frac{A(x)\boldsymbol{K}'}{a(x)}\right)\left[E'\left(\sqrt{\frac{a^2(x)-y^2}{a^2(x)-b^2(x)}}\right) - F'\left(\sqrt{\frac{a^2(x)-y^2}{a^2(x)-b^2(x)}}\right)\frac{\boldsymbol{E}'}{\boldsymbol{K}'} + \frac{|y|}{a(x)}\sqrt{\frac{y^2-b^2(x)}{a^2(x)-y^2}}\right] \quad (1)$$

The elliptic integrals are of modulus $k' = \sqrt{1-k^2}$, where $k = b(x)/a(x)$. The complete elliptic integrals are indicated by boldface italic type. The sine of the amplitude of the incomplete elliptic integrals is indicated inside the parentheses. Eq. (1) corresponds to the integrated form of Eq. (16) in reference 4. The shape of the pressure distribution curve depends only on $a(x)$ and $b(x)$. The unknown function $A(x)$ appears only as a scale factor. The chordwise variation of net lift is

$$\frac{dL}{dx} = 2\pi\rho V a(x)\left(1 - \frac{\boldsymbol{E}'}{\boldsymbol{K}'}\right)\left(\frac{A(x)\boldsymbol{K}'}{a(x)}\right) \quad (2)$$

which corresponds to Eq. (18) of reference 4. The unknown function $A(x)$ is obtained from the following integral equation:

$$\alpha V\sqrt{a^2(x)-a_0^2} = \int_{c_0}^{x}\left(\frac{A(t)\,\boldsymbol{K}'}{a(t)}\right)\left\{\left(1-\frac{\boldsymbol{E}'}{\boldsymbol{K}'}\right)\times\left[F\left(\frac{a(t)}{a(x)}\right)-\boldsymbol{K}\right]-\left[E\left(\frac{a(t)}{a(x)}\right)-\boldsymbol{E}\right]+\frac{a(t)}{a(x)}\sqrt{\frac{a^2(x)-b^2(t)}{a^2(x)-a^2(t)}}\right\}dt \quad (3)$$

Eq. (3) contains the complete elliptic integrals $\boldsymbol{K}$ and $\boldsymbol{E}$, and it is in this respect that it differs from Eq. (15) in reference 4. Robinson's error arises from his treatment of his Eq. (12). He properly states that a function of x [say $f(x)$] can be added to Eq. (12) but claims that this function may be taken to be zero. Actually, this function is not arbitrary, and it is not equal to zero. If the solution of the swept wing is considered as a superposition of a simple delta wing and a cancellation wing,[5] then $f(x)$ can be shown to equal the value of the cross-flow stream function on the $w = 0$ portion of the cancellation wing.

Let the leading and trailing edges be straight lines with slopes $\tan\gamma_1$ and $\tan\gamma_2$, respectively. Define the slope ratio $r \equiv \tan\gamma_2/\tan\gamma_1$. Then, limiting solutions of Eq. (3) are:
For $r \to \infty$,

$$\frac{A(x)\,\boldsymbol{K}'}{a(x)} = \frac{\alpha V\tan\gamma_1}{\sqrt{1-[b^2(x)/a^2(x)]}} \quad (4a)$$

for $r \to 0$,

$$A(x)\boldsymbol{K}'/a(x) = \alpha V\tan\gamma_1 \quad (4b)$$

for $r = 1$, $x \to \infty$,

$$A(x)\boldsymbol{K}'/a(x) = \alpha V\tan\gamma_1 \quad (4c)$$

for $b(x)/a(x) \ll 1$,

$$\frac{A(x)\,\boldsymbol{K}'}{a(x)} = \alpha V\tan\gamma_1\left[1+\frac{4}{r}\int_0^{b(x)/4a(x)}\frac{ds}{\ln s}+\frac{1}{2}\left(\frac{b(x)}{a(x)}\right)^2+\ldots\right] \quad (4d)$$

Eq. (4a) is the same as Robinson's limiting solution to his integral equation. The correction to the integral equation does not effect the $r \to \infty$ case. Eq. (4c) corresponds to a two-dimensional swept wing. Eq. (4d) was obtained by an approximation in which it is difficult to estimate the error involved, but it is an excellent agreement with numerical solutions of the integral equation.

When the leading and trailing edges are parallel ($r = 1$), the parameter

$$A(x)\,\boldsymbol{K}'/a(x)\alpha V\tan\gamma_1$$

equals one for $x = c_0$, then decreases (with increasing x) to a minimum value of 0.94 at $b(x)/a(x) \cong 0.5$, and then increases gradually to a value of 1. Thus, use of the constant value 1 seems justified for this case.

The writer has developed a general procedure for calculating the aerodynamics of highly swept wings. Expressions similar to Eqs. (1) to (4) have been obtained for the rolling and pitching case. Early publication is intended.

REFERENCES

[1] Munk, M. M., *The Aerodynamic Forces on Airship Hulls*, N.A.C.A. Report No. 184, 1924.

[2] Jones, R. T., *Properties of Low Aspect Ratio Pointed Wings at Speeds Below and Above the Speed of Sound*, N.A.C.A. Report No. 835, 1946.

[3] Lomax, H., and Heaslet, M. A., *Linearized Lifting-Surface Theory for Swept-Back Wings with Slender Plan Forms*, N.A.C.A. T.N. No. 1992, 1949.

[4] Robinson, A., *Aerofoil Theory for Swallow Tail Wings of Small Aspect Ratio*, The Aeronautical Quarterly, Vol. IV, August, 1952.

[5] Mirels, H., *A Lift-Cancellation Technique in Linearized Supersonic-Wing Theory*, N.A.C.A. Report No. 1004, 1951.

Effects of Angle of Attack on Local Skin-Friction Coefficients at $M_0 = 4$

John Joseph Martin
Research Engineer, North American Aviation, Inc., Downey, Calif.

November 11, 1952

GENERALLY, SKIN-FRICTION COEFFICIENTS are based on properties of air immediately outside the boundary layer, and

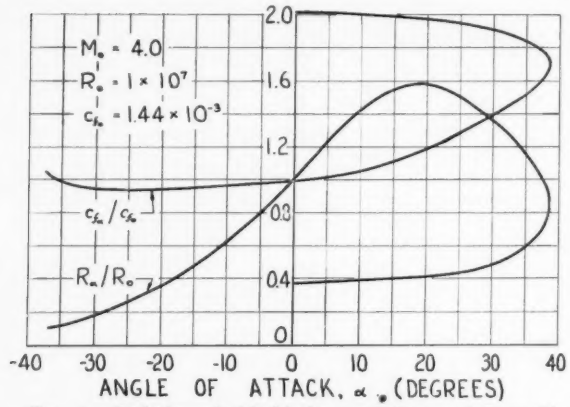

FIG. 1. Variation of skin-friction coefficient and Reynolds Number ratios with angle of attack for $M_0 = 4.0$ and $R_0 = 1 \times 10^7$.

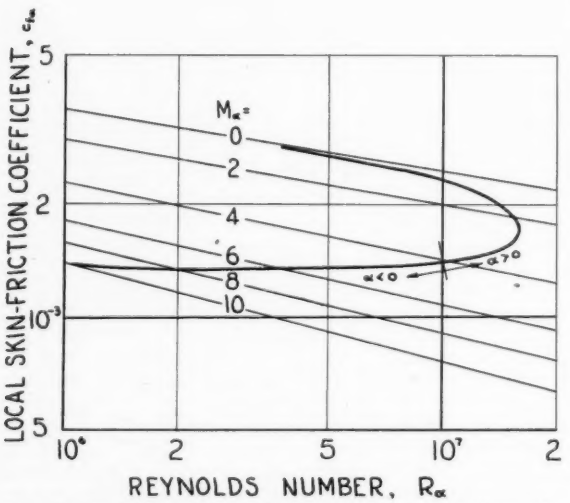

FIG. 2. Variation of skin-friction coefficient with Reynolds Number for parameters of Fig. 1.

this leads to no particular difficulty in supersonic flow, since, when there is a change in the properties of air through a shock, results of this change may be calculated or obtained from tabulations for this purpose. It is the intent of this note, however, to show how local skin friction, and therefore in some measure heat transfer, may vary for a particular case with angle of attack.

Specifically, the case is that of a flat plate with* $M_0 = 4$

$$R_0 = 1 \times 10^7$$

$$T_w/T_\alpha = 1 + {}^1/_2(\gamma - 1)M_\alpha^2$$

(i.e., T_w = a constant = insulated plate temperature) with shock wave attached. The local coefficients were computed on the basis of reference 1 in which

$$c_{f\alpha} = c_{f\alpha}(M_\alpha, R_\alpha, T_w/T_\alpha)$$

Then, given values of M_0 and R_0, these need be converted to M_α, R_α, and T_w/T_α for the plate at an angle of attack; further, from these, $c_{f\alpha}$ may be found.

* Subscripts denote angle of attack; M_0 is free-stream Mach Number for plate at $\alpha = 0$; M_α is free-stream Mach Number for plate at angle of attack α.

Now,

$$R_\alpha = M_\alpha a_\alpha \rho_\alpha/\mu_\alpha = R_0\left(\frac{M_\alpha}{M_0}\cdot\frac{a_\alpha}{a_0}\cdot\frac{\rho_\alpha}{\rho_0}\cdot\frac{\mu_0}{\mu_\alpha}\right)$$

and if

$$\mu_\alpha/\mu_0 = [1.505(T_\alpha/T_0)^{3/2}]/[1 + 0.505/(T_\alpha/T_0)]$$

as is so for air when $T_0 = 393$ °R. (see reference 1), then

$$T_w/T_\alpha = 1 + (1/2)(\gamma - 1)M_\alpha^2$$

as indicated. Also,

$$R_\alpha = M_\alpha a_\alpha \rho_\alpha/\mu_\alpha = R_0\left[\frac{M_\alpha}{M_0}\cdot\frac{\rho_\alpha}{\rho_0}\cdot\frac{1 + 0.505/(T_\alpha/T_0)}{1.505}\right]$$

and M_α as a function of α may be found in tabulations[2,3] or calculated. Then, since $c_{f\alpha}$ is a function of M_α, R_α, and T_w/T_α, computations† may be made, and the results are plotted in Fig. 1 as functions of angle of attack. In this figure, for $\alpha > 0$, the upper branch of $c_{f\alpha}/c_{f0}$ and the lower branch of R_α/R_0 are for a strong shock and the remainder of the curves are for a weak shock. Fig. 2 is a graph of the calculations on the usual plot of $c_{f\alpha}$ vs. R_α, with M_α as a parameter, and shows the relationships among $c_{f\alpha}$, R_α, and M_α that obtain in Fig. 1.

REFERENCES

[1] Van Driest, E. R., *Turbulent Boundary Layer in Compressible Fluids*, Journal of the Aeronautical Sciences, Vol. 18, No. 3, pp. 145–161, March, 1951.

[2] Ferri, A., *Elements of Aerodynamics of Supersonic Flows*, pp. 430–431; The Macmillan Company, New York, 1949.

[3] *Notes and Tables for Use in the Analysis of Supersonic Flow*, N.A.C.A. T.N. No. 1428, December, 1947.

† These were very kindly done by Mrs. R. B. Davis.

Comments on "Remarks on Dynamic Loads in Landing"

Frederic M. Hoblit
Lockheed Aircraft Corporation, Burbank, Calif.
December 10, 1952

IN A PAPER, "Remarks on Dynamic Loads in Landing," in the April, 1952, JOURNAL, Zahorski gives an example of calculated dynamic loads. In this example, dynamic magnification factors are calculated for four cases, with maximum values at the wing tip as follows:

Maximum landing weight, limit drop	1.4
Maximum landing weight, ultimate drop	2.2
Normal landing weight, limit drop	3.3
Normal landing weight, ultimate drop	6.3

This variation is rather startling, and several conclusions might be drawn therefrom.

Zahorski's conclusion is that, in a dynamic landing analysis, it is important to use the correct forcing function and, in particular, to base the dynamic analysis on the *limit* loading rather than the *ultimate* loading. The desired factor of safety is then applied to the resulting accelerations after the calculations are completed. The writer heartily concurs in this conclusion.

A second conclusion that some readers may have drawn is that, since the four forcing functions appeared to be of roughly the same shape, the results of a dynamic analysis are too sensitive to small changes in parameters to be of use in establishing design load factors.

This conclusion is entirely too pessimistic. A major part of the variation in dynamic factor in the present case is not due to small differences in the forcing functions. Instead, what appear

to be small differences in the forcing function are actually in some cases substantial differences, and in other cases the mode shapes change considerably with changes in airplane gross weight. Furthermore, whatever degree of sensitivity does actually exist can be detected and estimated by examining the mode shapes and the response time histories in the various modes.

The change in mode shape between the normal and maximum landing weight cases is due to the fact that not only the total mass changes but also the distribution of mass. Unfortunately, Zahorski did not include either the mass distributions or the mode shapes, but one can deduce from the data given that the differences in mode shape between the two cases are rather drastic. For example, the signs of the accelerations for the first mode indicate a shift of the node from inboard of the gear for normal landing weight to outboard of the gear for maximum landing weight, possibly as a result of a large addition of fuel in wing-tip tanks. Naturally, a significant difference in dynamic factor should be expected, even if the forcing functions were identical.

The shape of the forcing function for any given one-time loading is characterized by (1) the time required to reach maximum load or "loading period," (2) the period of time the maximum load is sustained, and (3) the time required for removal of load. Each of these can have a great effect on the dynamic response. In comparing the limit-drop and ultimate-drop cases, it is seen that item (2) above is completely different in the two cases, since the forcing function in one case is a triangle and in the other is a long trapezoid. A considerable difference in dynamic factor is therefore to be expected.

Some of the variation between the limit and ultimate cases cannot be accounted for by the above considerations and probably must be attributed to rather small changes in forcing function (although some question might be raised whether a 40 to 50 per cent change in loading period is a "small change"). In any event, this variation could have been anticipated by examining the time histories of the responses in the various modes.

First, it is noted that, in this example, the higher frequency modes—the second and third—contribute a large part of the total acceleration. The time at which the maximum total acceleration occurs, however, is governed largely by the rigid-airplane and first-mode accelerations. If at this time the second and third modes should be in phase, they would add a large amount to the total; whereas if they are exactly out of phase, their contribution would be negligible. Comparing Zahorski's limit-drop and ultimate-drop cases at maximum weight (his Figs. 5 and 6), it is seen that the second and third modes both add at the critical time in the ultimate-drop case but are of opposite sign in the limit-drop case. If in the limit-drop case both of these modes had added, the dynamic magnification factor would have increased from 1.4 to 1.8, which is much closer to the ultimate-drop value of 2.2.

In this instance the difference in phasing is due to a difference in loading period. For the phasing to change as much as in the example would appear to be possible only when the loading period changes by an amount that is about the same as, or greater than, half the natural period of one of the two modes. In other words, the modes involved would have to have a relatively high natural frequency.

Incidentally, significant changes in phasing can also result from small changes in natural frequency, especially when the maximum total acceleration occurs a considerable time after the initial disturbance. If, for example, the critical time occurs after two cycles of the second mode and three cycles of the third mode, it is clear that only a 16 per cent change in the frequency of the higher mode will completely reverse the phase relation at the critical time, so that if these two modes originally added, they would then subtract. Considerable uncertainty as to natural frequency is to be expected, since calculated natural frequencies depend upon approximations to the stiffness properties of the structure and upon a mass distribution that may depart considerably in service from that chosen as a basis for the analysis.

Consequently, consideration should always be given to the effect of possible phase variation between the various modes at the critical time. The effect of phase variation on total acceleration is, of course, limited to the sum of the acceleration amplitudes of the two modes for which the phase relation is in doubt.

The shape of forcing function also affects the maximum acceleration independently of the relative phasing between modes. Zahorski notes from his Eq. (14) that, for a trapezoidal forcing function, if the natural period of a mode is contained exactly 1, 2, 3, etc., times in the loading period, the ensuing amplitude of acceleration in the mode is zero. If this number of times is in the neighborhood of 2, as for Zahorski's third mode, it is seen that only about a 20 per cent change in natural frequency or loading period would make the difference between zero amplitude and a peak amplitude. So again the maximum response is seen to be sensitive to both the shape of the forcing function and the natural period of the mode. This sensitivity can be anticipated by looking at the time history for a single case, and the possible range of response can readily be determined.

It should be emphasized that, when the dynamic analysis indicates sensitivity of accelerations to shape of forcing function or to natural frequency, this sensitivity is a real phenomenon that would show up as scatter of test data if tests were made and will occur in service, especially as the airplane mass distribution varies.

In summary, a dynamic analysis can be of real value. Accelerations obtained from a calculated time history must, however, be interpreted with judgment rather than accepted blindly; due consideration should—and readily can—be given to the possible range of results which might occur with reasonable variation of conditions.

A Reply—Single Degree Flutter of an Aileron

H. L. Runyan, H. J. Cunningham, and C. E. Watkins
Langley Aeronautical Laboratory, N.A.C.A., Langley Field, Va.
October 3, 1952

THE SUBJECT OF single degree of freedom flutter of a control surface has been discussed in reference 1, and some of the material was presented in reference 2. In these references it was analytically demonstrated that a control surface having no aerodynamic balance (hinged at its leading edge) could flutter in a single degree of freedom. At about the time these papers were published, another treatment of this problem was published,[3] with conclusions that appeared to contradict those of references 1 and 2—that is, the conclusions of reference 3 stated that only ailerons with large amounts of aerodynamic balance could flutter. Accordingly, an attempt was made to point out the basic reason for the apparent discrepancy between the two conclusions in a Readers' Forum note.[4] This note was then followed by another Readers' Forum item[5] by the authors of reference 3 in which they strongly reiterated their previously made deductions.

Inasmuch as aileron flutter in a single degree of freedom is theoretically possible without aerodynamic balance and, under certain conditions, may be dangerously significant, we are induced to present this brief reply to reference 5 with hopes that the matter will be laid to rest without false impressions of the theoretical possibilities of this type of flutter. This can be simply achieved with the equations and notation of reference 3 itself.

In the absence of structural damping, the conditions of aileron stability or instability are directly determined by the algebraic sign of T_I, the coefficient of the imaginary part of the complex moment term T, of reference 3. Positive values of T_I indicate

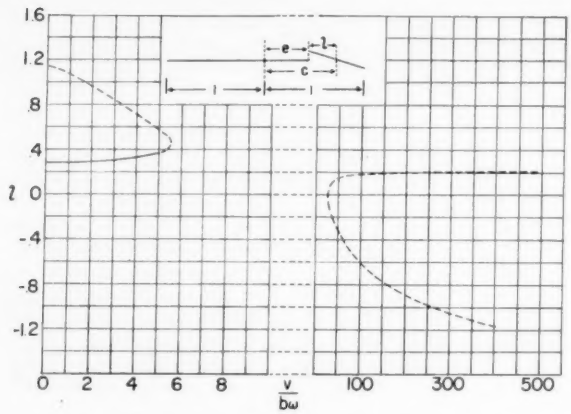

Fig. 1. Values of l and $v/b\omega$ for which T_l vanishes. ($e = 0.4$)

dynamic instability, negative values indicate stable conditions, and the vanishing of T_l indicates the existence of a borderline state of equilibrium separating damped and undamped aileron motions. We are thus behooved to consider the nature of T_l as a function of the various parameters considered in reference 3—namely, aileron leading-edge position e, hinge position c, aerodynamic balance $l = c - e$, and reduced speed parameter $v/b\omega$. If for a given value of e in the range $0 \leq e < 1$ corresponding values of l and $v/b\omega$ for which T_l vanishes are plotted, it will be found that such plots invariably consist of two distinct loops or branches, one loop corresponding to small values of $v/b\omega$ and the other to large values of $v/b\omega$. Fig. 1 of reference 3 consists of partial plots of the first loop of $T_l = 0$ just described—that is, for small values of $v/b\omega$—for several values of e in the range $0 \leq e \leq 0.7$. A more complete plot of $T_l = 0$ for one representative value of e ($e = 0.4$) is shown here in Fig. 1. The only portion of the curves in this plot which is presented in reference 3 is indicated by the solid curve, and results of more extended calculations are indicated by dashed curves. Values of T_l corresponding to points inside the loops are positive, indicating instability, and values corresponding to points outside the loops are negative, indicating stability. It will be noted that for $l = 0$ (no aerodynamic balance) that T_l vanishes for $v/b\omega = 33$ (approximately) and for some value of $v/b\omega > 33$ for positive values of l in the range $0 \leq l \leq 0.204$. This corroborates the statement here and the conclusions of references 1 and 2 that aileron flutter is possible without aerodynamic balance. (Negative values of l correspond to hinge positions ahead of the aileron leading edge and are excluded from the present discussion.)

As a final remark, it is pointed out that the mass moment of inertia parameter I_β is an important parameter that strongly affects the degree of stability or instability of an aileron. For any combination of values of $v/b\omega$ and l which causes the value of T_l to vanish, there exists real positive value of I_β for which real values of flutter frequency are given by the equation of reals in Eq. (5) of reference 3. Furthermore for values of l corresponding to hinge position ahead of the aerodynamic center of pressure on the aileron (about 34 per cent aileron chord), the ratio of flutter frequency to aileron frequency will invariably be greater than unity, a conclusion apparently at variance with reference 3.

References

[1] Runyan, Harry L., *Effect of Various Parameters Including Mach Number on Single-Degree-of-Freedom Flutter of a Control Surface in Potential Flow*, N.A.C.A. T.N. No. 2551, December, 1951.

[2] Runyan, Harry L., Cunningham, Herbert J., and Watkins, Charles E., *Theoretical Investigation of Several Types of Single Degree of Freedom Flutter*, Journal of the Aeronautical Sciences, Vol. 19, No. 2, pp. 101–110, 126, February, 1952.

[3] Abichandani, K. P., and Rosenberg, Reinhardt M., *Aileron Flutter in a Single Degree of Freedom*, University of Washington, Engineering Experiment Station, Bulletin 118, Seattle, 1951.

[4] Runyan, Harry L., Cunningham, Herbert J., and Watkins, Charles E., *Single Degree of Freedom Aileron Flutter of an Aileron*, Readers' Forum, Journal of the Aeronautical Sciences, Vol. 19, No. 3, pp. 215–216, March, 1952.

[5] Abichandani, K. P., and Rosenberg, Reinhardt M., *Once More—Single Degree of Freedom Flutter of an Aileron*, Readers' Forum, Journal of the Aeronautical Sciences, Vol. 19, No. 7, pp. 503–504, July, 1952.

Authors' Closure

R. M. Rosenberg
Boeing Airplane Company, Seattle
October 30, 1952

THESE COMMENTS—it is hoped that they constitute a closure—are written without the collaboration of my coauthor in the paper "Aileron Flutter in a Single Degree of Freedom"[1] because the distance between us makes such a cooperative venture difficult. In spite of the omission of K. P. Abichandani's name from this contribution to the Readers' Forum, its content is based largely on his thesis[2] for the M.S. degree in Aeronautical Engineering, completed and entered into the records of the University of Washington in December, 1950.

It is anomalous that a paper, having had but little circulation should become the subject of discussions[3,4] that are now entering into the third issue of the JOURNAL OF THE AERONAUTICAL SCIENCES where the paper under discussion was *not* published. However, Runyan, Cunningham, and Watkins did not have the opportunity to discuss this paper in its originating publication because the *Bulletin* of the University of Washington Engineering Experiment Station is not a periodical. As a result, readers have been presented with the discussion of a paper that most of them have had no opportunity to examine; they probably enjoy it no more than hearing the punchline of an unknown joke.

The above Readers' Forum contribution by Runyan, Cunningham, and Watkins is substantially in agreement with some recent findings by Abichandani, reported to me in a personal communication,[5] and it largely resolves the apparent discrepancies that have formed the subject of the earlier discussions.

It appears that the earlier work by Runyan[6] and by Runyan, Cunningham, and Watkins,[7] concerned with single degree of freedom flutter of ailerons that are not aerodynamically balanced, was necessarily restricted to deal with that loop of their Fig. 1 above which lies in $v/b\omega \geq 33$. We shall call it the "outer loop." If one considers the curves of their Fig. 1 as the solution to the equation

$$l = f(v/b\omega) \tag{1}$$

then one may regard the problem of references 6 and 7 as that of finding the zeros of $f(v/b\omega)$. But, $f(v/b\omega)$ has apparently only one zero in the outer loop; therefore, the authors were actually concerned with locating that value of $v/b\omega$ at which the outer loop crosses the line $l = 0$.

We posed the more general problem of solving Eq. (1); however, by using the tables of flutter coefficients tabulated by Smilg and Wasserman,[8] we were necessarily restricted to deal with the "inner loop" of Fig. 1 above because we considered the solution of this equation only in the interval $0 \leq v/b\omega \leq 16.67$, the range of $v/b\omega$ in reference 8.

Although the upper branch of the inner loop was not *plotted* in our original paper,[1] it was not overlooked. In this paper, we wrote out the above Eq. (1). It is Eq. (8) of reference 1,

$$l = \frac{b_1 + b_2}{2b_4} \pm \sqrt{\frac{(b_1 + b_2)^2}{4b_4^2} - \frac{b_2}{b_4}} \tag{2}$$

and the b_i are defined by

$$\left.\begin{aligned} P_\beta &= a_1 + ib_1 \\ T_z &= a_2 + ib_2 \\ T_\beta &= a_3 + ib_3 \\ P_z &= a_4 + ib_4 \end{aligned}\right\} \text{all functions of } v/b\omega$$

It was remarked[4] that l is a double-valued function of $v/b\omega$, and, in the earlier thesis[2] by Abichandani, *both* values of l have been computed for a variety of values of e; they are listed in reference 2, Tables 2.01 to 2.08. However, the upper branch of the inner loop was not plotted for the following reason: From the geometric relations of the illustration accompanying Fig. 1 of the above reply, it will be seen that the aileron chord is $1 - e$. Thus, values of $l > 1 - e$ imply that the overhanging portion of the aileron is larger than the entire aileron chord or that the aileron is hinged aft of its trailing edge. We may conclude that not only are values of $l < 0$ excluded, as observed in the above reply, but so are the values of $l > 1 - e$ or that l must lie in $0 \leq l \leq 1 - e$. This excludes the major portion of the upper branch of the inner loop of the above illustration, because, in the example chosen, $1 - e = 0.6$. In fairness to Runyan, Cunningham, and Watkins, it should be pointed out that we stated[1] that the positive sign in Eq. (2) always implies that the aileron is hinged aft of its trailing edge. Actually, this statement is true only for certain values of e; but in those cases where it is not strictly true, it holds nevertheless for most values of $v/b\omega$. For instance, in the example of the Readers' Forum item above, the lower branch only of the inner loop has significance in the interval $0 \leq v/b\omega \leq 4.8$ (approximately), while both branches are of interest in $4.8 < v/b\omega \leq 5.5$.

It remains to consider the parting remark of the above reply. This is a repetition of an earlier statement by the same authors.[3] We find that we can no more agree with it now than we could earlier. In our original paper[1] there is an equation that is repeated here for convenience. It is Eq. (18) of reference 1

$$(v_f/v_d)^2 = [1 - (\omega/\omega_\beta)^2]/\eta \qquad (3)$$

The same paper also contains the statement that the aileron divergence speed v_d is imaginary if the aileron is hinged foreward of the aerodynamic center of pressure of the aileron. It will be observed that for this hinge location $(v_f/v_d)^2 < 0$ if the flutter speed v_f is real, which is the case discussed by Runyan, Cunningham, and Watkins. But if $(v_f/v_d)^2$ is negative, then Eq. (3) above demands that $(\omega/\omega_\beta)^2$ be larger than unity (because η is a real nonnegative quantity). Thus, not only *is* the last statement of the above reply in accord, but any other statement would *not* be in accord, with our results.

In spite of some minor discrepancies that appear to exist still, we have reasons to note with pleasure the results of this discussion in the Readers' Forum. In investigations that obviously were independently conducted, the problem of single degree of freedom flutter of ailerons has been investigated. Prior, it was not even known that ailerons are capable of this type of flutter; as a result, the phenomenon was only imperfectly understood. In particular, only one régime of this flutter (the inner loop) was discussed in reference 1, and only one point on the outer loop was discussed in references 6 and 7. Now, both observations are drawn into a single fold, and, as a consequence, the phenomenon is better understood. This pleasant result appears to have made these discussions well worth while.

References

[1] Abichandani, K. P., and Rosenberg, R. M., *Aileron Flutter in a Single Degree of Freedom*, University of Washington, Engineering Experiment Station, Bulletin 118, Seattle, 1951.

[2] Abichandani, K. P., *Single Degree of Freedom Aileron Flutter*, Thesis for the degree of Master of Science in Aeronautical Engineering, University of Washington, Seattle, 1950.

[3] Runyan, H. L., Cunningham, H. J., and Watkins, C. E., *Single Degree of Freedom Flutter of an Aileron*, Readers' Forum, Journal of the Aeronautical Sciences, Vol. 19, No. 3, pp. 215–216, March, 1952.

[4] Abichandani, K. P., and Rosenberg, R. M., *Once More—Single Degree of Freedom Flutter of an Aileron*, Readers' Forum, Journal of the Aeronautical Sciences, Vol. 19, No. 7, pp. 503–504, July, 1952.

[5] Abichandani, K. P., *On Single Degree of Freedom Flutter for Large Values of $v/b\omega$*, Personal Communication, April 21, 1952.

[6] Runyan, H. L., *Effect of Various Parameters Including Mach Number on Single-Degree-of-Freedom Flutter of a Control Surface in Potential Flow*, N.A.C.A. T.N. No. 2551, December, 1951.

[7] Runyan, H. L., Cunningham, H. J., and Watkins, C. E., *Theoretical Investigation of Several Types of Single Degree of Freedom Flutter*, Journal of the Aeronautical Sciences, Vol. 19, No. 2, pp. 101–110, 126, February, 1952.

[8] Smilg, B., and Wasserman, L. S., *Application of Three-Dimensional Flutter Theory to Aircraft Structures*, A.A.F. T.R. No. 4798, July, 1942.

Approximate Calculation of Axisymmetric Flow Near the Vertex of a Body Traveling at High Supersonic Speeds

A. J. Eggers, Jr., and Samuel Kraus

Ames Aeronautical Laboratory, N.A.C.A., Moffett Field, Calif.

November 3, 1952

Introduction

STEADY, INVISCID FLOW in the region of the vertex of a curved noninclined body of revolution with attached shock wave has been studied by Shen and Lin[1] and Cabannes[2] by perturbing the conical flow solution of Taylor and Maccoll.[3] It was found that fluid properties in this region may be obtained by performing rather lengthy numerical integrations of the perturbed conical flow equations. It has recently been indicated,[4,5] however, that flow about such a body traveling at high supersonic speeds, corresponding to values of the hypersonic similarity parameter in excess of 1, may be calculated with relative simplicity using a generalized shock-expansion method. This note describes the application of the method to the determination of flow in the region of the vertex.

Shock-Wave Curvature at the Vertex

A curved axisymmetric body creates pressure disturbances that alter the inclination of the vertex shock wave. Fig. 1 illustrates the geometry of this phenomenon. The pressure disturbances (expansion waves for a convex body) travel along the first family Mach lines, F_1, and interact with the shock wave. The reflected disturbances have been shown[6,7] to be so weak as to create relatively small pressure changes along these lines, provided that neither the Mach Number nor the ratio of specific heats of the disturbed fluid is too close to 1. Now, at the high supersonic speeds under consideration, the variation of Mach Number from the surface to the shock wave is extremely small in

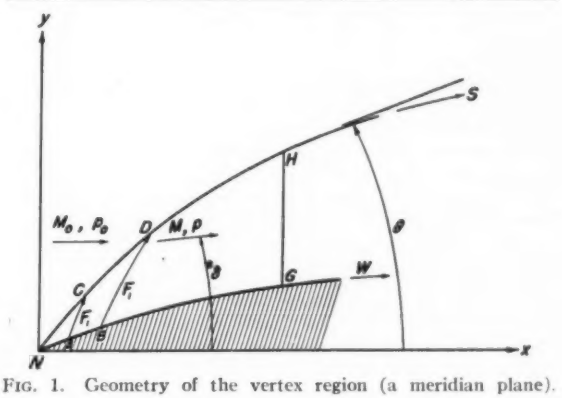

FIG. 1. Geometry of the vertex region (a meridian plane).

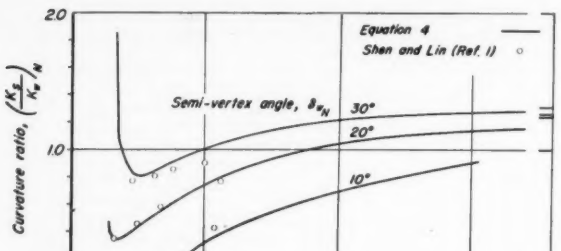

FIG. 2. Variation of curvature ratio with free-stream Mach Number for various semivertex angles.

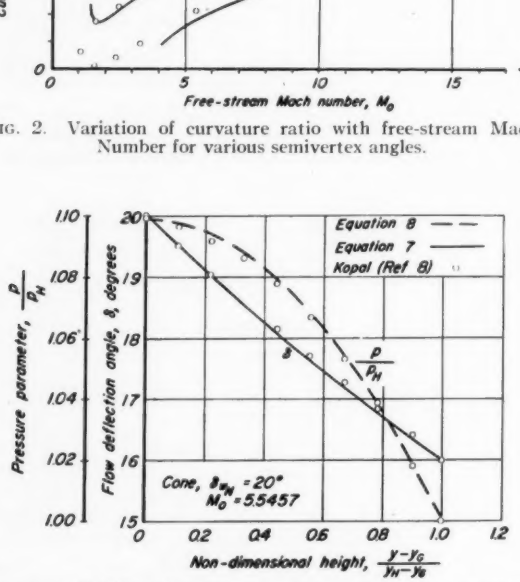

FIG. 3. Variation of pressure parameter and flow deflection angle with nondimensional height.

the unperturbed conical flow; therefore, the variation of pressure is also small. Thus, in the perturbed conical flow field created by the curved body, it is suggested that the variation of pressure along first family Mach lines is small. With this point in mind, it is clear, referring to Fig. 1, that the equation

$$\int_A^C \frac{\partial p}{\partial F_1}\,dF_1 + \int_C^D \frac{\partial p}{\partial S}\,dS = \int_A^B \frac{\partial p}{\partial W}\,dW + \int_B^D \frac{\partial p}{\partial F_1}\,dF_1 \quad (1)$$

relating pressures on the surface w to those just downstream of shock wave s reduces to

$$\int_C^D \frac{\partial p}{\partial S}\,dS \cong \int_A^B \frac{\partial p}{\partial W}\,dW \quad (2)$$

since the quantity

$$\int_A^C \frac{\partial p}{\partial F_1}\,dF_1 - \int_B^D \frac{\partial p}{\partial F_1}\,dF_1$$

is indicated to be small indeed. But $\partial p/\partial W$, the gradient of pressure with distance along the body, is, to the accuracy of this analysis,[4] the Prandtl-Meyer value. Noting that $\partial\theta/\partial s = K_s$, the shock-wave curvature, and $\partial\delta_w/\partial W = K_w$, the body curvature, we have, then, from Eq. (2), in the limit as points A, B, C, and D approach the vertex, the following expression for the ratio of shock-wave to body curvature:

$$\left(\frac{K_s}{K_w}\right)_N = \frac{(\partial p/\partial \delta_w)_N}{(\partial p/\partial \theta)_N} \lim_{A,\,B,\,C,\,D \to N} \cdot \frac{\int_A^B dW}{\int_C^D dS} \quad (3)$$

The pressure gradient along the shock wave $(\partial p/\partial\theta)_N$ can be evaluated using the oblique-shock-wave equations, while the pressure gradient along the body $(\partial p/\partial\delta_w)_N$ is given by the Prandtl-Meyer equation. With the knowledge that the local Mach Number is essentially constant and the difference between flow inclination angle and ray angle is small compared to 1 in the conical flow at the vertex,[4] the ratio of integrals in this relation is readily evaluated. Thus, according to the generalized shock-expansion method, the expression for the curvature ratio may be written

$$\left(\frac{K_s}{K_w}\right)_N = \frac{2\gamma M_0^2 \sin^2\theta_N - (\gamma - 1)}{M_0^2 \sin 2\theta_N \sin 2\beta_N}\left[1 - \frac{2\tan(\theta_N - \delta_{w_N})}{\tan\beta_N}\right]^{1/2} \quad (4)$$

where β_N, the Mach angle just downstream of the shock, and θ_N may be determined from existing conical flow calculations[3, 4, 5] for given M_0 and δ_{w_N}.

Results of calculations of curvature ratio using Eq. (4) for several free-stream Mach Numbers and semivertex angles are compared in Fig. 2 with those presented by Shen and Lin. The agreement at higher Mach Numbers would seem to justify application of the generalized shock-expansion method to the solution of this problem.

Flow Conditions Along a Line a Short Distance Downstream of the Vertex

The variation of a fluid property, ϕ, along the vertical line GH (see Fig. 1) can be expressed by a Taylor expansion as follows:

$$\phi = \phi_R + (\partial\phi/\partial y)_R(y - y_R) + (\partial^2\phi/\partial y^2)_R(y - y_R)^2/2 + \dots \quad (5)$$

where R is a reference point on the line. Since the shape of the shock wave has been related to the shape of the body, we may proceed with this relation to calculate flow conditions along GH. To illustrate, at the high supersonic speeds of interest here, the rate of change of δ with y at point G for axisymmetric flow can easily be shown[4] to be

$$(\partial\delta/\partial y)_G = -\sin\delta_G \cos\delta_G/y_G \quad (6)$$

The second derivative $(\partial^2\delta/\partial y^2)_G$ is evaluated using the boundary conditions at G and H. Thus the variation of δ with y along the line GH is

$$\delta \cong \delta_G - (\sin\delta_G \cos\delta_G/y_G)(y - y_G) + [\delta_H - \delta_G + (\sin\delta_G \cos\delta_G/y_G)(y_H - y_G)][(y - y_G)/(y_H - y_G)]^2 \quad (7)$$

Similarly, knowing that the variation of static pressure p with F_1 at G is zero, the following relation for p obtains:

$$p \cong p_G - \frac{2\gamma p_G K_{w_G} \cos(\beta + \delta)_G}{\sin\beta_G \sin 2\beta_G}(y - y_G) + \left[p_H - p_G + \frac{2\gamma\, p_G K_{w_G} \cos(\beta + \delta)_G}{\sin\beta_G \sin 2\beta_G}(y_H - y_G)\right] \times [(y - y_G)/(y_H - y_G)]^2 \quad (8)$$

The variations of δ and p/p_H with $(y - y_G)/(y_H - y_G)$ [Eqs. (7) and (8)], are compared in Fig. 3, in the limit of purely conical flow, with the variations obtained from M.I.T. tables.[6] Good agreement is observed.

It is convenient to expand the total pressure p_t about the point H, since the gradient of p_t with y is readily calculated at this point. In an analogous manner, then, the variation of total-pressure with height is given by the expression

$$p_t \cong p_{t_H} + [(\partial p_t/\partial\theta)_H K_{s_H} \cos\delta_H/\sin(\theta - \delta)_H](y - y_H) + [p_t - p_{t_H} - \{(\partial p_t/\partial\theta)_H K_{s_H} \cos\delta_H/\sin(\theta - \delta)_H\}(y_G - y_H)] \times [(y - y_H)/(y_G - y_H)]^2 \quad (9)$$

Knowing δ, p, and p_t, other pertinent fluid properties can be determined along the line GH. Thus, this line may be used as a starting line for generalized shock-expansion solutions of flow about noninclined bodies of revolution traveling at high super-

sonic speeds. The method may also prove useful in starting characteristics solutions for flow about a body.

REFERENCES

[1] Shen, S. F., and Lin, C. C., *On the Attached Curved Shock in Front of a Sharp-Nosed Axially Symmetrical Body Placed in a Uniform Stream*, N.A.C.A. T.N. No. 2505, October, 1951.

[2] Cabannes, H., *Étude de L'Onde de Choc Attachée dans les Écoulements de Révolution, Première Partie: Cas d'un Obstacle Terminé par un Ogive*, La Recherche Aeronautique No. 24, pp. 17–23, November-December, 1951.

[3] Taylor, G. I., and Maccoll, J. W., *The Air Pressure on a Cone Moving at High Speeds—I and II*, Proc. Roy. Soc. of London, Ser. A, Vol. 139, No. 883, pp. 278–311, February 1, 1933.

[4] Eggers, A. J., Jr., and Savin, Raymond C., *Approximate Methods for Calculating the Flow About Nonlifting Bodies of Revolution at High Supersonic Airspeeds*, N.A.C.A. T.N. No. 2579, December, 1951.

[5] Eggers, A. J., Jr., *On the Calculation of Flow About Objects Traveling at High Supersonic Speeds*, N.A.C.A. T.N. No. 2811, October, 1952.

[6] Eggers, A. J., Jr., and Syvertson, Clarence A., *Inviscid Flow About Airfoils at High Supersonic Speeds*, N.A.C.A. T.N. No. 2646, March, 1952.

[7] Kraus, Samuel, *An Analysis of Supersonic Flow in the Region of the Leading Edge of Curved Airfoils, Including Charts for Determining Surface Pressure Gradient and Shock Wave Curvature*, N.A.C.A. T.N. No. 2729, May, 1952.

[8] *Tables of Supersonic Flow Around Cones*, Staff of the Computing Section, under direction of Zdenek Kopal, M.I.T., Department of Electrical Engineering, Center of Analysis: Tech. Rep. No. 1, 1947.

Statement on References: On Air Forces on Oscillating Wings of Low Aspect Ratio

I. E. Garrick

Chief, Dynamic Loads Division, Langley Aeronautical Laboratory, N.A.C.A., Langley Field, Va.

November 21, 1952

IN THE INTERESTING PAPER by Lawrence and Gerber,[1] reference is made to an extension of some low aspect ratio wing theory of R. T. Jones to nonstationary flows attributed to me.[2] For the sake of the record, I should like to make it clear that the particular work referred to was done jointly by Dr. Eric Reissner and myself, as indicated in reference 3, during June, 1948, while Dr. Reissner was at the Langley Aeronautical Laboratory for a few weeks' stay. It is pertinent to note that Miles has also contributed to the same subject.[4]

REFERENCES

[1] Lawrence, H. R., and Gerber, E. H., *The Aerodynamic Forces on Low Aspect Ratio Wings Oscillating in an Incompressible Flow*, Journal of the Aeronautical Sciences, Vol. 19, No. 11, pp. 769–781, November, 1952.

[2] Garrick, I. E., *Some Research on High-Speed Flutter*, Proceedings of the Third Anglo-American Aeronautical Conference, R.Ae.S.-I.A.S., Appendix B, 1951.

[3] Garrick, I. E., *A Review of Unsteady Aerodynamics of Potential Flows*, Applied Mechanics Reviews, March, 1952.

[4] Miles, John W., *On Nonsteady Motion of Slender Bodies*, Aeronautical Quarterly, Vol. 2, Part 3, pp. 183–194, November, 1950.

Compressible Flow Past a Cascade of Thin Airfoils

G. V. R. Rao

General Electric Company, Lynn, Mass.

November 5, 1952

THE WIDER USE of high-velocity flows through axial-flow compressors has shown the need for a theory of compressible flow past a cascade at high velocities and small turning angles. The well-known thin airfoil theory has been extended to an airfoil in cascade.[1, 2] By use of affine transformation, a linearized compressible flow can be obtained past a cascade of airfoils. As shown in reference 2 for the incompressible flow, the method adopted here can be easily extended to the case of a staggered cascade.

The perturbation velocities caused by the airfoil profiles in cascade are assumed to be small compared with the velocity of the mean uniform flow. Each airfoil in the cascade can be replaced by a distribution of vortices situated on the chord lines of the profiles. Further, if the camber is small, these vortices can be located on lines parallel to the mean flow direction, as shown in the figure. Consider the row of vortices located at a distance x_0 from the cascade axis. These all have the same strength $\gamma(x_0)$ and have the coordinates given by $z_n = x_0 + int$, where n takes all values from $-\infty$ to $+\infty$ including zero (Fig. 1).

The following affine transformation is applied:

$$x = \xi$$
$$\beta y = \eta$$
$$\beta = \sqrt{1 - M^2}$$

where M is the Mach Number of the mean flow.

It can be easily shown[3] that, by choosing a singularity strength $\gamma(\xi_0) = \beta\gamma(x_0)$ in ζ-plane, the perturbation potential will satisfy Laplace's equation. Thus, from the incompressible flow in the ζ-plane, the velocity at a point $(\xi, 0)$, induced by a row of vortices βt apart and located at distance ξ_0 from the point $(\xi, 0)$, is given by

$$v(\xi, 0) = -\sum_{-\infty}^{\infty} \frac{\gamma(\xi_0)}{2\pi(\xi - \xi_0 - in\beta t)}$$

The velocity at the corresponding point in the linearized compressible flow is given by

$$v(x, 0) = v(\xi, 0) = -\sum_{-\infty}^{\infty} \frac{\gamma(\xi_0)}{2\pi(\xi - \xi_0 - in\beta t)}$$

In terms of the coordinates of the physical plane in which the compressible flow occurs,

$$v(x, 0) = -\sum_{-\infty}^{\infty} \frac{\beta\gamma(x_0)}{2\pi(x = x_0 - in\beta t)}$$

The above summation can be easily identified as

$$v(x, 0) = \frac{-\gamma(x_0)}{2t} \coth \frac{\pi(x - x_0)}{\beta t}$$

Adding up the effect of all the rows of vortices given by $-c/2 \leq x \leq c/2$

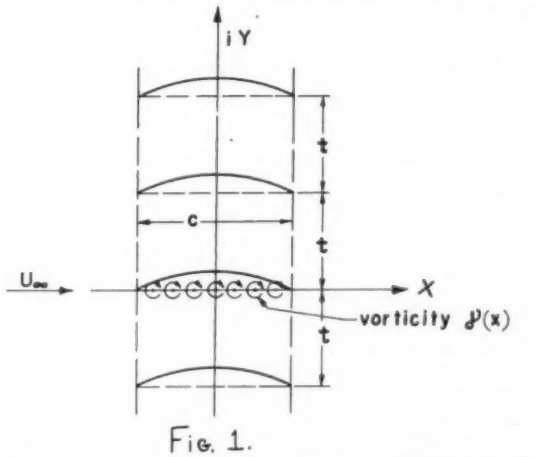

FIG. 1.

$$v(x, 0) = \frac{-1}{2t} \int_{x_0 = -c/2}^{c/2} \gamma(x_0) \coth \frac{\pi(x - x_0)}{\beta t} \, dx_0$$

As $t \to \infty$ the above reduces to the perturbation velocity for an isolated airfoil,

$$v_{\text{isol.}}(x, 0) = \frac{-1}{2} \int_{x_0 = -c/2}^{c/2} \gamma(x_0) \left[\frac{\beta}{\pi(x - x_0)} \right] dx_0$$

Hence, the effect of the rest of the airfoils in cascade can be given as

$$v_{\text{casc.}} - v_{\text{isol.}} = \frac{-1}{2t} \int_{x_0 = -c/2}^{c/2} \gamma(x_0) \left[\coth \frac{\pi(x - x_0)}{\beta t} - \frac{\beta t}{\pi(x - x_0)} \right] dx_0$$

Spurr and Allen in their investigation[4] using a different approach give this effect as

$$- \frac{\pi}{6\beta t^2} \int_{-c/2}^{c/2} \gamma(x_0) \cdot (x - x_0) \, dx_0$$

after neglecting powers of $[(x - x_0)/nt]$ higher than second in the summation. These two expressions for the additional effect in the vertical velocity can be shown to agree if $\coth \pi(x - x_0) \div \beta t$ were expanded and powers of $(x - x_0)/\beta t$ higher than second neglected. It can be readily seen that such an approximation overestimates the vertical induced velocity, thereby giving a higher incidence at the airfoil. Hence, their investigation showed a decrease in the lift-curve slope for an airfoil in cascade of high solidity at high Mach Numbers. Based on this they concluded: "The interference effects of the airfoils in cascade increase so rapidly with Mach Number that, contrary to the usual expectation, a decrease in lift-curve slope occurs for high solidities."

Using the more complete expression for the additional induced velocity, the calculations by this author showed no such adverse effect.

References

[1] Pistolesi, E., *On the Calculation of Flow Past an Infinite Screen of Thin Airfoils*, N.A.C.A. T.M. No. 968, February, 1941.

[2] Scholz, N., *On the Calculation of the Potential Flow Around Airfoils in Cascade*, Readers' Forum, Journal of the Aeronautical Sciences, Vol. 18, No. 1, p. 68, January, 1951.

[3] Milne-Thomson, L. M., *Theoretical Aerodynamics;* D. Van Nostand Company, New York, 1948.

[4] Spurr, Robert A., and Allen, H. Julian, *A Theory of Unstaggered Airfoil Cascades in Compressible Flow*, N.A.C.A. Report No. 888, 1947.

The Pressure Distribution on Low Aspect Ratio Wings in Steady or Unsteady Incompressible Flow

H. R. Lawrence
Cornell Aeronautical Laboratory, Inc., Buffalo, N. Y.

November 17, 1952

METHODS FOR COMPUTING the chordwise lift and rolling moment distribution on low aspect ratio wings with straight trailing edges in steady and unsteady linearized incompressible flow have appeared recently in this JOURNAL.[1, 2] In this note, the results of references 1 and 2 will be extended in two directions. A physical interpretation will be supplied for certain mathematical procedures employed in these papers, and a method for computing the distribution of lifting pressure will be derived.

The notation of reference 2, which applies to the unsteady state, will be employed, but the steady-state results may be found by allowing the reduced frequency k to vanish.

The lift per unit area may be expressed in terms of the perturbation velocity potential as follows:

$$dL/dS = 2\rho U^2[\phi_x(x,y) + ik\phi(x,y)] \tag{1}$$

A major result of references 1 and 2 is a method for computing the spanwise integrals $g(x)$ and $m(x)$ defined below.

$$g(x) = \int_{-\beta(x)}^{\beta(x)} dy \, \phi(x,y) \tag{2}$$

$$m(x) = \int_{-\beta(x)}^{\beta(x)} dy \, y\phi(x,y) \tag{3}$$

In the steady case, the functions $2\rho U^2 g'(x)$ and $2\rho U^2 m'(x)$ represent the lift and rolling moment per unit chord. Although a knowledge of the above spanwise integrals of the potential is sufficient to compute a number of important aerodynamic properties of a wing, the distribution of lift pressures can only be calculated when the velocity potential $\phi(x,y)$ is known.

In order to compute the velocity potential $\phi(x,y)$ from a knowledge of the functions g and m, an additional physical assumption must be introduced. Following reference 2, the integral equation for a lifting surface may be written in the form

$$w(x, y) - w_i(x,y) = w_a(x,y) = \frac{1}{\pi} \int_{-\beta(x)}^{\beta(x)} \frac{d\eta}{y - \eta} \phi(x,\eta) \tag{4}$$

where $w_i(x,y)$, the induced angle of attack, represents the additional terms in the integral equation for the lifting surface and $w_a(x,y)$, the aerodynamic angle of attack, is defined by Eq. (4). The potential $\phi(x,y)$ may be expressed in terms of the aerodynamic angle of attack $w_a(x,y)$ by inverting the integral Eq. (4) as follows:

$$\phi_y(x,y) = \frac{-1}{\pi\sqrt{\beta^2(x) - y^2}} \int_{-\beta(x)}^{\beta(x)} \frac{d\eta \, w_a(x,\eta) \sqrt{\beta^2(x) - \eta^2}}{y - \eta} \tag{5}$$

For a wing of very low aspect ratio, the induced angle of attack $w_i(x,y)$ becomes negligible compared with $w(x,y)$, and the integral Eq. (4) becomes a form of the Jones[3] low aspect ratio theory for steady flow or the Garrick[4] extension of this theory for unsteady flow. For wings of higher aspect ratio, where the induced angle of attack $w_i(x,y)$ can no longer be neglected relative to the geometric angle of attack $w(x,y)$, a procedure similar to that employed in developing the Prandtl[5] lifting-line theory may be used to obtain an approximate expression for the induced angle of attack $w_i(x,y)$. In the case where the spanwise lift distribution is symmetric, the induced angle of attack will be assumed to be constant over the span or $w_i(x,y) = w_i^{(s)}(x)$. This assumption is seen to be directly analogous to the assumption of constant downwash angle over the chord in Prandtl lifting-line theory. In the case where the spanwise lift distribution is antisymmetric, the induced angle of attack will be assumed to be a linear function of the spanwise coordinate or for $w_i(x,y) = y w_i^{(a)}(x)/\beta(x)$. It is clear that the general unsymmetric case is directly analogous to the Weissinger[6] assumption that the induced angle of attack is a linear function of the chordwise coordinate.

The induced angle of attack may be calculated in the following manner. In the symmetric case, Eq. (4) is multiplied by $\sqrt{\beta^2(x) - y^2}$ and is integrated over the span. There results the formula

$$w_i^{(s)}(x) = [f(x) - g(x)]/(\kappa/2)\beta^2(x) \tag{6}$$

where the function f is defined as follows:

$$f(x) = \int_{-\beta(x)}^{\beta(x)} dy \, w(x,y) \sqrt{\beta^2(x) - y^2} \tag{7}$$

It will be noted that, in the steady case, $2\rho U^2 f'(x)$ is the lift per unit chord of a Jones[3] wing.

An expression for the induced angle of attack in the antisymmetric case may be obtained by multiplying Eq. (1) by $y\sqrt{\beta^2(x) - y^2}$ and integrating over the span.

There results the formula

$$w_i^{(a)}(x) = [e(x) - m(x)]/(\kappa\beta^2/16) \, . \tag{8}$$

where the function e is defined as follows

$$e(x) = \frac{1}{2}\int_{-\beta(x)}^{\beta(x)} dy\, y\sqrt{\beta^2(x) - y^2}\, w(x,y) \qquad (9)$$

In the steady case, $2\rho U^2 e'(x)$ represents the rolling moment per unit chord of a Jones[3] wing.

It will be noted that the sign in Eq. (9) has been reversed when compared with references 1 and 2 in order to obtain a more consistent notation.

References

[1] Lawrence, H. R., *The Lift Distribution of Low Aspect Ratio Wings at Subsonic Speeds*, Journal of the Aeronautical Sciences, Vol. 18, No. 10, p. 683, October, 1951.

[2] Lawrence, H. R., and Gerber, E. H., *The Aerodynamic Forces on Low Aspect Ratio Wings Oscillating in an Incompressible Flow*, Journal of the Aeronautical Sciences, Vol. 19, No. 11, p. 769, November, 1952.

[3] Jones, R. T., *Properties of Low Aspect Ratio Pointed Wings at Speeds Below and Above the Speed of Sound*," N.A.C.A. T.N. No. 1032, 1946.

[4] Garrick, I. E., *Some Research on High-Speed Flutter*, Proceedings of the Third Anglo-American Aeronautical Conference, R.Ae.S.-I.A.S., Appendix B, 1951.

[5] Prandtl, L., *Tragflügeltheorie, I Mitteilung, Nachrichten der K. Gesellschaft der Wissenschaften zu Göttingen*, Math.-Phys. Klasse, pp. 451–477, 1918.

[6] Weissinger, J., *The Lift Distribution on Swept-Back Wings*, N.A.C.A. T.M. No. 1120, March, 1947.

Busemann Coefficients for a Supersonic Airfoil

D. Naylor

Research Student, University of London, King's College, London, England

November 11, 1952

Introduction

There has been considerable debate on the correct values of the Busemann coefficients for the pressure on an airfoil in supersonic flow. This is entirely due to the lengthy analysis usually involved.[1–4] Computation is liable to errors and is not easily checked, but by resorting to an equation for the pressure in terms of the local Mach Number much of the algebra can be avoided.

The coefficients are first found when there is no shock; their values for the combined case when a simple wave follows the shock are easily deduced.

Simple Wave

Steady isentropic supersonic flow in two dimensions is considered in which the velocity vector reduces to a function of one independent variable w, say. If p, ρ, q, and a denote, respectively, the pressure, density, velocity, and acoustic speed of the gas and if θ is the angle the velocity makes with some initial line, then the equations of continuity and motion along a stream line are

$$(\rho q)_s + \rho q \theta_n = 0$$
$$p_s + \rho q q_s = 0$$

where suffixes s, n denote differentiation along and normal to a stream line.

Using $dp = a^2 d\rho$ and eliminating ρ_s/ρ yields the equation for the velocity in the form

$$(a^2 - q^2)q_s + qa^2\theta_n = 0$$

or, since $q = q(w)$ and $\theta = \theta(w)$,

$$(a^2 - q^2)q_w w_s + qa^2\theta_w w_n = 0$$

Similarly, the equation of irrotational flow

$$q\theta_s = q_n$$

becomes

$$q\theta_w w_s = q_w w_n$$

Therefore, eliminating w_s/w_n,

$$(a^2 - q^2)q_w^2 + q^2a^2\theta_w^2 = 0$$

or

$$dq/q\, d\theta = \pm 1/B$$

where $B = (M^2 - 1)^{1/2}$ and $M = q/a$.

Now, $q\, dq + (dp/\rho) = 0$ and $a^2 = \gamma p/\rho$; therefore, the required equation for the pressure is

$$dp/p\, d\theta = \gamma M^2/B \qquad (1)$$

the positive sign being taken if the flow is one of expansion in the direction θ decreasing.

Logarithmic differentiation of $M = q/a$ gives

$$dM/M\, d\theta = (dq/q\, d\theta) - (da/a\, d\theta)$$
$$= [1 + (1/2)(\gamma - 1)M^2]dq/q\, d\theta$$

since

$$q\, dq + [2ada/(\gamma - 1)] = 0$$

therefore, using $dq/q\, d\theta = -1/B$,

$$dM/d\theta = -[1 + (1/2)(\gamma - 1)M^2]M/B \qquad (2)$$

Differentiating Eq. (1) with respect to θ and using Eq. (2) to substitute for $dM/d\theta$ yields

$$d^2p/p\, d\theta^2 = \gamma M^2[(\gamma + 1)M^4 - 4B^2]/2B^4 \qquad (3)$$

Differentiating again gives, after short calculation,

$$d^3p/p\, d\theta^3 = \gamma M^2[(\gamma + 1)M^8 + (2\gamma^2 - 7\gamma - 5)M^6 + 10(\gamma + 1)M^4 - 12M^2 + 8]/2B^7 \qquad (4)$$

In the case of an initial undisturbed stream parallel to the axis $\theta = 0$, with Mach Number M_1 and pressure p_1, Eqs. (1), (3), and (4) give at once the first three coefficients of the pressure series expansion appropriate to a small expansive deflection θ, actually negative for the clockwise expansion considered,

$$p/p_1 = 1 + c_1\theta + c_2\theta^2 + c_3\theta^3 + 0(\theta^4) \qquad (5)$$

where

$$c_1 = \gamma M_1^2/B_1, \qquad B_1 = (M_1^2 - 1)^{1/2}$$
$$c_2 = \gamma M_1^2[(\gamma + 1)M_1^4 - 4B_1^2]/4B_1^4$$
$$c_3 = \gamma M_1^2[(\gamma + 1)M_1^8 + (2\gamma^2 - 7\gamma - 5)M_1^6 + 10(\gamma + 1)M_1^4 - 12M_1^2 + 8]/12B_1^7$$

The following expansions are readily obtained from Eq. (5):

$$p_\theta/p = c_1 + (2c_2 - c_1^2)\theta + (3c_3 - 3c_1c_2 + c_1^3)\theta^2 + 0(\theta^3) \qquad (6)$$

$$p_{\theta\theta}/2p = c_2 + (3c_3 - c_1c_2)\theta + 0(\theta^2) \qquad (7)$$

$$p_{\theta\theta\theta}/6p = c_3 + 0(\theta) \qquad (8)$$

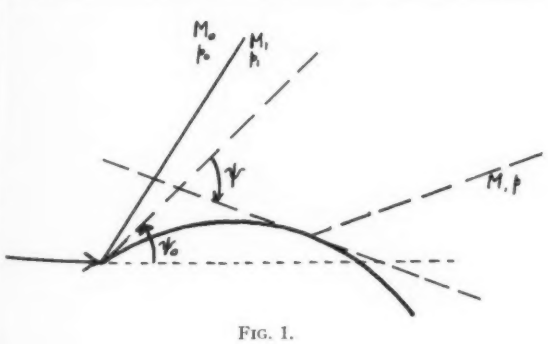

Fig. 1.

By virtue of Eqs. (1), (3), and (4), these are just the expansions for the three Busemann coefficients, evaluated on the Mach line where the deflection is θ, as a power series whose coefficients are functions of the Mach Number M_1.

If ψ denotes the actual magnitude of the expansive deflection, then Eq. (5) can be written

$$p/p_1 = 1 - c_1\psi + c_2\psi^2 - c_3\psi^3 + 0(\psi^4) \qquad (9)$$

Oblique Shock Followed by Simple Wave

Let M_0 and p_0 denote the Mach Number and pressure in front of the shock and ψ_0 denote the deflection through it (Fig. 1). From shock theory the pressure p_1 immediately behind the shock is given by

$$p_1/p_0 = 1 + b_1\psi_0 + b_2\psi_0^2 + (b_3 - D)\psi_0^3 + 0(\psi_0^4) \qquad (10)$$

where b_1, b_2, b_3 are the same functions of M_0 as c_1, c_2, c_3 are of M_1, and

$$D = \gamma(\gamma + 1)M_0^6[(5 - 3\gamma)M_0^4 - 4(3 - \gamma)M_0^2 + 8]/96B_0$$

$$B_0 = (M_0^2 - 1)^{1/2}$$

Because the formulas for the pressure, density, and velocity immediately behind the shock differ from the corresponding formulas if the change had been a small isentropic compression through the same deflection ψ_0 only in the third order terms, it follows that in expressing each of the functions c_1, c_2, c_3 as power series in ψ_0, the formulas (6), (7), and (8) may be used if c_1, c_2, c_3, and θ are replaced by b_1, b_2, b_3, and ψ_0. Therefore,

$$c_1 = b_1 + (2b_2 - b_1^2)\psi_0 + (3b_3 - 3b_1b_2 + b_1^3)\psi_0^2 + 0(\psi_0^3)$$

$$c_2 = b_2 + (3b_3 - b_1b_2)\psi_0 + 0(\psi_0^2)$$

$$c_3 = b_3 + 0(\psi_0)$$

Substituting these values in Eq. (9) and using Eq. (10) to eliminate p_1 by simple multiplication gives the final expansion,

$$p/p_0 = 1 + b_1\phi + b_2\phi^2 + b_3\phi^3 - D\psi_0^3 + 0(\phi^3)$$

where $\phi = \psi_0 - \psi$, the resultant compressive deflection.

These results agree with those derived by Jones in reference 4, while the derivation of Eq. (10) is given by Laitone in reference 2.

References

[1] Busemann, A., *Atti del V Convegno "Volta,"* Rome, Reale Academia d'Italia.

[2] Laitone, E. V., *Exact and Approximate Solutions of Two-Dimensional Oblique Shock Flow*, Journal of the Aeronautical Sciences, Vol. 14, No. 1, p. 25, January, 1947

[3] Puckett, A. E., and Li, T. Y., Letter to the Editor, Journal of the Aeronautical Sciences, Vol. 14, No. 6, p. 336, June, 1947.

[4] Jones, W. P., A.R.C. Report 10,871, September, 1947.

A Note on the Solution for the Rectangular Membrane

S. F. Borg*

Stevens Institute of Technology, Hoboken, N. J.

October 27, 1952

The exact solution for the uniformly loaded rectangular membrane stresses and deflections has not been obtained. Hencky[1] described a rather lengthy numerical finite difference solution but applied it only to a square membrane. The Hencky computations for the rectangular membrane have not as yet been carried through. A solution may be obtained based on a Fourier series analysis similar to the Levy Solution[2] for the nonlinear large deflections problem of plates, but this also is a lengthy numerical procedure and has not been done.

An approximate solution obtained by Föppl[3] assumes values for the membrane deformations which satisfy the boundary and symmetry conditions and evaluates the unknown constant coefficients by minimizing the total energy of the membrane. He applied this solution to the square membrane only and obtained the stress and deflection at the center, which values differ slightly from Hencky's. Neubert and Sommer[4] carried through the Föppl computations for the rectangular case and drew curves for stresses and deflections. In addition, these authors obtained reasonably satisfactory experimental verification for the Föppl and Hencky solutions for the square membrane, as did also Head and Sechler.[5] The latter authors suggest a discrepancy between experimental and Föppl stresses for higher aspect ratio membranes. Neubert and Sommer did not test the rectangular membrane.

Thus the status of the membrane problem appears to be as follows: (a) No complete exact solution has been obtained; (b) the approximate square membrane solutions of Föppl and Hencky have been verified experimentally; and (c) only the approximate Föppl solution is available for the rectangular membrane.

There is, however, a serious discrepancy in the Föppl solution which casts doubt on its validity for a large range of rectangular membranes.† It is possible to obtain an exact solution for the semi-infinite membrane. This may be done, for example, by taking the limit of the semi-infinite tied-plate solution[6] as the plate stiffness approaches zero. Doing this, the value for the center stress in a direction parallel to the short side is

$$\sigma_x = 0.357\sqrt[3]{p^2a^2E/h^2} \qquad (1)$$

† Since writing this note, the writer has been advised of a recent N.A.C.A. Technical Note by Flügge (No. 2612, "Stress Problems in Pressurized Cabins," February, 1952), in which a brief statement is made concerning this weakness of the Föppl-type solution.

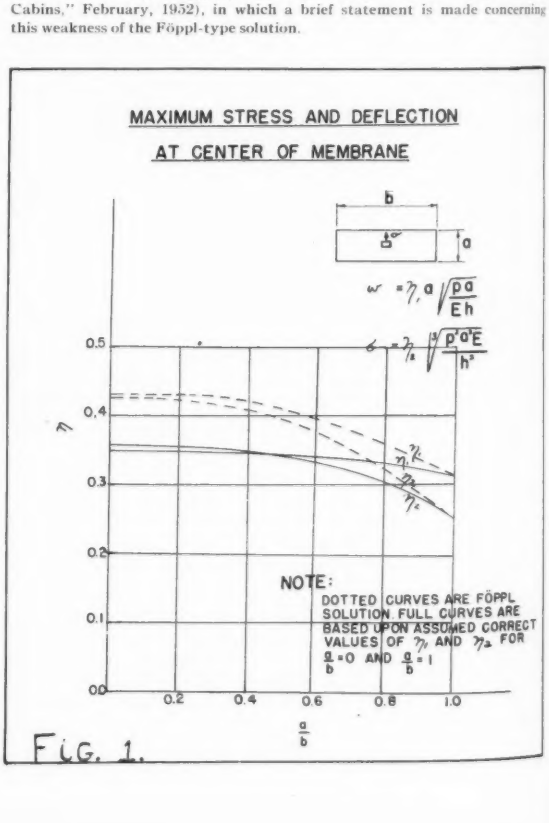

FIG. 1.

* This work was done while the writer was a Research Engineer for Grumman Aircraft Engineering Corporation.

in which

p = transverse uniform load
a = short side of membrane
E = modulus of elasticity
h = membrane thickness

If the Föppl solution is carried through to its limit, the semi-infinite membrane stress σ_x is given by

$$\sigma_x = 0.425 \sqrt[3]{p^2a^2E/h^2} \qquad (2)$$

a difference of 19.1 per cent. (A similar comparison and discrepancy may be obtained for the center deflections.)

The reason for this discrepancy is not difficult to trace. The trigonometric function assumed by Föppl becomes less accurate as the aspect ratio increases. In the limit, $b/a = \infty$, the deflection function should be a constant but instead maintains the sinusoidal form.

Experiments indicate[5] that for rectangular membranes of aspect ration $b/a \geq 3$, the center portion of the membrane is, for all practical purposes, in the same stress and deflection condition as the semi-infinite membrane.

The experimental and theoretical requirements outlined above are embodied in the curves of Fig. 1. The dotted lines are for σ_x and w (the center deflection) as determined by the Föppl method. The full lines drawn between the known limits $b/a = 1$ (Föppl) and $a/b = 0$ (exact) in such a way as to satisfy the known experimental requirements may be taken to represent actual conditions closely enough for all engineering and design purposes.

The values of the stresses and deflections in the rectangular membrane are of importance not only for problems involving pure membrane design but also in conjunction with approximate split-rigidity designs of plates subjected to large deflections.[3]

References

[1] Hencky, H., *Die Berechnung dunner rechteckiger Platten mit verschwindender Biegungsteifigkeit*, ZAMM, p. 8, April, 1921.

[2] Levy, Samuel, *Square Plate with Clamped Edges under Normal Pressure Producing Large Deflections*, N.A.C.A. T.N. No. 847, 1942.

[3] Föppl, A. L., *Drang und Zwang*, p. 226; R. Oldenbourg, Munich, Germany, 1924.

[4] Neubert, M., and Sommer, A., *Rectangular Shell Plating under Uniformly Distributed Hydrostatic Pressure*, N.A.C.A. T.M. No. 965, December, 1940.

[5] Head, R. M., and Sechler, E. E., *Normal Pressure Tests on Unstiffened Flat Plates*, N.A.C.A. T.N. No. 943, September, 1944.

[6] Timoshenko, S., *Theory of Plates and Shells*, p. 4; McGraw-Hill Book Co., Inc., New York and London, 1940.

A Measurement of Turbulent Boundary-Layer Profiles and Heat-Transfer Coefficient at $M = 7$

Peter P. Wegener, Eva M. Winkler, and M. Sibulkin
U.S. Naval Ordnance Laboratory, White Oak, Silver Spring, Md.

October 28, 1952

Measurements in a naturally turbulent boundary layer with heat transfer to the surface were made in the continuous 12- by 12-cm. N.O.L. hypersonic tunnel.[1] The survey station was located on the centerline of one of the diverging walls of a straight-walled two-dimensional nozzle. The free-stream Mach Number (M_∞) at the survey station was 7.0, and the free-stream velocity was 3,400 ft. per sec.; the free-stream Mach Number gradient inherent in this type of nozzle was approximately $0.05M$ per in. Wind-tunnel supply pressure (p_0) and temperature (T_0) were kept constant, T_0 being 50°C. higher than the temperature needed to avoid air condensation during the expansion. Wall surface temperature (T_w) was kept constant at $T_w/T_\infty = 5.7$ by a water cooling system in the nozzle wall. The static pressures measured on the wall and at the edge of

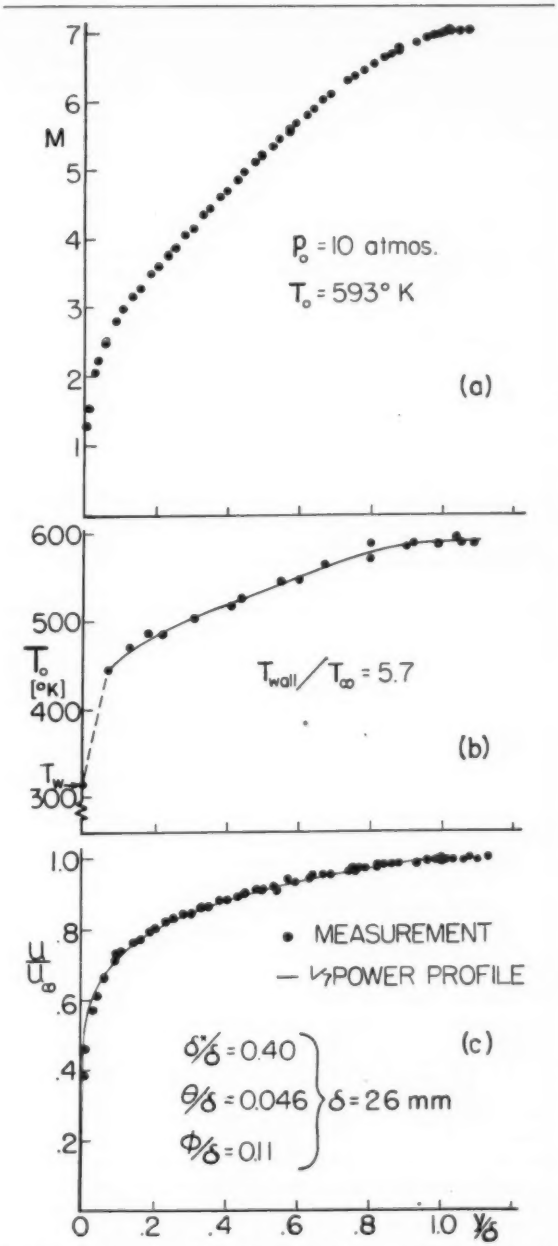

Fig. 1. Measured turbulent boundary-layer profiles with heat transfer at a free-stream Mach Number of 7.

boundary layer agreed, and this value of static pressure was assumed to exist through the boundary layer. Pitot pressure was surveyed from wall to free stream, with a probe large enough to avoid errors due to slip flow effects.[2] The Mach Number determined from the Rayleigh formula is shown on Fig. 1a. (The use of the perfect gas law and $\gamma = 1.4$ implied in this procedure is valid for our test conditions.) Total temperature (T_0') distribution was surveyed with a double-shielded total temperature probe. This probe was calibrated in the free stream at about the same M and Re encountered in the boundary layer. The T_0' profile obtained after applying these calibration factors is shown in Fig. 1b. Velocity was calculated using the M data

points and values of T_0' obtained from a curve faired through the measured T_0' points. A straight line was drawn between the last T_0' point and the measured value of T_w. This velocity profile is shown in Fig. 1c, which combines the results of four independent runs at identical operation conditions. A $^1/_7$-power profile is also shown in Fig. 1c for comparison. Since all the flow properties in the boundary layer are known, displacement thickness (δ^*) and momentum thickness (θ) could be computed and are indicated in Fig. 1c. The Reynolds Number based upon free-stream conditions and displacement thickness is 43,000, while an equivalent flat plate Re would be of the order of 10^7.

Other measurements show that tunnel supply temperature (T_0) is constant across the nozzle inlet. Therefore, the rate of heat transfer per unit nozzle width (Q) from the nozzle inlet to the boundary-layer station may be computed from

$$Q = c_p \rho_\infty u_\infty (T_w - T_0)\phi \tag{1}$$

$$\phi = \int_0^\infty \frac{\rho u}{\rho_\infty u_\infty} \left(\frac{T_0' - T_0}{T_w - T_0} \right) dy \tag{2}$$

Eq. (2) represents a definition of an "energy thickness" that permits the calculation of Q from the mass flow weighted defect of T_0' with respect to T_0 across the boundary layer at the survey station. On the other hand, Q may also be determined by measuring the discharge rate and temperature increase of the nozzle cooling water after a steady state of heat transfer has been established. It was found that these two values of Q were in agreement suggesting the reliability of the T_0' measurement in the boundary layer.

Measurements in the steel nozzle wall showed that the temperature dropped linearly with distance from the surface at the survey station after a steady state of heat transfer had been established. Knowing the temperature gradient (dT/dy) and the thermal conductivity (k) in the steel wall, the rate of heat transfer per unit area,

$$q = k(dT/dy) = h(T_e - T_w) \tag{3}$$

could be computed, where h is the heat-transfer coefficient. However, to determine the Stanton Number (St_∞) (also called the dimensionless heat-transfer coefficient $C_{H\infty}$),

$$St_\infty = \frac{h}{c_p \rho_\infty u_\infty} = \frac{k(dT/dy)}{c_p \rho_\infty u_\infty (T_e - T_w)} \tag{4}$$

we need to know the insulated flat-plate temperature (T_e), a quantity that we were not able to measure. Assuming the relation between our recovery factor (r) and Prandtl Number (Pr) to be $r = Pr^{1/3}$ and taking $Pr = 0.73$, we can calculate T_e and in turn obtain $St_\infty = 0.00075$ from Eq. (4) and the measured data. Using $Pr = 1$ (and thus $T_e = T_0$), we find $St_\infty = 0.00061$. However, after applying the relation[3] $c_{f\infty}/2 = St_\infty Pr^{2/3}$, we obtain $c_{f\infty} = 0.0012$ regardless of which of these Pr we choose. Knowing the local friction coefficient ($c_{f\infty}$), we calculate the shear stress at the wall (τ_w). While the heat-transfer measurement

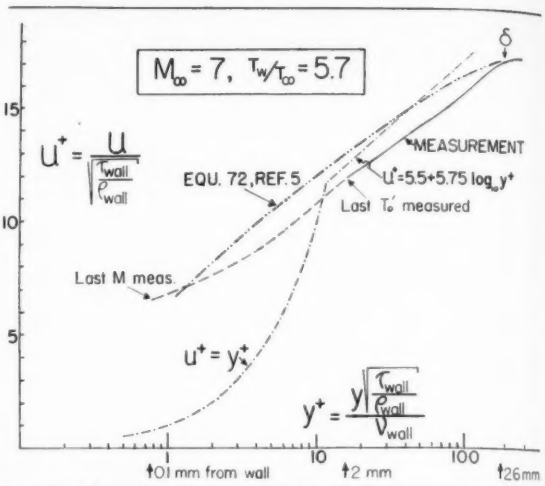

FIG. 2. The u^+, y^+ representation of the measured velocity profile at $M_\infty = 7$ and comparison with theory.

may not be too reliable, we are now able to tentatively plot our velocity profile in the u^+, y^+ parameters[4] as shown on Fig. 2. Since these parameters are of most value near the wall, the density and kinematic viscosity were based upon wall properties. The portion of the velocity profile derived from measured M but only interpolated T_0' (note actual distances from wall) is represented by a dashed line. For comparison, von Kármán's incompressible flow semilogarithmic law[4] and assumed linear velocity distribution ($u^+ = y^+$) in the laminar sublayer are shown on Fig. 2. Finally, a compressible flow profile calculated from Eq. (72) of Van Driest's analysis[5] for our M_∞ and T_w/T_∞ is shown. (Aside from other assumptions inherent in this analysis, the profile has the boundary condition $u = u_\infty$ at $y = \delta$.)

It appears from Figs. 1c and 2 that the measured velocity profile is similar to that found in low-speed flow except in the region extremely close to the wall, and this difference may be due to the lack of T_0' measurements in that region.

REFERENCES

[1] Wegener, Peter P., *Summary of Recent Experimental Investigation in the N.O.L. Hyperballistics Wind Tunnel*, Journal of the Aeronautical Sciences, Vol. 18, No. 10, p. 665, October, 1951.

[2] Kane, E. D., and G. J. Maslach, *Impact-Pressure Interpretation in a Rarefied Gas at Supersonic Speeds*, N.A.C.A. T.N. No. 2210, October, 1950.

[3] Johnson, H. A., and M. W. Rubesin, *Aerodynamic Heating and Convective Heat Transfer—Summary of Literature Survey*, Trans. A.S.M.E., Vol. 71, No. 5, Eq. (20), p. 452, July, 1949.

[4] von Kármán, Th., *Turbulence and Skin Friction*, Journal of the Aeronautical Sciences, Vol. 1, No. 1, p. 1, January, 1934.

[5] Van Driest, E. R., *Turbulent Boundary Layer in Compressible Fluids*, Journal of the Aeronautical Sciences, Vol. 18, No. 3, p. 145, March, 1951.

INSTITUTE *of the* AERONAUTICAL SCIENCES

1932–1953

Since its incorporation in October, 1932, as a scientific membership society to advance the art and science of aeronautics, the Institute of the Aeronautical Sciences, in over twenty years of service to aviation, has become the representative technical society for the aviation industry and profession. It is the only organization in the United States which brings together all of the sciences and branches of engineering and technology which are applied to aeronautics.

Publications

Papers presented at meetings or submitted to the Editorial Board are published in the JOURNAL OF THE AERONAUTICAL SCIENCES or the AERONAUTICAL ENGINEERING REVIEW. The JOURNAL prints in each issue full-length scientific papers on new research and developments in various fields applied to aviation. The REVIEW keeps members and subscribers up to date on aeronautical news and literature through reviews of new books and periodical articles, government publications and trade literature and publishes papers on applied engineering and aircraft production.

The AERONAUTICAL ENGINEERING CATALOG, published yearly, is a guide to sources and specifications of materials, parts, and accessories used in the design and production of aircraft, aircraft engines, and parts.

Research Facilities

Through the Aeronautical Archives of the Institute, members have for their use the most complete aeronautical library and reference research facilities maintained by any technical society. At the New York building of the Institute, The W. A. M. Burden Library of books, reports and periodicals, the Aeronautical Index of subject files, biographic files and bibliography, and the historical and art collections in the Archives are available for study. The Pacific Aeronautical Library at 7660 Beverly Boulevard, Los Angeles, maintains a reference collection and reading room for members and loans books to company libraries in the area. Through the Paul Kollsman Lending Library, aeronautical books are lent by mail without charge to members anywhere in the continental United States. In addition to a complete collection of standard aeronautical reference works, the Kollsman Lending Library has available for loan new aviation books as they are reviewed in the AERONAUTICAL ENGINEERING REVIEW.

Membership

In addition to membership in professional societies representing their particular fields, specialists applying their knowledge and experience to aeronautics find membership in the Institute of great value in the contacts made with others engaged in aeronautical work and in the broad coverage of all aeronautical problems furnished through its meetings and publications. All applications for membership are carefully reviewed by the Membership Committee, which recommends the grade of membership for which the applicant is found eligible. There are advanced grades of membership—Fellow and Honorary Fellow—to which members may be elected as their experience warrants. Thus, a member receives due recognition—more valuable because it is given by his colleagues—for his contributions to the progress of aeronautics. New applicants may be elected by the Membership Committee to the grade of Associate Fellow if they have been engaged for not less than ten years in the practice of the aeronautical sciences and shall have been in responsible charge of important scientific or engineering work, or shall have otherwise made outstanding contributions to the aeronautical sciences; to the grade of MEMBER if they have been engaged in professional work for at least eight years and have acquired a recognized standing in engineering, design, or other special work applied to aeronautics; to the grade of Associate Member if they have acquired a recognized standing in an administrative capacity in the aviation industry; to the grade of Technical Member if they are recent engineering school graduates or are engaged in technical aeronautical work. Student Members are admitted by application through Student Branches organized at their schools. Aeronautical companies, as well as individuals, are affiliated with, and participate in, the support of the Institute through Corporate Membership.

Dues

An entrance fee of $10 is required of all new members who apply for admission to a grade of membership to be specified by the Membership Committee (Corporate Members, Foreign Members, and Student Members being excepted).

Annual membership dues include a subscription to the AERONAUTICAL ENGINEERING REVIEW. Dues for the various grades of membership are as follows: Fellows—$16.50; Associate Fellows—$16.50; MEMBERS—$13.50; Associate Members—$13.50; Technical Members—(26 years of age and over) $13.50, (under 26) $6.50.

The regular subscription price for the JOURNAL OF THE AERONAUTICAL SCIENCES and the AERONAUTICAL ENGINEERING REVIEW is $12 and $3.00 per year, respectively. Members may subscribe to the JOURNAL at $4.00 per year.

Those who are engaged in aeronautical work or who have an interest in any technical phase of aviation will find the services of the Institute to be a necessary aid in keeping abreast of developments in these times of such rapid progress. An application form and further information about membership can be obtained from an Institute member or by writing to the Secretary.

INSTITUTE OF THE AERONAUTICAL SCIENCES, INC.

2 EAST 64TH STREET

NEW YORK 21, N.Y.

SUGGESTIONS *for* CONTRIBUTORS *to the Publications of the* INSTITUTE *of the* AERONAUTICAL SCIENCES

The Institute of the Aeronautical Sciences invites both members and nonmembers from any country to submit papers for publication in the JOURNAL OF THE AERONAUTICAL SCIENCES and the AERONAUTICAL ENGINEERING REVIEW. The Institute, following the practice of other societies, does not pay for contributions.

The following directions for the preparation of papers, if followed by authors, will save correspondence, avoid the return of papers for changes, minimize the work of preparation for the printer, and save the expense due to the charges made for "author's corrections."

MANUSCRIPTS: The original typewritten copy of the paper is desired, double or triple spaced on one side of white paper sheets, consecutively numbered. There should be wide margins to allow for the marking of directions to the printer. Correcting, changing, or adding to papers after they are in type is costly. It is, therefore, imperative that papers submitted be in final form. Typographical errors may be corrected on proofs, but if authors wish to add material, they may do so at their own expense. In mailing, drawings may be rolled but manuscripts should be sent flat. Send by first-class mail (register if you wish for your own protection) to the Editorial Office, Institute of the Aeronautical Sciences, 2 East 64th Street, New York 21, N.Y. All manuscripts will be examined by the Editorial Committee and by the Editor. Authors will be advised as promptly as possible whether the paper is acceptable for publication.

TITLES: The title of the paper should be brief. The name and initials of the author should be written as he prefers. The use of the full name of an author is advocated because of the frequent duplication of initials and surnames which sometimes makes it difficult to establish the identity of the author. This is particularly important for large annual indexing and abstracting services. All titles and degrees or honors are omitted. The name of the organization with which the author is associated should be placed after his name on a separate line. The date on which the paper is received will be inserted by the Editor. The author's title should be indicated in a footnote.

SUMMARIES OR ABSTRACTS: An abstract to be printed at the beginning should accompany each article. It should be adequate as an *index* and as a *summary*. It should contain a statement of major conclusions reached, since summaries in many cases constitute the only source of information used in compiling scientific reference indexes. Abstracts printed in other journals, especially foreign, in most cases, consist of summaries from printed papers. The summary should explain as adequately as possible the major conclusions to a nonspecialist in the subject and should contain from 100 to 300 words, depending on the length of the paper.

SUBHEADINGS: Subheadings should be inserted by the author at frequent intervals. The work of editorial preparation will be simplified by the author providing many subheadings.

MATTER USUALLY DELETED: Photographs or illustrations of little technical interest and not showing advances in general practice. Too detailed tabular matter (general results of such tables may be included in the text). Lengthy descriptions of materials or processes or of preliminary experiments or theories that preceded final results; salient features only are of interest.

REFERENCES AND FOOTNOTES: References should appear as footnotes only, numbered consecutively and grouped together at the end of the manuscript. The arrangement should be as follows: (For books)—[1] Durand, W. F. *Aerodynamic Theory*, 1st Ed., Vol. 1, p. 23; Julius Springer, Berlin, 1934. (For Magazines)—[1] England, C. R., Crawford, A. B., and Mumford, W. W., *Some Results of a Study of Ultra-Short-Wave Transmission Phenomenon*, Proc. I.R.E., Vol. 20, No. 12, pp. 481–482, March, 1933. Please give author, title, edition, volume, page, publisher, and date of publication as indicated. Omission of one required fact causes much extra editorial work and possible inaccuracies.

ILLUSTRATIONS: Illustrations should accompany manuscripts, and each should always be referred to in the text, by number. Drawings or graphs should not be larger than 12 × 16 inches, and must be made with jet black India ink on white paper or tracing cloth, the latter being preferred. *Do not use typewriter for lettering.* The smallest lettering on 8- × 10-inch figures should be no less than $^1/_4$ inch high. Cross-section paper (white with black lines) may be used but it should not have more than 4 lines per inch. If finer ruled paper is used, the major division lines should be drawn in with black ink, omitting the finer divisions. In the case of finely ruled paper, only blue-lined paper can be accepted. *Tracing paper and blueprints* are not acceptable. Lettering and all markings must be large enough to be readable after reduction. Mail rolled or flat; never fold. Drawings that cannot be reproduced (including pencil drawings) will be returned to the author for redrawing thus delaying publication of the paper. Photographs should be distinct and show clear black and white contrasts. They must be on glossy white paper. Avoid round and oval photographs.

CAPTIONS AND LEGENDS: Legends or captions must accompany each drawing or photograph submitted. If written on the drawing or photograph, they should be placed below and well outside the part to be reproduced. Each table should have a caption such as Table 1, Table 2, Table 3, etc. Captions should be complete in themselves so as to make the data intelligible to the reader without reference to the text. A duplicate list of captions for figures should be included as the last page of the manuscript. Use "Fig. 1" (not Figure 1), Figs. 3 and 4, etc., in both the text and the numbering of illustrations. In the text, "Eq. (1)" or "Eqs. (1) and (2)" is used, not "Equation (1)." In captions and legends, except for "Fig." and "Eq.," and in table headings write all words in full; do not abbreviate.

MATHEMATICAL WORK: Only the simplest formulas should be typewritten; all others should be carefully written in pen and ink, the writing to be large enough so that ample room is provided to mark mathematical matter for the printer. A considerable spacing for marking should be allowed above and below all equations. All complicated equations should be repeated on separate sheets with plenty of space left for marking. The solidus should be used for simple fractions appearing within the text. Make all expressions clear to the typesetter. Greek letters used in formulas should be clearly designated by name on the margin of the manuscript. All symbols should be clearly written and carefully checked. The difference between capital and lower-case letters should be clearly distinguished and care taken to avoid confusion between zero (0) and the letter (o), between the numeral (one) and the letter (ell) and the prime ($'$), between alpha and a, kappa and k, u and mu, v and nu, n and eta. All subscripts and exponents should be clearly marked, and dots and bars over letters or mathematical expressions should be avoided. Avoid complicated exponents and subscripts. When it is necessary to repeat a complicated expression, it should be represented by some convenient symbol.

NOMENCLATURE AND ABBREVIATIONS: Standard abbreviations should be used, and it should be noted that most abbreviations are lower case such as m.p.h., b.m.e.p., i.hp., b.hp., hp., . . . etc.